



National Institute of
Environmental Research



National Aeronautics and
Space Administration

KORUS-AQ Final Science Synthesis Report

한-미 협력 국내 대기질 공동조사 KORUS-AQ 최종 종합보고서



KORUS-AQ Final Science Synthesis Report

한-미 협력 국내 대기질 공동조사 KORUS-AQ 최종 종합보고서

Co-authors: James Crawford¹, Yongpyo Kim², Alan Fried³, Barry Lefer⁴, Carolyn Jordan⁵, Gangwoong Lee⁶, Isobel Simpson⁷, Jay Al-Saadi¹, Jhoon Kim⁸, Junghun Woo⁹, Louisa Emmons¹⁰, Seongyeon Cho¹¹, Taehyoung Lee⁶, Rokjin Park¹², Daigon Kim¹³, jinsoo Park¹³, jinsoo Choi¹³

¹NASA Langley Research Center, Hampton, Virginia, US

²Ewha Womans University, Seoul, KR

³University of Colorado, Boulder, Colorado, US

⁴NASA Headquarters, Washington, DC, US

⁵National Institute of Aerospace, Hampton, Virginia, US

⁶Hankuk University of Foreign Studies, Seoul, KR

⁷University of California, Irvine, California, US

⁸Yonsei University, Seoul, KR

⁹Konkuk University, Seoul, KR

¹⁰National Center for Atmospheric Research, Boulder, CO, US

¹¹Inha University, Incheon, KR

¹²Seoul National University, Seoul, KR

¹³National Institute of Environmental Research, Air Quality Research Division, Incheon, KR

KORUS-AQ Final Science Synthesis Report

CONTENTS

Chapter 1: Introduction	9
Chapter 2: Fine Particle Pollution	21
Chapter 3: Ozone Pollution	40
Chapter 4: Emissions	51
Chapter 5: Air Quality Modeling	77
Chapter 6: Satellite Remote Sensing	85
Chapter 7: Policy Recommendations	105
References	113
Appendix	123

Figure 1-1. Schematic representation of the observing strategy used to address KORUS-AQ science goals and explore the synergy between multi-perspective observations from the ground, air, and space. Details for each listed asset are provided in the text. p.13

Figure 1-2. Ground based observations during KORUS-AQ included (a) monitors comprising the AirKorea monitoring network and (b) research sites incorporating combinations of in situ observations (red), Pandora spectrometers (green), and AERONET sunphotometers (blue). Panel (c) offers an expanded view of sites located in the Seoul Metropolitan Area. Details on ground observations at these sites are provided in Tables 1-4 of the Appendix. p.14

Figure 1-3. Google Earth images overlaid with flight tracks for each of the KORUS-AQ aircraft. Special Use Airspace affecting flight access is overlaid with circles representing airports and polygons representing Military Operations Areas (white), Restricted Areas (teal), and Prohibited Areas (magenta). Expanded views of flight patterns conducted over the Seoul Metropolitan Area by each aircraft are shown in the bottom images with Olympic Park (red) and Taehwa Forest (green) research sites marked. ... p.17

Figure 1-4. Daily statistics for $PM_{2.5}$ and ozone observed across the AirKorea network during KORUS-AQ. Box whisker plots indicate the median, interquartile range, and 5th and 95th percentiles. Flight days are shown in green. Red lines indicate the air quality standards in place at the time of the study. Periods of stagnation (yellow) and sustained low-level pollution transport (orange) are highlighted. The primary dynamic period and blocking pattern are denoted by black arrows. Cold front passages are numbered sequentially (F#) at the bottom of each panel. (Figure adapted from Peterson et al., 2019) p.18

Figure 2-1. *Left panel:* map of AirKorea sites divided into five sectors. The Seoul Metropolitan Area (SMA) encompasses Seoul City, Incheon, and Gyeonggi. Southeastern coastal sites include Busan and Ulsan. Southwestern sites include Gwangju and Jeju island. Sites across central Korea are referred to as “Rest of Korea”. The number of sites in each sector is provided in parentheses. *Right panel:* time series of hourly $PM_{2.5}$ concentrations averaged across each of the five sectors shown in left panel. The four major meteorological periods are annotated across the top of the figure. (Figure panels from Jordan et al., 2020) p.23

Figure 2-2. Mean PM_1 composition observed at the KIST ground site in Seoul for each of the 4 meteorological periods during KORUS-AQ. The size of the pie charts is scaled to the total mean aerosol concentration of the period. The outer black arc on each pie signifies primary aerosols, while the green

outline encompasses secondary aerosols. (Figure from Jordan et al., 2020) p.24

Figure 2-3. *Top panel:* campaign time series of KIST AMS data shown with meteorological periods annotated at the top of the panel. The sum of the individual constituents (black) is used as a proxy for PM₁ aerosol over the entire KORUS-AQ campaign. *Bottom panel:* hourly PM₁ and PM_{2.5} concentrations measured at Olympic Park. (Figure panels from Jordan et al., 2020 main text and supplemental information) p.25

Figure 2-4. Calculated SOA production for KORUS-AQ. The SOA precursor classes are defined in Table 2-3. Note, toluene is part of aromatics class 1 (light purple), but it is shown separately. The error bars represent the uncertainty in OA ($\pm 38\%$). (Figure from Nault et al., 2018) p.29

Figure 2-5. Time series of Olympic Park T and RH (top panel) and ALW with nitrate and sulfate (bottom panel) during the Stagnant and 1st half of Transport/Haze periods. ALW calculated from E-AIM thermodynamic model. Note the elevated RH throughout the day and night during Transport/Haze compared to Stagnant, along with the reduced daytime temperature for the Transport/Haze period. (Figure from Jordan et al., 2020) p.32

Figure 2-6. Time series of the hourly average PM_{2.5} during the KORUS-AQ period for AirKorea sites in Seoul (top panel). Time series of hourly average mixed layer height (MLH) measured at Olympic Park in Seoul by a CL51 ceilometer (bottom panel) along with a 24-hr running mean showing MLH over the previous 24 hrs. BL depth based on daily soundings in the afternoon (3 p.m. local time) at Osan Air Base are also shown in the bottom panel. (Figure from Jordan et al., 2020) p.33

Figure 2-7. Time series of the hourly average PM_{2.5} concentrations during the KORUS-AQ period for AirKorea sites in Seoul City. Median CO/CO₂ slopes are shown for DC-8 flight days and are taken from descent profiles over Seoul. Statistics for the CO/CO₂ slopes (median and interquartile range) are shown for 1-minute data periods with slopes having a significant correlation ($R^2 > 0.5$). Symbol size is proportional to the fraction of data having significant CO/CO₂ correlation. Statistics are shown for both the boundary layer (BL, orange circles) and lower free troposphere (LFT, green squares). (Figure from Jordan et al., 2020) p.34

Figure 2-8. a) Time series of hourly PM_{2.5} measurements for Jun 01 through June 30, 2016 with the Baengnyeong site (~210 km NW of central Seoul) compared to measurements in central Seoul and the Yellow Sea coast. b) Time series of the differences in hourly PM_{2.5} between the central Seoul average and

the coastal average. Note the much higher values in Seoul versus the coastal region for some of the days with highest PM_{2.5} levels, especially June 22–23 and June 28. (Figure from Eck et al., 2020)

..... p.36

Figure 2-9. Observations from the DC-8 show that the relationship between the calculated concentrations of H⁺_(aerosol) and sulfate depend on the form of sulfate in the aerosol (left panel). The nitrate/sulfate molar ratio increases as a function of “excess ammonium” (right panel). (Figure from T. Park et al., in preparation) p.39

Figure 3-1. Vertical distribution of ozone observed by the DC-8 during fifty-two profiles conducted in the vicinity of the Taehwa Research Forest southeast of Seoul. Boxes showing median and interquartile values for 1 km increments of altitude are plotted over the individual measurements. p.42

Figure 3-2. Modeled distributions of net ozone production, P(O₃), over Seoul from the “base case” calculations (black dashed line in each panel) including all VOC precursors compared with calculations removing different VOC types (orange line in each panel). Each panel indicates the VOCs removed from the calculations and the integrated reduction in P(O₃). (Figure from Schroeder et al., 2020) p.44

Figure 3-3. Spatial distributions of simulated OPE, O₃, and NO_x lifetime changes. Spatial distributions of changes (modified emissions run minus base run) in simulated surface a) OPE, b) O₃ levels, and c) NO_x lifetime as a response to emission changes. Major metropolitan and industrial areas are indicated with stars and circles, respectively. (Figure from Oak et al., 2019) p.46

Figure 3-4. Diurnal variations of O₃, PM_{2.5}, cloud coverage, and UV (upper panel), and aromatics, NO_x, HCHO, and H₂O₂ (lower panel) for four high O₃ episodes associated with diverse meteorological conditions, e.g., (a) Stagnant period (C1), (b) Blocking period (C2), and (c-d) Transport period (C3 and C4). Non-episode conditions (e) are offered for comparison. (Figure from H. Kim et al., 2020) p.48

Figure 3-5. Correlation between ozone and HONO. Hourly average data (open circles) show a negative relationship. Triangles representing daily maximum levels of HONO (occurring in the morning) and ozone (occurring in the afternoon) have a positive correlation (Figure from Gil et al., unpublished). p.49

Figure 4-1. KORUS v5 modeling NO_x emissions for Asia (left) and South Korea (right) domains p.53

Figure 4-2. Annual average emission changes for China (left) and Korea (right) based on subsequent

versions of the KORUS modeling emissions for (a) Inorganic precursors and (b) Organic precursors (Woo et al., 2020b, in-preparation). p.55

Figure 4-3. Comparison of DC-8 observations with model simulations for SO₂ (left), NO_x (center) and toluene (right) in the lower atmosphere over the Seoul metropolitan area during KORUS-AQ. Symbols indicate mean values. The full range of DC-8 observations at each altitude are also shown using a box-whisker format (center line = median, box = interquartile range, lines = 10th to 90th percentiles). The number of values contributing to the statistics for each altitude bin are shown on the right. Gray shading indicates the spread in model values. p.57

Figure 4-4. Top 15 most abundant VOCs measured during the MAPS-Seoul and KORUS-AQ campaigns, plotted in descending order based on average mixing ratio. (a) Ground-based data at KIST in May 2015 during MAPS-Seoul ($n = 23$). Low-altitude airborne samples (< 0.5 km) during KORUS-AQ over (b) Seoul ($n = 177$), (c) Daesan, ($n = 63$), and air sampled over the Yellow Sea downwind of (d) China ($n = 68$). A maximum Daesan propane value of 62.5 ppbv is not shown. (Figure from Simpson et al., 2020) p.59

Figure 4-5. Spatial distributions of (a) toluene and (b) carbonyl sulfide (COS) during KORUS-AQ. Toluene was most elevated over the Seoul Metropolitan Area (red points), while carbonyl sulfide was most enriched in air arriving from China. Each graph is color-coded by VOC mixing ratio. We note that the KORUS-AQ campaign targeted Seoul, and we recognize that other major urban centers in Korea are also impacted by VOC emissions and ozone pollution. (Figure from Simpson et al., 2020) p.60

Figure 4-6. (a) Top 20 most abundant VOCs measured at low altitude (< 0.5 km) over Seoul during KORUS-AQ, (b) their OH reaction rate constants, and (c) their OH reactivity. Selected aromatics are colored in green and selected alkenes in orange. The top 4 OH reactivity rankings are labeled in panel (c). (Figure from Simpson et al., 2020) p.61

Figure 4-7. Relative potential of different VOC groups to form O₃ in Seoul during KORUS-AQ based on (a) OH reactivity calculations (Simpson et al., 2020) and (b) photochemical box modeling calculations (Schroeder et al., 2020). Light alkanes are C₂–C₃ and heavy alkanes are C₄ and higher. (Figure from Simpson et al., 2020) p.62

Figure 4-8. Source apportionment results for selected VOCs measured over Seoul during KORUS-AQ. Colored bars show major sources of reactive alkenes (orange) and aromatics (green). (Figure from Simpson et al., 2020) p.64



Figure 4-9. Flight tracks at altitudes around 300-m in the morning around 10:50 (local) on June 5, 2016. The Daesan complex is shown as the gray shaded region along with the largest individual VOC emission sources sized by their yearly emissions in MT/year. The flight legs are colored and sized by the HCHO concentrations measured on the DC-8. The large black arrow shows the average wind direction ($70.7^\circ \pm 13.5^\circ$) and wind speed (4.5 ± 0.7 m/s) from analysis of DC-8 wind measurements. The plume outflow boundaries are indicated here by the  symbols, and the upwind inflow period by the  symbols. (Figure adapted from Fried et al., 2020) p.67

Figure 4-10. (a) Top-down total Daesan VOC yearly emission estimate with error bars reflecting the measurement imprecision (1σ level) and comparison with the bottom-up inventory estimate. (b) Similar analysis for HCHO and its four major precursors (Figure adapted from Fried et al., 2020). p.69

Figure 4-11. Summary of Daesan VOC emission inventory determinations in MT/year during the 2016 KORUS-AQ study. The inventory value is from Woo et al. (2020b, in-preparation), and the 3 measurements are: 1) Fried et al. (2020) from DC-8 VOC measurements employing mass balance analysis for June 2, 3, 5, 2016 plumes; 2) Cho et al. (2020) from Hanseo King Air measurements of HCHO on May 22, 2016 coupled with a 0-D box model analysis of HCHO build-up and loss; and 3) Kwon et al. (2020) from HCHO vertical column density measurements from the GeoTASO instrument on the NASA B-200 coupled with GEOS-Chem simulations for HCHO net production assuming yields from various organic precursors. The error bars represent the estimated 1σ total uncertainties for each top-down determination..... p.70

Figure 4-12. Top-down SO_2 yearly emission estimate based on the Daesan plumes sampled by the DC-8 on the 3 sampling days. The grand average of six measurements is $13,000 \pm 3,800$ MT/Yr (1σ standard deviation). The 2016 CAPSS SO_2 emission inventory for the Seosan Province (the province where Daesan is located) includes 3 different categories, which comprise 97% of the SO_2 emissions in this province (Figure adapted from Fried et al., 2020). p.72

Figure 4-13. (a) Point sources sampled by the DC-8 along the west coast of Korea (A: Hyundai Steel, B: Dangjin PP, C: Boryeong PP, D: Seocheon PP, E: Gunsan IC); (b) DC-8 flight track around Dangjin PP colored by SO_2 concentration (red dots: over 70ppb); (c) Close-up of the Dangjin PP stacks. 1-4 (blue) indicate original stacks and 5-6 (red) indicate newly added capacity..... p.73

Figure 4-14. Inter-comparison between model and Δ measurement for (a) NO_x and (b) SO_2 concentration at Dangjin PP. 'Model 1' shows model calculations that include only stacks 1-4, and 'Model 2' show

calculations for all six stacks. ‘ΔMeasurement’ means difference between upwind and downwind locations of DC-8 measurements. The x-axis indicates sequential DC-8 measurement points across the plume. The blue shaded part of the graphs indicates the amount of additional emissions from stacks 5-6 (i.e. Model 2 – Model 1) (M. Park et al., 2020, submitted).………… p.74

Figure 5-1. Measurements from the DC-8 aircraft binned by altitude in black for the Seoul plume (SW corner: 37.1 °N, 127.05°E; NE corner: 37.75°N, 127.85°E). Co-located WRF-Chem within the same altitude bin as the aircraft observations are plotted (vertically offset from the observations) in red for the original and in orange for the $2.13 \times \text{NO}_x$ emissions simulation. Square dots represent the median values. Boxes represent the 25th and 75th percentiles, while whiskers represent the 5th and 95th percentiles. Comparisons are for (a) NO_2 , (b) NO_y , and (c) the NO_2 – NO_y ratio when coincident NO_2 and NO_y measurements are available. (Figure from Goldberg et al., 2019)………… p.79

Figure 5-2. Simulated and observed daytime (8-hour average) O_3 (top) and daily $\text{PM}_{2.5}$ (bottom) concentrations averaged at AirKorea surface sites located in Seoul, Busan, Incheon, Gwangju, Yeosu, and Gangwon. Observations are in black solid lines and individual models are in different colors with the ensemble model mean in red solid lines. Model ranges are shown in gray shades. The Pearson correlation coefficient (R), normalized mean bias (NMB), and root mean square error (RMSE) of each model and the ensemble model are denoted in the upper-left corners. (Figure from R. Park et al., 2020).………… p.82

Figure 5-3. Comparison of simulated and observed mean PM_1 chemical compositions in surface air for different synoptic regimes during the campaign. Each chemical component is indicated in different colors and the observations are from AMS at the KIST ground site (127.045°E, 37.601°N). Model results from the lowest model layer were sampled coherently with the observations. (Figure from R. Park et al., 2020)………… p.80

Figure 6-1. GeoTASO observations of tropospheric vertical column NO_2 (left) and HCHO (right) on June 9, 2016, acquired at 4 times of day progressing from early morning (top) through late afternoon (bottom). (Figure adapted from Judd et al., 2018).………… p.88

Figure 6-2. GeoTASO observations of tropospheric vertical column NO_2 (left) and HCHO (right) on May 17, 2016, acquired over a large SMA domain in the morning (top) and afternoon (bottom). (Figure adapted from Judd et al., 2018).………… p.89

Figure 6-3. Comparison of DC-8 observations, ground and GeoTASO and satellite remote sensing, and

model simulations for column NO_2 , HCHO , and HCHO/NO_2 over Taehwa Research Forest according to the measurement time. Upper three rows show NO_2 , HCHO and HCHO/NO_2 ratio from DC-8, Pandora, GeoTASO and GOME-2B measurements, and lower three rows show the same from OMI measurements and model results from GEOS-Chem, WRF-Chem and CAM-Chem. (Figure taken from Koo et al., in preparation) p.92

Figure 6-4. Enlarged views of GeoTASO SO_2 observations over the northern Chungnam area. The seven flights shown covered this region on (a) 11 May 08:58-11:23 LT; (b) 17 May 08:39-11:05 LT; (c) 17 May 14:10-16:31 LT; (d) 22 May 09:52-11:52 LT; (e) 2 June 10:19-11:47 LT; (f) 5 June 13:26-16:55 LT; and (g) 9 June 07:48-11:51 LT. Mean wind speed and direction obtained from the ERA5 data during each GeoTASO flight over this area is indicated in yellow. Nine SO_2 emission sources listed in the Stack Tele-Monitoring (TMS) reports for this region are numbered and marked with circles and triangles. The circles indicate SO_2 sources with SO_x emission rates of >1 kt yr $^{-1}$ on average during 2015-2017, while the triangles represent the sources with mean SO_x emission rates lower than 1 kt yr $^{-1}$ for the same period. A radius of each circle is proportional to the logarithm of a mean SO_x emission rate measured by Stack TMS devices at each facility in 2015-2017. The emission type of each numbered source and the corresponding 3-year mean SO_x emission rate from the Stack TMS reports are indicated. (Maps were created using Google Earth Imagery.) (Figure taken from Chong et al., 2020). p.96

Figure 6-5. Average of AHI fusion AOD during the KORUS AQ campaign (left top: Dynamic period, right top: Stagnant period, left bottom: Transport period, right bottom: Blocking period). (Figure taken from Kim, Al-Saadi et al., in preparation) p.97

Figure 6-6. Airborne LIDAR measurements of vertical extinction profile through the N-S cross section over the Yellow Sea with GOCI observations of daily average AODs on May 25th, 2016. (Figure taken from Kim, Al-Saadi et al., in preparation) p.98

Figure 6-7. GOCI AOD composites and wind vectors at 850-hPa pressure level for the 5 highest AOD days (upper) and 5 lowest AOD days (bottom) at Baengnyeong, Olympic Park and Anmyon during KORUS-AQ (Figure taken from Lee et al., 2019) p.99

Figure 6-8. Meridional mean GOCI AOD over the Yellow Sea and the Korean Peninsula (35–38 °N, 123–128 °E) at 0.2 longitude intervals on (a) 25 May and (b) 5 June 2016. Overlaid arrows represent meridionally averaged zonal wind at 850 hPa. (Figure taken from M. Choi et al., 2019) p.101

Figure 6-9. (a) Time series of the AERONET almucantar retrievals of volume median radius and measured AOD at 675 nm for the Yonsei University site in central Seoul from May 01 through June 10, 2016. (b) AERONET size distribution retrievals show an order of magnitude greater fine mode aerosol volume on the days of pollution transport (May 25, 26, & 31) as compared to the stagnant days (May 17 & 18) with primarily local sources, low RH and no clouds. This is partly due to enhanced aerosol water on the high RH pollution transport days. (Figure taken from Eck et al., 2020). p.102

Figure 6-10. Framework for air quality application of satellite observations. p.104

Table 2-1. PM₁ aerosol composition measured at KIST, along with meteorological parameters and calculated ALW. Means \pm standard deviations with the number of values in the mean in parentheses. (Table from Jordan et al., 2020) p.27

Table 2-2. Differences in the means from Table 2-1, between those observed during each meteorological period from the campaign as a whole. Bold values highlight the largest differences from the campaign mean that occurred during the Stagnant and Transport/Haze periods. (Table from Jordan et al., 2020) p.28

Table 2-3. Definition of classes used in Fig. 2-4. The VOCs listed were all measured aboard the DC-8. (Table from Nault et al., 2018) p.30

Table 3-1. Ozone chemistry sensitivity to emission reduction scenarios in GEOS-Chem (Table from Oak et al., 2020) p.46

Table 5-1. Source contributions [%] to South Korea pollution for a variety of pollutants and metrics during KORUS-AQ. p.84

Executive Summary

Despite various efforts to reduce air pollution levels, air quality in Korea remains in a very unhealthy condition, particularly with regard to fine particulate matter ($PM_{2.5}$) and O_3 . The effectiveness of current air quality policy and successful provision of future strategies require thorough scientific and technological assessments of their present status. Integrated research with intensive field studies, including ground, airborne, research vessel, satellite measurements, and 3-D chemical transport models is the primary scientific tool for understanding chemical, physical, and meteorological aspects of air pollution linked to precursor emissions, chemical production, transport, and deposition processes. KORUS-AQ is the first collaborative and fully integrated program for air quality study in Korea, utilizing the latest research tools and assembling Korean and US researchers to form a strong partnership between NIER and NASA.

The object of this report is to outline the scientific findings and advances in understanding air quality in Korea during the KORUS-AQ campaign period mostly reflecting the analysis of many participating experts and based on published manuscripts in peer-reviewed scientific journals. This report supersedes the KORUS-AQ preliminary report (RSSR) published in 2017 and offers both new and revised information resulting from a deeper and more complete analysis of the data collected during the study. This update is intended to provide the public and policy makers with in-depth explanations and scientific information useful to assessing the comprehensive air quality issues currently facing Korea. Topical highlights from each chapter of the report are provided below.

1) Fine particle ($PM_{2.5}$) pollution

- **$PM_{2.5}$ pollution is mainly due to secondary production and closely affected by weather patterns.** $PM_{2.5}$ mass across the Korean peninsula was dominated by material formed in the atmosphere (secondary production) from precursor gases rather than directly emitted (primary emissions) and changes in the abundance and chemical composition of $PM_{2.5}$ were mainly driven by synoptic meteorology.
- **Organic and inorganic composition of $PM_{2.5}$ varied with synoptic conditions.** During stagnant conditions photochemical (light driven) processes led to aerosols that were predominantly organic (secondary organic aerosol, SOA) from locally emitted VOCs. By contrast, during conditions driven by

frontal passages associated with transboundary transport, heterogeneous (gas-to-particle conversion) processes led to aerosols that were predominantly inorganic (secondary inorganic aerosol, SIA) produced under humid conditions with enhanced air mass transport from China such that the local production of aerosol in turn promoted the development and persistence of haze.

- **Controlling both local NO_x and VOCs emissions are necessary to help reduce $\text{PM}_{2.5}$ pollution.** Reductions in local NO_x and VOC emissions (particularly, highly reactive C_7+ aromatics) will help alleviate secondary production of aerosols with VOCs having a greater impact under dry stagnant conditions when SOA dominates and NO_x having a greater impact when SIA dominates under humid cloudy/foggy/hazy conditions. Additional steps to limit heterogeneous nitrate production may have the added benefit of limiting the extent and persistence of severe haze events.
- **A simple measure of combustion efficiency can provide a useful indicator of Chinese influence on air quality in Korea.** At the current time, overall combustion efficiency in China is much lower than in Korea. This results in a higher ratio of CO/CO_2 in Chinese air. While care must be taken into the future as emissions change, CO/CO_2 is a useful indicator to determine periods of strong transboundary versus local influence.

2) Ozone pollution

- **Ozone pollution is mainly driven by local emissions but there is also a highly elevated regional background ozone.** While local emissions significantly contribute to ozone production in the Seoul Metropolitan Area, alarmingly consistent background levels with a median of ~ 80 ppbv in the lower free troposphere also point to a much broader regional problem across East Asia. This calls for immediate and coordinated attention from both Korea and its neighbors to address ozone precursor emissions.
- **Aromatic hydrocarbons are the most important VOC species to ozone production in Seoul.** Observation-constrained sensitivity calculations show that C_7+ aromatics play a dominant role in ozone production with other important contributions from alkenes, including isoprene that results from natural emissions from vegetation.
- **NO_x reductions are key to limiting the regional extent of ozone production, but initial reductions will likely lead to increased ozone in urban areas in the short-term.** While NO_x reductions will

decrease overall ozone production, it will lead to greater ozone production efficiency in urban areas that are currently in a NO_x-saturated (VOC-limited) condition. Thus, VOC reductions play an important role in mitigating short-term ozone increases until NO_x reductions are large enough to provide benefit across both urban and rural areas.

3) Emission sources

- **Emissions in Korea were updated with much improved accuracy.** During the KORUS-AQ research period, KORUS emissions were developed based on feedbacks from the observation and modeling communities guided by scientific findings from the KORUS-AQ. Top-down emissions estimates were particularly valuable in identifying discrepancies, but emission inventory updates were strictly based on bottom-up information, such as new energy information, temporal allocation surrogates, or chemical speciation profiles, to maintain connectivity to the policy.
- **Solvents and traffic were identified as the main sources of aromatics and alkenes, respectively.** Aromatic and alkenes were identified as the VOCs most important to local ozone chemistry in Seoul. Observation-based analysis indicated solvents to be the main source of aromatics in Seoul, with both paint and non-paint sources of aromatics being particularly important targets for VOC reductions. Traffic was identified as the main source of alkenes such as ethene.
- **Petrochemical emission sources have distinct chemical composition.** The VOC mixture at the Daesan petrochemical facility is different from Seoul. For example, Seoul is toluene-rich whereas Daesan is benzene-rich. Ethene, *n*-hexane, propane and benzene were major VOC species emitted from the Daesan facility.
- **VOC emissions from Daesan are significantly underestimated.** Top-down estimates of the VOC emissions from the Daesan petrochemical complex by 3 independent approaches (i.e. mass balance, GeoTASO, and measurement-driven 0-D box model) indicate that present bottom-up inventories for Daesan VOCs are underestimated by a factor of 2.5 to 4.0. Additionally, top-down Daesan estimates of formaldehyde and its 4 major precursors (ethene, propene, 1,3-butadiene, and 1-butene) are underestimated by a factor of 4.3 ± 1.5 relative to bottom-up inventories. This result is specific to Daesan, but it raises questions of whether petrochemical facility emissions in Korea are underestimated

in general.

- **NO_x and SO₂ emissions inventories including points sources are well established with relatively small uncertainty.** Top-down estimates of sulfur dioxide and nitrogen oxides emissions are in agreement with the improved bottom-up inventory. The agreement ratio (top-down/bottom-up) for point sources is particularly good, ranging between 0.8-1.3 and 0.7-1.0 for NO_x and SO₂ respectively, based on NASA DC-8 measurements.
- **The risk associated with Hazardous Air Pollutants (HAPs) from Daesan warrants more attention.** The large underestimate in VOC emissions from Daesan carries additional concern due to the presence of HAPs (e.g., 1,3-butadiene, benzene, formaldehyde, etc.). Large abundances of toxic compounds were observed by the DC-8 in the Daesan plume at distances of many 10's of kilometers downwind over the Yellow Sea. These pollutants pose health risks to facility workers and pose additional risk to local populations under onshore wind conditions.

4) Air quality modeling

- **Air quality modeling is a key instrument in improving emission inventories.** Modeling analyses, combined with remote sensing and in-situ measurements, were applied to evaluate the anthropogenic emissions in South Korea. Simulations with initial emission inventories suggested 40-50% increases in NO_x emissions and also showed disagreement for aromatic VOCs when compared to observations. These model-observation discrepancies were investigated and resolved with bottom-up data for the updated inventory.
- **The strategies to reduce ozone and PM levels have been thoroughly tested in various conditions.** The chemical characteristics of PM and ozone for different synoptic patterns were analyzed to identify the NO_x and/or VOC dependencies of PM and ozone production throughout the country. Models allowed the sensitivity of air quality chemistry to be explored and led to an emphasis on concurrent reduction of both local NO_x and VOC emissions to alleviate PM_{2.5} and O₃ pollution especially in the major metropolitan areas.
- **A hierarchy models is needed to place bounds on quantitative assessments of how closely local air quality is affected by regional transport.** Individual models have strengths and weaknesses

related to their varying scales (regional-to-global), resolution, and complexity in representing physical and chemical processes. Thus, models can provide better answers when used as an ensemble, which outperforms individual models in reproducing observations. Models also provide a range of estimates for local versus regional influence.

5) Remote sensing

- **KORUS-AQ provided unique opportunity to test prototype GEMS observations.** The NASA King Air carrying the GeoTASO instrument was flown in a regular grid pattern to provide first-ever continuous high-spatial-resolution maps up to 4 times per day of NO_2 and HCHO , two key species that will be measured by GEMS. These data illustrate for the first time the tremendous spatial and temporal variability of the distributions of important precursors to ozone and aerosol formation across the SMA.
- **Airborne and satellite remote sensing are particularly useful to track large point source emissions.** SO_2 column retrievals from the GeoTASO sensor provided 2-dimensional snapshots of SO_2 emissions from point sources along the west coast, particularly in the northern west coast area of Chungnam Province. On one occasion, the SO_2 plume from the Daesan complex reached close to southern Gyeonggi Province decaying by a factor of $1/e$ at ~ 1 km away from source.
- **GEO satellites have the advantage of monitoring regional long-range transport of PM.** During KORUS-AQ, multiple satellite sensors provided AOD products with high accuracy, which enabled the monitoring of the spatio-temporal aerosol distribution in East Asia. The composite image of GOCI AOD with the wind field clearly showed significant enhancement of aerosol loading throughout the vertical column with heavy aerosol plumes over the Yellow Sea advected from east-central China.
- **GEMS will provide a new era of air quality monitoring in Asia.** Korea's own GEMS (launched on February 19, 2020) retrieves the detailed map of column amounts of aerosol, ozone, and their precursors (NO_2 , SO_2 , CH_2O , CHOCHO) across east Asia. It is expected to advance many scientific aspects of air quality forecasting, top-down emission rate estimates, data assimilation, public service, and so on.

6) Policy Recommendations

- **Improving both $PM_{2.5}$ and ozone pollution relies on coordinated reductions in both NO_x and VOCs, specifically higher (C_7+) aromatic compounds.** While reductions in NO_x and VOCs will yield immediate benefits for $PM_{2.5}$, the rate of reduction between NO_x and VOCs is important for ozone. The more rapidly NO_x is reduced relative to VOCs raises the expectation of increases in ozone, especially in urban areas. In the face of such setbacks, it will be important to be patient and confident that continued reductions will lead to success in the long term.
- **Specific sources for higher (C_7+) aromatic compounds need to be determined to enable effective control strategies to be developed.** Source sampling in Seoul and other urban centers of Korea may help to identify the specific VOC products that are top priorities to target. Without this information, meaningful VOC reductions will be more difficult to achieve.
- **Large underestimates of VOC emissions from industrial point sources warrant continued scrutiny and verification.** The discrepancies at Daesan raise questions about whether similar underestimates exist at other facilities, both large and small, across Korea. A top-down airborne survey of point sources may be the most efficient way to determine the extent of this underestimate.
- **Model simulations of air quality require a hierarchy of models to obtain the best representation and understanding of uncertainties to support decision making.** Ongoing model development, leading to more accurate simulations of ozone and secondary aerosol formation in individual models, is needed to guide policies on emissions controls and improve air quality forecasting.

7) Future Directions

- **Monitoring Investments:** With the combination of the extensive AirKorea monitoring network and hourly monitoring from GEMS as well as GOCI-II, Korea will have unprecedented information to support continuous air quality monitoring of Korea and the larger regional impacts across Asia. Minimal investment in a few other measurements at a research site in Seoul could add valuable information for interpreting changes in air quality throughout the year. These include:
 - High-quality measurements of CO and CO_2 to assess the strength of transboundary influence based on the

large difference in combustion efficiency in Korea as compared to China.

- Continuous research-grade observations of aerosol composition to better understand changes in the local rate of secondary aerosol production.
- Observations of humidified and dry aerosol scattering for calculation of aerosol liquid water to better understand the coupled chemical and meteorological processes driving haze events.
- High-quality ammonia measurements to fully constrain the evaluation of inorganic aerosol formation, aerosol acidity, and related aerosol reaction pathways.

Finally, to provide increased attention on the role of mixed layer dynamics on $PM_{2.5}$ abundance, a real-time mixing height data product from the currently operating ceilometer network should be developed to provide continuous information on the diurnal cycle of mixing and ventilation of near-surface pollution.

- **NIER-NASA MOU:** In December 2018, NIER and NASA signed a Memorandum of Understanding concerning “Cooperation in Pollution Studies, Calibration, and Validation”. This agreement demonstrates the commitment to continued cooperation between the United States and Korea to the calibration and validation of GEMS and TEMPO observations and more importantly to the interpretation of the information from these satellites to inform air quality forecasts, improve understanding, and provide value to decision making.
- **Pandora Asia Network (PAN):** The recent development of PAN allows for Pandora spectrometers to be placed in all of the countries in the GEMS field of view. This has been critical to expanding collaboration across Asia and globally through membership in the Pandora Global Network (PGN). This effort not only brings scientists together, but under the sponsorship of KOICA and the United Nations Economic and Social Commission for Asia and the Pacific (UNESCAP), PAN brings decision makers into the discussion of local and shared impacts to air quality across Asia.
- **Continued Need for Field Studies:** Current plans are already underway for flights of the GCAS instrument for GEMS validation. Other intensive measurement periods including in situ sampling from ground sites and aircraft will be valuable to the interpretation of GEMS observations, testing of models, and verification of emissions. Over the longer term, Korean and US scientists will continue to explore and discuss ideas for field study collaborations to evaluate the changing landscape of emissions and the resulting changes in air quality as we work to achieve our respective national goals.

8) Acknowledgement

We would like to acknowledge all of the contributions and support that made it possible for us to ensure this report's credibility in presenting the research findings of KORUS-AQ clearly and concisely. First, members of the KORUS-AQ science team are recognized for their tremendous efforts and hard work in collecting the KORUS-AQ observations and providing insightful analysis and interpretation. We also recognize the critical commitments and program support from NIER in Korea and NASA in the United States which made the KORUS-AQ study possible. Additional support and cooperation from civilian and military air traffic controllers was essential to the execution of research flights in busy airspace over Korea. Special thanks goes to Osan Air Base for hosting the aircraft and study team. Finally, thanks to the US Embassy and relevant Korean agencies who worked hard to evaluate our research plans and negotiate the access and permissions needed for this international collaboration to succeed.

Chapter 1: Introduction

1.1. Background

Air quality is an environmental concern of fundamental importance across the globe. In the Republic of Korea (Korea), air quality has been improved during the last four decades, but it is still worse than most developed countries. Among the criteria air pollutants, fine particles, in particular, pose a serious concern not only in Korea but across Northeast Asia including China. Also, ozone levels have increased during the last two decades in Korea. Rising public interest and concern about fine particle pollution affects almost every aspect of society and daily life in Korea. Scientific understanding of the sources and fate of fine particles is essential to support the process of policy making and identifying the most effective solution against fine particles in the context of the socio-economic framework of Korea.

The need to monitor and understand air quality requires continual effort as the landscape of emissions evolves in response to changes in population, energy use, and industrial activity. Air quality goals have also evolved with improved understanding of health effects, demonstrating the added benefit of setting lower targets for exposure of humans and ecosystems to ozone, fine particles, and other toxic pollutants in the air (e.g., WHO 1987, 1995, 2000, 2006; Bachmann 2007). Historically, efforts to diagnose regions of poor air quality have relied primarily on ground-based observations along with modeling to develop mitigation strategies. However, in recent years in Korea, higher quality data for the observations and emission inventory of air pollutants have been demanded by the public. In addition, in Korea there has been lively discussion on the degree of external contribution to the abundance of air pollutants observed in Korea. To obtain reliable estimation of the external contribution, it is essential to have multi-dimensional observations including airborne measurements and remote sensing observations.

In recent years, satellites in low Earth orbit (LEO) have demonstrated the ability to observe the critical constituents affecting air quality. However, the impact of LEO satellites has been limited due to their frequency of observation (approximately once per day) and coarse resolution (horizontal scales of tens of km) that fail to resolve the source distributions and chemical evolution controlling air quality conditions that develop over timescales of a single day. This has recently improved with the launch of

TROPOMI, providing unprecedented resolution ($3.5 \times 5.5 \text{ km}^2$) with daily global coverage. This enables the identification of specific point sources and fine-scale urban source distributions (Beirle et al., 2019; Goldberg et al., 2019). Geostationary (GEO) observations are needed to provide the additional requirement for more continuous observations over the course of the day as emissions, transport, and chemistry evolve. The drawback of GEO is the limited viewing domain, preventing global observations with a single satellite. This has led to an international effort to launch a constellation of satellite instruments focused on air quality over the major population centers of the northern hemisphere: Asia, North America, and Europe. These GEO instruments will provide hourly observations of those regions throughout the day at horizontal resolutions of better than 10 km.

The constellation approach requires a commitment to strong collaboration, especially regarding common strategies for satellite calibration and validation. Joint work on the interpretation of satellite observations and best practices for integrating information from satellites with more traditional ground monitoring is also needed. This need for collaboration played a key role in the genesis of the Korea-United States Air Quality (KORUS-AQ) Field Study. The study was jointly sponsored by the two organizations responsible for geostationary satellite observations of air quality over Asia and North America: the National Institute of Environmental Research (NIER) in Korea and the National Aeronautics and Space Administration (NASA) in the United States. The collaboration also involved the broader atmospheric chemistry community by organizing a team of scientists from dozens of institutions across governmental, academic, and private sectors.

There were other reasons that KORUS-AQ has been carried out around the Korean peninsula. Foremost was the recognition that Korea faces air quality conditions that warrant urgent attention. Its location on the Asian Pacific Rim places it in a unique location where large gradients exist in atmospheric composition. The Korean peninsula is distinct, isolated by surrounding waters that offer the ability to assess upwind influences and downwind outflows under the right meteorological conditions. Interesting gradients also exist within Korea. The city of Seoul and the surrounding metropolitan area (the Seoul Metropolitan Area (SMA)) occupies the northwest corner of the country. While only accounting for 12% of the land area, it is home to 25 million people or roughly half of the country's population. Combined with the industrial activities and power plants along the northwest coast of Korea, a dominant fraction of emissions is contained in a relatively small area. This provided an ideal setting to examine air quality across megacity,

country, and regional scales.

In Korea, a scientific research program integrating in-situ observations for a field study named the Megacity Air Pollution Studies – Seoul (MAPS-Seoul) was carried out in May-June 2015. Focused on the SMA, MAPS-Seoul also included the use of remote and satellite sensors and air quality modeling. The main goal of MAPS-Seoul was to study pollution in the SMA governed by secondary chemical processes and transport processes with a focus on ozone (O_3) and particulate matter with an aerodynamic diameter less than or equal to the nominal value of $2.5\ \mu\text{m}$ ($PM_{2.5}$). MAPS-Seoul also served as a preliminary test study preceding the KORUS-AQ Field Study.

The KORUS-AQ Field Study was conducted during May-June 2016. The timing of the KORUS-AQ study was focused on the pre-monsoon period from late spring into early summer. While pollution associated with fine particulate matter peaks earlier in the year during late winter and early spring, the pre-monsoon is associated with the most photochemically active period during which both ozone and fine particle pollution episodes can occur. The pre-monsoon also focuses more attention on the impact of local emissions since transboundary transport is maximized in the March-April timeframe.

After the study, the KORUS-AQ Rapid Science Synthesis Report (RSSR) was published in July 2017 to provide policy makers in Korea important preliminary scientific findings that would be later finalized through deeper analysis. In the KORUS-AQ RSSR, preliminary answers for the following five questions were given:

Question 1: Can we identify a) the portion of aerosol derived from secondary production in SMA and across Korea, and b) the major sources and factors controlling its variation?

Question 2: Is ozone formation in Seoul NO_x limited or VOC limited? Can we determine the biogenic or natural contributions to ozone production?

Question 3: How well do KORUS-AQ observations support current emissions estimates (e.g., NO_x , VOCs, SO_2 , NH_3) by magnitude and sector?

Question 4: How significant is the impact of the large point sources along the west coast to the air quality of SMA temporally and spatially?

Question 5: How is Seoul affected by transport of air pollution from sources from regional to continental to hemispheric scales?

In this KORUS-AQ Final Science Synthesis Report (FSSR), the findings and recommendations that are discussed and summarized have resulted from analyses that have been published or will soon appear in peer-reviewed journals. Thus, the KORUS-AQ FSSR provides an important update to early feedback previously provided in the KORUS-AQ RSSR in 2017.

The chapters of this report provide KORUS-AQ study results and scientific findings on fine particle pollution (Chapter 2), ozone pollution (Chapter 3), emissions (Chapter 4), air quality modeling (Chapter 5), satellite remote sensing (Chapter 6) and policy recommendations (Chapter 7). In the remainder of this chapter, an overview of the observations collected, execution of research flights, and air quality conditions and meteorology during the study are presented. These details provide important context for discussions in later chapters.

1.2. Observational Assets

The KORUS-AQ study was conducted from 2 May to 10 June 2016. The study implemented a multi-perspective observing strategy intended to explore the synergy between operational air quality networks, air quality models, and geostationary satellite observations that was realized with the launch of the Geostationary Environment Monitoring Spectrometer (GEMS) over Asia in early 2020. This observing strategy is represented schematically in Figure 1-1 to show how the KORUS-AQ observational assets were deployed and used to address the fundamental science of air quality in Korea, enable model evaluation and improvement, and contribute to the development of strategies for the validation and interpretation of GEMS observations. Intensive observations were collected from three aircraft, two supersites, additional ground site augmentations, and two ships. A suite of air quality models was also employed to guide the collection of observations, particularly for the aircraft flight planning. The assets listed in Figure 1-1 also include existing satellite instruments: Korea's Geostationary Ocean Color Imager (GOCI), Japan's Advanced Himawari Imager (AHI), and the Ozone Monitoring Instrument (OMI) jointly administered by the US, Netherlands, and Finland. Information from these existing space-borne assets supported both planning during the campaign and post-campaign analysis and interpretation of KORUS-AQ observations.

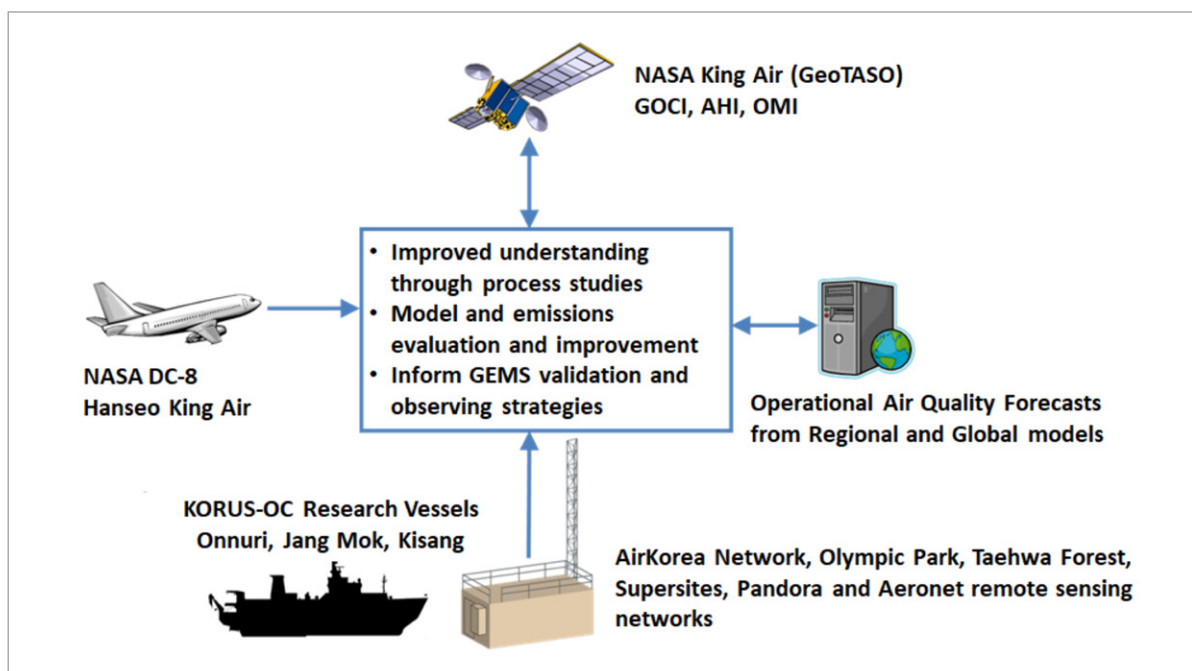


Figure 1-1. Schematic representation of the observing strategy used to address KORUS-AQ science goals and explore the synergy between multi-perspective observations from the ground, air, and space. Details for each listed asset are provided in the text.

1.2.1 Ground Observations

The ground observations in support of KORUS-AQ provided a critical continuous record and direct determination of surface air quality conditions. The AirKorea monitoring network (<https://www.airkorea.or.kr/eng>) provided the anchor for KORUS-AQ observations. Organized under Korea's Ministry of Environment and implemented by NIER, hourly observations of criteria pollutants including fine particulate matter and ozone are collected across the Korean peninsula from more than 300 instrumented sites (see Figure 1-2a). This operational monitoring system was supplemented by supersites at Olympic Park in Seoul and Taehwa Forest Research Station (see Figure 1-2c). Additional augmentation of ground measurements was implemented at numerous sites across the peninsula as well as Baengnyeong and Jeju islands. Networks of Pandora spectrometers and AERONET sunphotometers (see Figure 1-2b) provided an additional element of ground-based remote sensing useful in understanding how to bridge

the gap between surface in situ observations and remotely sensed quantities observed by satellites. Observations were also collected from three research vessels (see Figure 1-1) as part of an associated effort focused on Ocean Color called KORUS-OC. Details on measurements at each research site and on each ship can be found in Table 3 of the Appendix.

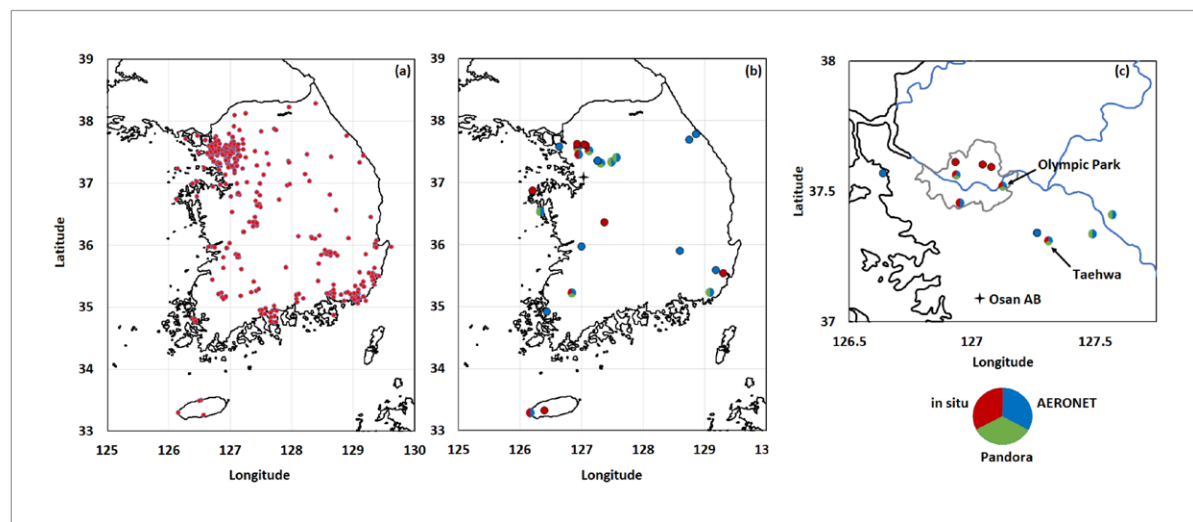


Figure 1-2. Ground based observations during KORUS-AQ included (a) monitors comprising the AirKorea monitoring network and (b) research sites incorporating combinations of in situ observations (red), Pandora spectrometers (green), and AERONET sunphotometers (blue). Panel (c) offers an expanded view of sites located in the Seoul Metropolitan Area. Details on ground observations at these sites are provided in Tables 1-4 of the Appendix.

1.2.2 Airborne Observations

KORUS-AQ included three research aircraft that conducted flights from Osan Air Base located ~50 km south of Olympic Park (see Figure 1-2c). The specific role of each platform is described below. Details on the investigators, instruments, and observed quantities for each aircraft are provided in Table 5 of the Appendix.

NASA DC-8: The largest of the three airborne platforms carried a comprehensive payload for in situ

sampling of trace gas and aerosol composition. Remote sensing capability included measurements of actinic flux to diagnose photochemical rates, active remote sensing of ozone and aerosols above and below the aircraft, and passive remote sensing above the aircraft for aerosol optical depth and trace gas abundances of water vapor, ozone and, NO_2 .

Hanseon King Air: This smaller in situ platform carried a payload to measure the key subset of trace gases that can be remotely sensed by satellites and ground-based remote sensors: ozone, NO_2 , SO_2 , CO, CH_2O , CH_4 , CO_2 , and water vapor.

NASA King Air: This aircraft was dedicated specifically to remote sensing of NO_2 , CH_2O , and ozone. Flying above the ground sites and in situ aircraft in the study region, it provided an analog for the satellite observations of air quality that can be anticipated from geostationary satellites.

In addition to these three aircraft, another aircraft flew over the North China Plain in the vicinity of Xingtai in Hebei province during the same period. The study, called Air Chemistry Research in Asia (ARIAs) collected valuable information from a turboprop Y-12 airplane for an important upwind source region (Wang et al., 2018). Observations included aerosol optical properties (scattering and absorption), black carbon, trace gases (ozone, SO_2 , NO, NO_2 , NO_y , CO, CH_4 , CO_2 , and H_2O), and VOC grab samples.

1.2.3 Satellite Observations

The KORUS-AQ team leveraged information from existing satellites that played a critical role in providing wide area observations to interpret surface and airborne observations in conjunction with synoptic weather patterns. The specific role of each satellite platform is described below.

GOCI: The Geostationary Ocean Color Imager provided information on aerosol optical properties including aerosol optical depth (AOD), fine mode fraction (FMF), single scattering albedo (SSA) and aerosol type.

AHI: The Advanced Himawari Imager is a geostationary meteorological satellite providing key context regarding the weather patterns affecting KORUS-AQ observations as well as aerosol optical properties similar to GOCI.

OMI: The Ozone Monitoring Instrument provided daily observations of atmospheric pollutants (O_3 , NO_2 , SO_2 , HCHO, and aerosol properties) in the early afternoon from Low Earth Orbit (LEO) using a UV-visible hyperspectral instrument. OMI data served as a proxy for the information that GEMS will provide with higher temporal and spatial resolution.

1.3. Execution of Research Flights

During KORUS-AQ, flights were conducted on 23 days during the 40-day period from 2 May to 10 June. With only a few exceptions, most flight days included all three aircraft. Flight tracks for each aircraft are shown in Figure 1-3. These flight patterns required detailed negotiation in advance and constant coordination during their execution. Daily flight planning was led by an array of teams producing air quality model forecasts and meteorological forecasters providing the necessary context to determine the best days and flight paths for sampling.

The need for careful planning and the location of flight lines was mainly due to the Special Use Airspace over Korea also shown in Figure 1-3. The polygons covering the majority of the peninsula and coastal waters are reserved for military training. Navigation of this complicated airspace was only possible by flying along the jetways connecting the airports (shown by circular airspace). Special consideration was needed for sampling over Seoul and the surrounding metropolitan area. Here, airspace was even more restrictive with a prohibited area extending along the border with North Korea and covering Seoul north of the Han river.

In total, the DC-8 flew 20 sorties, the NASA King Air flew 30 sorties, and the Hanseo King Air flew 33 sorties.

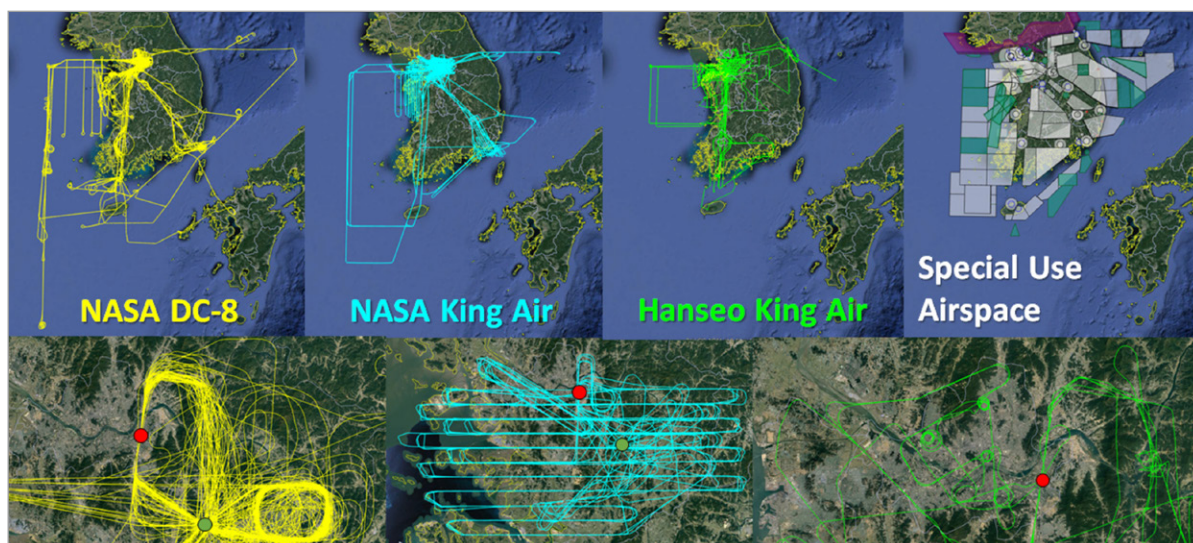


Figure 1-3. Google Earth images overlaid with flight tracks for each of the KORUS-AQ aircraft. Special Use Airspace affecting flight access is overlaid with circles representing airports and polygons representing Military Operations Areas (white), Restricted Areas (teal), and Prohibited Areas (magenta). Expanded views of flight patterns conducted over the Seoul Metropolitan Area by each aircraft are shown in the bottom images with Olympic Park (red) and Taehwa Forest (green) research sites marked.

1.4. Air Quality Conditions in Korea during the Study

The timeframe of the KORUS-AQ study was selected to occur during the pre-monsoon when there would be potential for both ozone and fine particulate pollution episodes. Based on climatology, this period was also expected to emphasize the role of local emission sources under the control of Korean policy makers. Figure 1-4 provides a statistical summary of air quality conditions during KORUS-AQ based on data collected from the AirKorea monitoring network for ozone and $PM_{2.5}$. While ozone exceeded the 60 ppbv daily 8-hour standard somewhere in the network on most days, the preponderance of high ozone values occurred during the latter half of May and into early June. Overall, 47% of the ozone data collected across the network during the study period exceeded the 8-hour standard. In addition, 15% of the data exceeded the 1-hour standard of 100 ppbv (not shown). Flight days, highlighted in green, show that the overall trend in ozone during the period is also well sampled for conditions aloft. The trend for $PM_{2.5}$ is also well captured but quite different, with a much narrower timeframe for peak values during the last

week of May. Values exceeding the 24-hour standard of $50 \mu\text{g}/\text{m}^3$ were recorded for only a few days. Overall, 8% of the $\text{PM}_{2.5}$ data collected across the network during the study period exceeded the 24-hour standard; however, under the recent reduction of the 24-hour standard to $35 \mu\text{g}/\text{m}^3$ (dotted line) in early 2018, exceedances increase to 26%.

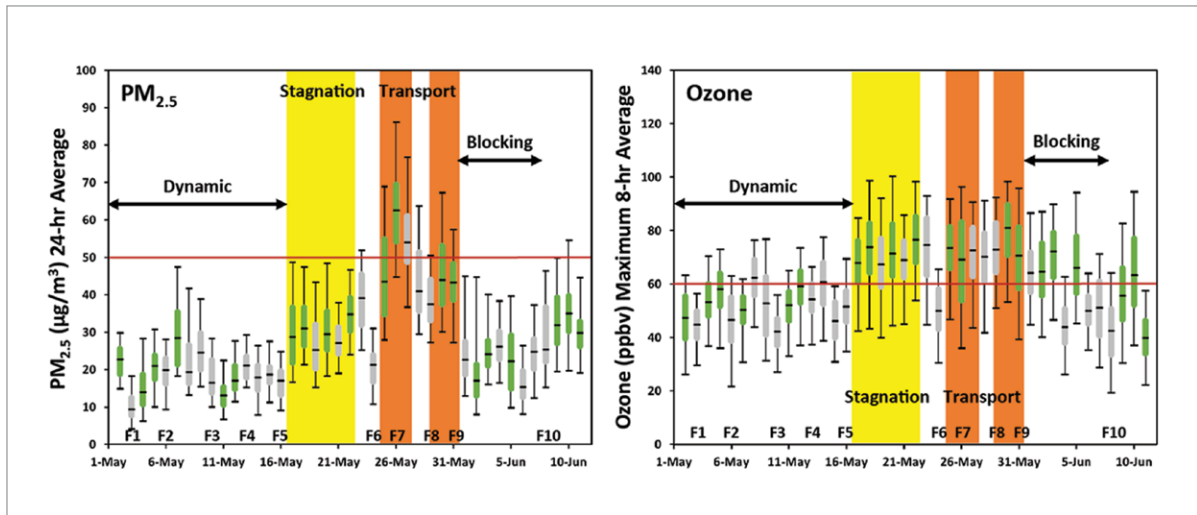


Figure 1-4. Daily statistics for $\text{PM}_{2.5}$ and ozone observed across the AirKorea network during KORUS-AQ. Box whisker plots indicate the median, interquartile range, and 5th and 95th percentiles. Flight days are shown in green. Red lines indicate the air quality standards in place at the time of the study. Periods of stagnation (yellow) and sustained low-level pollution transport (orange) are highlighted. The primary dynamic period and blocking pattern are denoted by black arrows. Cold front passages are numbered sequentially (F#) at the bottom of each panel. (Figure adapted from Peterson et al., 2019)

Figure 1-4 is annotated with the four distinct meteorological periods of the KORUS-AQ Field Study. The conditions associated with each period are described below and provide important context for the discussion of findings in subsequent chapters.

1-16 May: Dynamic meteorology and complex aerosol vertical profiles

Throughout this period, a series of strong frontal passages provided vertical lofting, along with horizontal

transport from sources upwind of Korea, that limited accumulation of aerosol at the surface and resulted in complex aerosol vertical profiles.

17-22 May: Stagnant conditions under a persistent anticyclone

Dry conditions under a persistent anticyclone resulted in clear skies and a wide diurnal temperature range. Transport of air from sources outside of Korea was limited such that local emissions and atmospheric processes dominated surface observations of atmospheric gases and aerosols.

25-31 May: Dynamic meteorology, low-level transport, and haze development

Four weak frontal passages transported polluted air from upwind sources in China, but with less vertical lofting than the Dynamic period leading to low-level surface transport. Each front was accompanied by extensive cloud cover and high humidity that led to haze and fog development within a stable shallow boundary layer.

1-7 June: Blocking pattern

A Rex Block (a high north of a low) limits horizontal transport leading to stagnant conditions. However, unlike the persistent anticyclone of the Stagnant period, the stagnant conditions arising from the Rex Block did not last long enough for surface pollutants to accumulate.

These periods played a particularly important role in the analysis and interpretation of the timeline for $PM_{2.5}$, especially given the role of local versus transboundary influences between the stagnant and low-level transport/haze periods in the latter part of May. By contrast, the stronger role of local emissions on the photochemical production of ozone resulted in less dramatic shifts in response to synoptic meteorology. Instead, strong ozone gradients were more common on the shorter timescales associated with sea breeze fronts.

1.5. Concluding Remarks

Analysis of observations from the KORUS-AQ Field Study has contributed to over sixty peer reviewed publications to date. These publications form the basis for findings highlighted in this report and the resulting recommendations. Going forward, the KORUS-AQ data will continue to enable valuable science and inform strategies for future field observations that will be needed to assess progress in meeting Korea's air quality goals.

Chapter 2: Fine Particle Pollution

Key Findings

- Synoptic meteorology was the primary driver of $PM_{2.5}$ concentrations across the Korean peninsula leading to surprisingly similar observations across the country.
- $PM_{2.5}$ mass was dominated by material formed in the atmosphere (secondary production) rather than directly emitted (primary emissions).
- There are different processes that drive secondary production and those processes depend on the synoptic meteorology. Here, we observed that during the Stagnant period photochemical (light driven) processes led to aerosols that were predominantly organic (secondary organic aerosol, SOA), while during the Transport/Haze period heterogeneous (gas and particle interactions) processes led to aerosols that were predominantly inorganic (secondary inorganic aerosol, SIA)
- Stagnant period SOA were produced from local emissions of volatile organic compounds (VOCs, see also Chapter 4).
- Transport period SIA were produced under humid conditions with enhanced air mass transport from China such that the local production of aerosol in turn promoted the development and persistence of haze.
- Models do not yet fully represent various contributing factors to aerosol production (see also Chapter 5). For example, more work is needed to identify the gas-phase VOCs and/or the reaction pathways that lead to SOA production under Stagnant conditions. Nor do models fully capture the diurnal cycle of the depth of the surface layer (boundary layer) of air that can trap emissions and confine aerosol production near the surface driving poor air quality. Finally, more work is needed to identify the heterogeneous reactions that produce SIA in haze events.

KORUS-AQ $PM_{2.5}$ study results show reductions in local NO_x and VOC emissions (particularly, highly reactive aromatics with at least 7 carbon atoms or more, C_{7+}) will help alleviate secondary production of aerosols both under dry stagnant conditions that promote photochemical production of SOA and under humid cloudy/foggy/hazy conditions that foster

heterogeneous production of SIA. Steps to limit heterogeneous nitrate production may have the added benefit of limiting the extent and persistence of haze events.

Recommendations for future studies to fill remaining knowledge gaps

- A few additional targeted measurements at a Seoul ground site would greatly benefit future studies to further probe remaining questions to inform future PM_{2.5} mitigation strategies:
 1. High quality measurements of CO and CO₂ to apportion PM_{2.5} and its precursors from transboundary versus local sources (their ratio differs substantially between emissions from China and Korea)
 2. High temporal-resolution aerosol composition to better examine the interplay between secondary aerosol production and meteorology,
 3. Humidified and dry aerosol scattering from which aerosol liquid water can be calculated and used to examine feedbacks driving haze events, and
 4. High quality measurements of NH₃ to better constrain models of inorganic aerosol formation and the role of acidity in aerosol production mechanisms.
- In addition, the development of a boundary layer height data product from the current network of ceilometers in Korea is needed to capture its diurnal variability to resolve the roles of mixing, dilution, and ventilation in aerosol production and accumulation at the surface during PM_{2.5} events.

2.1. Synoptic meteorology drives PM_{2.5} concentrations across the peninsula

Figure 2-1 shows the time series of PM_{2.5} across Korea using regional averages calculated from all of the stations in the AirKorea network. Large changes in PM_{2.5} are driven by synoptic meteorology which include phenomena such as temperature, relative humidity, precipitation, transboundary transport, land/sea breeze circulations, and boundary layer depth. However, regional variability is present and arises from the fact that not all phenomena may extend across the entire country, e.g., cloud cover, fog occurrence, or a particular transport pathway. No sector (including the city of Seoul) was found to have consistently higher PM_{2.5} concentrations than any other sector. Average sector values over the course of the campaign differed from each other by < 1 µg/m³ from the peninsula-wide average of 28.4 µg/m³. However, when PM_{2.5} concentrations were large (> 50 µg/m³), Seoul tended to have higher concentrations than the rest

of the peninsula. Such conditions occurred several times between May 20th and June 1st, spanning both the Stagnant and Transport/Haze meteorological regimes (Figure 2-1). Given the focus of KORUS-AQ on identifying the drivers of high PM_{2.5} concentrations that contribute to bad air quality days in Korea, we closely examined the factors that contributed to enhanced PM_{2.5} during the Stagnant and Transport/Haze periods.

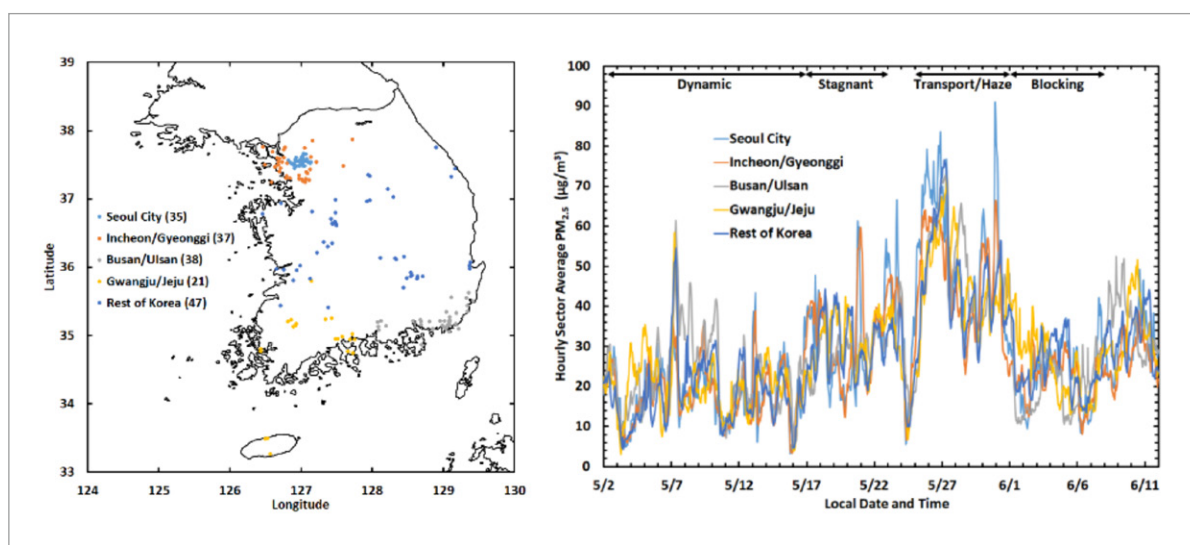


Figure 2-1. *Left panel:* map of AirKorea sites divided into five sectors. The Seoul Metropolitan Area (SMA) encompasses Seoul City, Incheon, and Gyeonggi. Southeastern coastal sites include Busan and Ulsan. Southwestern sites include Gwangju and Jeju island. Sites across central Korea are referred to as “Rest of Korea”. The number of sites in each sector is provided in parentheses. *Right panel:* time series of hourly PM_{2.5} concentrations averaged across each of the five sectors shown in left panel. The four major meteorological periods are annotated across the top of the figure. (Figure panels from Jordan et al., 2020)

2.2. PM_{2.5} mass is dominated by material formed by secondary production mechanisms

Early work at the Korea Institute of Science and Technology (KIST) (H. Kim et al., 2018) revealed that aerosol formed by secondary production mechanisms dominated the aerosol mass rather than particulates emitted directly into the atmosphere (primary emissions) as shown in Figure 2-2 by the pie

sections outlined in green. The fraction of secondary aerosol ranged from 71% to 83% across the 4 meteorological regimes of the campaign. The observations of aerosol composition and abundance at KIST are consistent with comparable observations at Olympic Park and the airborne measurements from the NASA DC-8. They are used here for their completeness of the time series at the surface in Seoul (Figure 2-3).

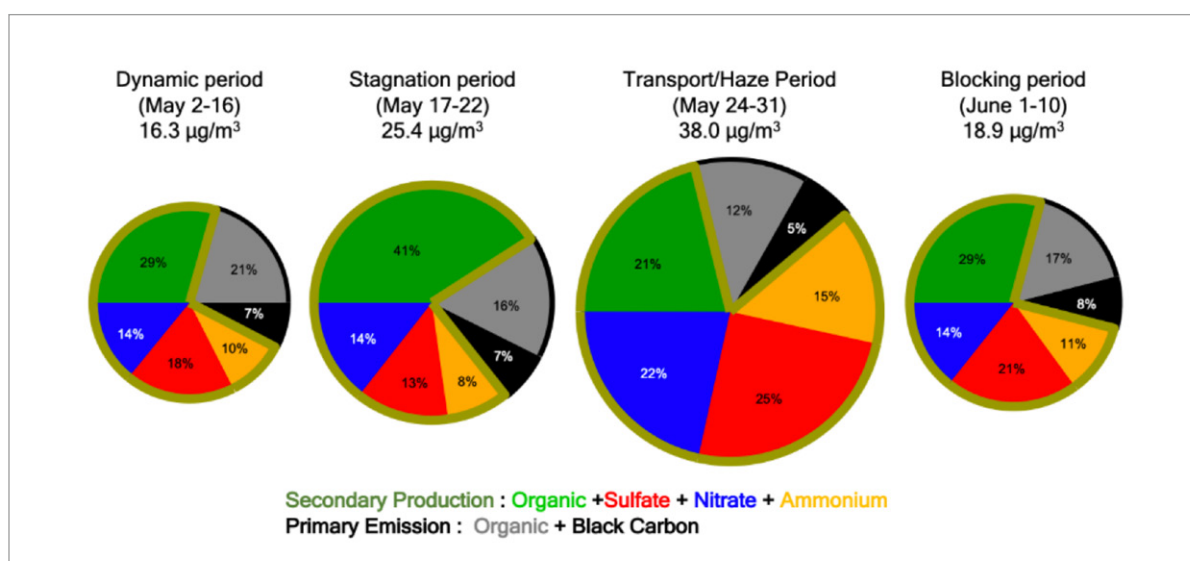


Figure 2-2. Mean PM_{10} composition observed at the KIST ground site in Seoul for each of the 4 meteorological periods during KORUS-AQ. The size of the pie charts is scaled to the total mean aerosol concentration of the period. The outer black arc on each pie signifies primary aerosols, while the green outline encompasses secondary aerosols. (Figure from Jordan et al., 2020)

These measurements relied on a technique (aerosol mass spectrometry) that is limited to particles with a diameter $< 1 \mu\text{m}$ (PM_{10} , as opposed to $\text{PM}_{2.5}$ that includes particle diameters up to $2.5 \mu\text{m}$). The top panel of Figure 3 shows the time series of the KIST data where the individual chemical compounds are summed as a proxy for PM_{10} . The bottom panel of Figure 3 shows the time series of hourly PM_{10} and $\text{PM}_{2.5}$ measurements from Olympic Park revealing that for much of the campaign there was little difference between the two. That is, most of the $\text{PM}_{2.5}$ mass was in the PM_{10} size fraction. However, during the Transport/Haze period the two sizes diverged indicating a shift to larger sizes. The most striking feature in

aerosol composition during the campaign was the shift from SOA dominant aerosol during the latter part of the Stagnant period to SIA dominant aerosol during the Transport/Haze period (Figures 2-2 and 2-3 upper panel). This indicated different atmospheric processes were responsible for enhanced secondary aerosol production between the two meteorological periods.

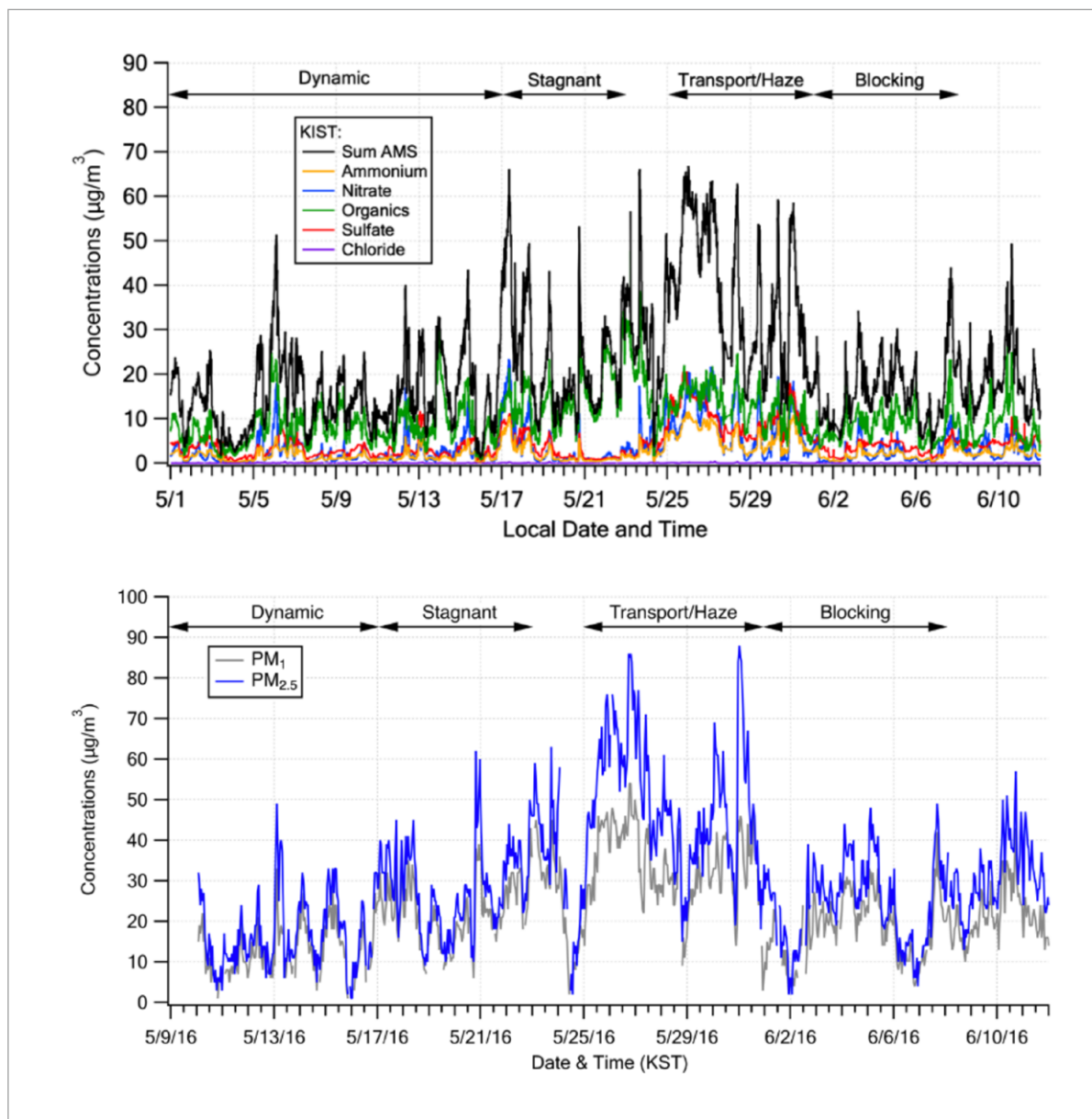


Figure 2-3. *Top panel:* campaign time series of KIST AMS data shown with meteorological periods

annotated at the top of the panel. The sum of the individual constituents (black) is used as a proxy for PM_{10} aerosol over the entire KORUS-AQ campaign. *Bottom panel:* hourly PM_{10} and $\text{PM}_{2.5}$ concentrations measured at Olympic Park. (Figure panels from Jordan et al., 2020 main text and supplemental information)

2.3. Different processes drive secondary production and those processes depend on the synoptic meteorology

Table 2-1 shows the mean for each chemical component of PM_{10} over the KORUS-AQ sampling period at KIST, along with mean values in temperature (T), relative humidity (RH), and aerosol liquid water (ALW). Means for each meteorological period are also shown. Table 2-2 shows the difference in the means of each meteorological period from the KORUS-AQ mean, highlighting the largest differences that were observed during the Stagnant and Transport/Haze periods. The largest enhancement in PM_{10} was found during the Transport/Haze period and was due to large enhancements in the secondary inorganic compounds of nitrate, sulfate, and ammonium (Table 2-2). In addition, RH was enhanced during this period contributing to enhanced ALW. PM_{10} was also elevated, but to a lesser extent during the Stagnant period. Here, the elevated PM_{10} was due to enhanced SOA. Note, during this time RH was much lower than the campaign mean as was ALW.

These results are consistent with the meteorological conditions described by Peterson et al. (2019) and outlined in Chapter 1. The Stagnant period was characterized by dry conditions under clear skies. A wide range in diurnal temperature led to a dynamic boundary layer that expanded under the warm afternoon temperatures and contracted at night under cooler temperatures. An anticyclone limited transboundary transport such that local emissions were dominant. These conditions promoted photochemical (sunlight driven) production of SOA from local gas-phase emissions of VOCs. With limited transport SOA accumulated within the boundary layer to high concentrations over a period of days.

In contrast, weak cold front passages during the Transport/Haze period increased transboundary transport from China bringing humid air masses under cloudy skies to Korea. The cold surface temperatures of the West Sea (Yellow Sea) along the coast of Korea induced fog formation in the humid overlying air along the coast. The cloudy/foggy conditions limited the diurnal temperature range suppressing boundary layer

dynamics minimizing its diurnal expansion and contraction. The high humidity of this stable boundary layer air led to water uptake onto hygroscopic (a term that refers to the ability to readily take up and retain water) inorganic aerosols (nitrate, sulfate, and ammonium) increasing ALW growing the aerosols to larger sizes increasing the surface area available for more heterogeneous production of nitrate and sulfate which accumulated more water. This positive feedback loop drove the rapid secondary heterogeneous production of SIA and growth in size of the $PM_{2.5}$ aerosols as shown in the bottom panel of Figure 2-3.

Table 2-1. PM_1 aerosol composition measured at KIST, along with meteorological parameters and calculated ALW. Means \pm standard deviations with the number of values in the mean in parentheses. (Table from Jordan et al., 2020)

	KORUS-AQ Mean	Dynamic Period	Stagnant Period	Transport Period	Blocking Period
POA ($\mu\text{g}/\text{m}^3$)	3.85 ± 3.18 (11605)	3.35 ± 3.25 (2803)	4.17 ± 2.66 (1200)	4.57 ± 3.29 (1478)	3.19 ± 2.26 (1858)
Black Carbon ($\mu\text{g}/\text{m}^3$)	1.52 ± 0.82 (28758)	1.21 ± 0.70 (7090)	1.74 ± 0.83 (2879)	2.09 ± 0.88 (3639)	1.48 ± 0.81 (4553)
Ammonium ($\mu\text{g}/\text{m}^3$)	2.56 ± 2.16 (14403)	1.60 ± 1.16 (3562)	2.14 ± 2.28 (1440)	5.54 ± 2.78 (1821)	2.07 ± 1.06 (2276)
Sulfate ($\mu\text{g}/\text{m}^3$)	4.40 ± 3.26 (14403)	2.99 ± 1.83 (3562)	3.25 ± 2.72 (1440)	9.50 ± 4.12 (1821)	3.92 ± 1.52 (2276)
Nitrate ($\mu\text{g}/\text{m}^3$)	3.78 ± 4.20 (14403)	2.30 ± 2.58 (3562)	3.66 ± 4.95 (1440)	8.20 ± 5.86 (1821)	2.70 ± 2.33 (2276)
SOA ($\mu\text{g}/\text{m}^3$)	5.91 ± 4.63 (11605)	4.78 ± 2.98 (2803)	10.4 ± 6.06 (1200)	8.04 ± 3.69 (1478)	5.51 ± 2.79 (1858)
Total PM_1 ($\mu\text{g}/\text{m}^3$)	22.1 ± 13.0 (14403)	16.3 ± 8.80 (3562)	25.4 ± 12.5 (1440)	38.0 ± 15.6 (1821)	18.9 ± 7.89 (2276)

Temperature (°C)	19.7 ± 4.5 (10773)	17.2 ± 5.0 (3562)	22.0 ± 5.0 (1439)	20.1 ± 3.4 (1820)	22.3 ± 3.3 (2275)
Relative Humidity (%)	60.1 ± 21.3 (10773)	66.3 ± 22.4 (3562)	40.5 ± 17.9 (1439)	70.2 ± 16.4 (1820)	61.3 ± 17.2 (2275)
ALW (µg/m ³)	12.5 ± 21.9 (10773)	11.4 ± 21.6 (3562)	3.8 ± 7.3 (1439)	29.8 ± 30.4 (1820)	9.5 ± 18.3 (2275)

Abbreviations: POA = Primary Organic Aerosol, SOA = Secondary Organic Aerosol, PM₁ = Particulate Matter with aerodynamic diameters < 1 µm, ALW = Aerosol Liquid Water

Table 2-2. Differences in the means from Table 2-1, between those observed during each meteorological period from the campaign as a whole. Bold values highlight the largest differences from the campaign mean that occurred during the Stagnant and Transport/Haze periods. (Table from Jordan et al., 2020)

	Dynamic Period	Stagnant Period	Transport Period	Blocking Period
POA (µg/m ³)	-0.5	0.3	0.7	-0.7
Black Carbon (µg/m ³)	-0.3	0.2	0.6	0.0
Ammonium (µg/m ³)	-1.0	-0.4	3.0	-0.5
Sulfate (µg/m ³)	-1.4	-1.2	5.1	-0.5
Nitrate (µg/m ³)	-1.5	-0.1	4.4	-1.1
SOA (µg/m ³)	-1.1	4.5	2.1	-0.4
Total PM ₁ (µg/m ³)	-5.8	3.3	15.9	-3.2
Temperature (°C)	-2.5	2.3	0.4	2.6
Relative Humidity (%)	6.2	-19.6	10.1	1.2
ALW (µg/m ³)	-1.1	-8.7	17.3	-3.0

Abbreviations: POA = Primary Organic Aerosol, SOA = Secondary Organic Aerosol, PM₁ = Particulate Matter with aerodynamic diameters < 1 µm, ALW = Aerosol Liquid Water

2.4. Stagnant period SOA was produced from local emissions of VOCs

Nault et al. (2018) used a simple box model and VOC concentrations measured aboard the DC-8 to calculate SOA production over Seoul. They found that the most important precursor compounds were from the semi-volatile and intermediate volatility group of organic compounds (collectively abbreviated as S/IVOC) and from the most reactive aromatic compounds (Fig. 2-4 and Table 2-3). These compounds have short photochemical lifetimes (all < 1 day, and < 4 hr for the average observed daytime OH concentration of 6×10^6 molecules/cm³). Typical wind speeds during KORUS-AQ were only ~ 4 m s⁻¹, leading to a transport range of about 60 km during daylight hours. **Hence, the source of these SOA precursors was local.**

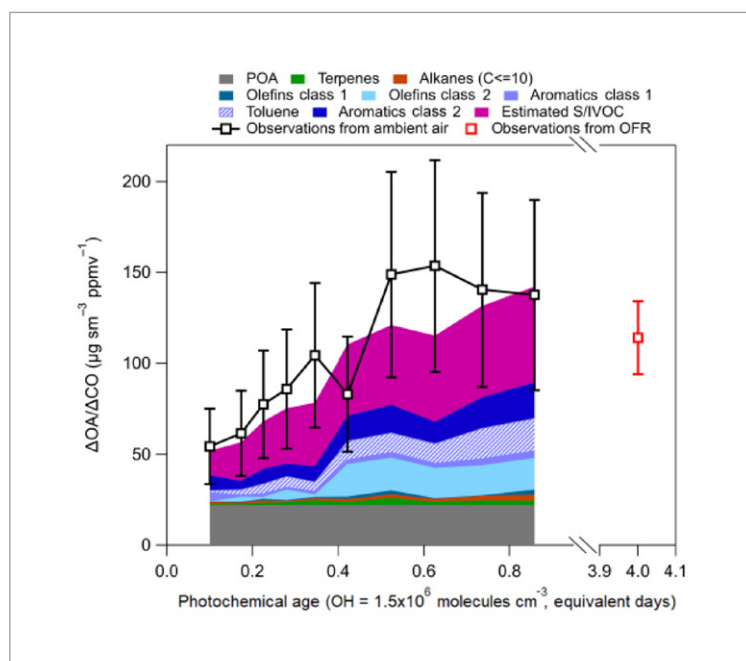


Figure 2-4. Calculated SOA production for KORUS-AQ. The SOA precursor classes are defined in Table 2-3. Note, toluene is part of aromatics class 1 (light purple), but it is shown separately. The error bars represent the uncertainty in OA (± 38 %). (Figure from Nault et al., 2018)

S/IVOC constitute a small fraction of the total VOCs in urban environments and they are challenging to measure, but their low volatility and high reactivity makes it easy to shift these compounds from gas to particle phase with the addition of any functional groups via photochemical reactions (Nault et al., 2018 and references therein). More work needs to be done to identify the compounds in this group.

In addition to the box model, Nault et al. (2018) performed further analyses all of which corroborated local emissions as the source of SOA precursors. These included correlations of SOA with other photochemically derived trace gases (e.g., O₃, HCHO, and peroxy acyl nitrates), comparisons with background CO and organic aerosol upwind of Seoul, and data from an oxidation flow reactor (OFR) on the DC-8 that showed air over Seoul had an SOA formation potential 3.5 times greater than air over the Yellow Sea.

Table 2-3. Definition of classes used in Fig. 2-4. The VOCs listed were all measured aboard the DC-8. (Table from Nault et al., 2018)

Class	Included compounds or parameterization
Terpenes	alpha-pinene, beta-pinene
Alkanes (C ≤10)	methyl-cyclopentane, cyclohexane, methyl-cyclohexane, <i>n</i> -heptane, <i>n</i> -octane, <i>n</i> -nonane, <i>n</i> -decane
Olefin class 1	1-butene, i-butene, <i>cis</i> -butene, <i>trans</i> -butene
Olefin class 2	styrene, 1,3-butadiene
Aromatics class 1	benzene, toluene, isopropylbenzene, <i>n</i> -propylbenzene, ethylbenzene
Aromatics class 2	<i>m</i> + <i>p</i> -xylene, <i>o</i> -xylene, 3-ethyltoluene, 4-ethyltoluene, 1,2,3-trimethylbenzene, 1,2,4-trimethylbenzene, 1,3,5-trimethylbenzene
Estimated S/IVOC	$6.7 \times \Delta\text{HOA}/\Delta\text{CO}$ ($\Delta\text{HOA}/\Delta\text{CO} = 23 \text{ } \mu\text{g}/\text{sm}^3\text{-ppmv}$)

Abbreviations: HOA = hydrocarbon-like organic aerosol

Given the known speciation of highly reactive aromatics and their large contribution to SOA

production (Fig. 2-4), we recommend targeting C₇+ aromatic VOCs for emission reductions to help alleviate bad air quality related to SOA under stagnant meteorological conditions.

2.5. Transport/Haze period SIA production was coupled to meteorology with a positive feedback that promotes the development and persistence of haze

A thermodynamic model (E-AIM, see Jordan et al., 2020, for details) was used to calculate ALW from measured aerosol nitrate, sulfate, ammonium, gas-phase HNO₃, and the meteorological parameters RH and T. High humidity and low temperatures shift gas-phase NH₃ and HNO₃ into aerosol phase ammonium nitrate (NH₄NO₃). Aerosol nitrate readily takes up more water into the aerosol, promoting further partitioning of gas phase NH₃ and HNO₃ into the particles in a positive feedback loop. This tightly coupled system leads to dramatic increases in ALW and nitrate such that they co-vary (Fig. 2-5). Similarly, gas-phase SO₂ participates in this system as well, but the curves in Figure 2-5 differ because sulfate once formed remains in the aerosol phase, while semi-volatile nitrate does not.

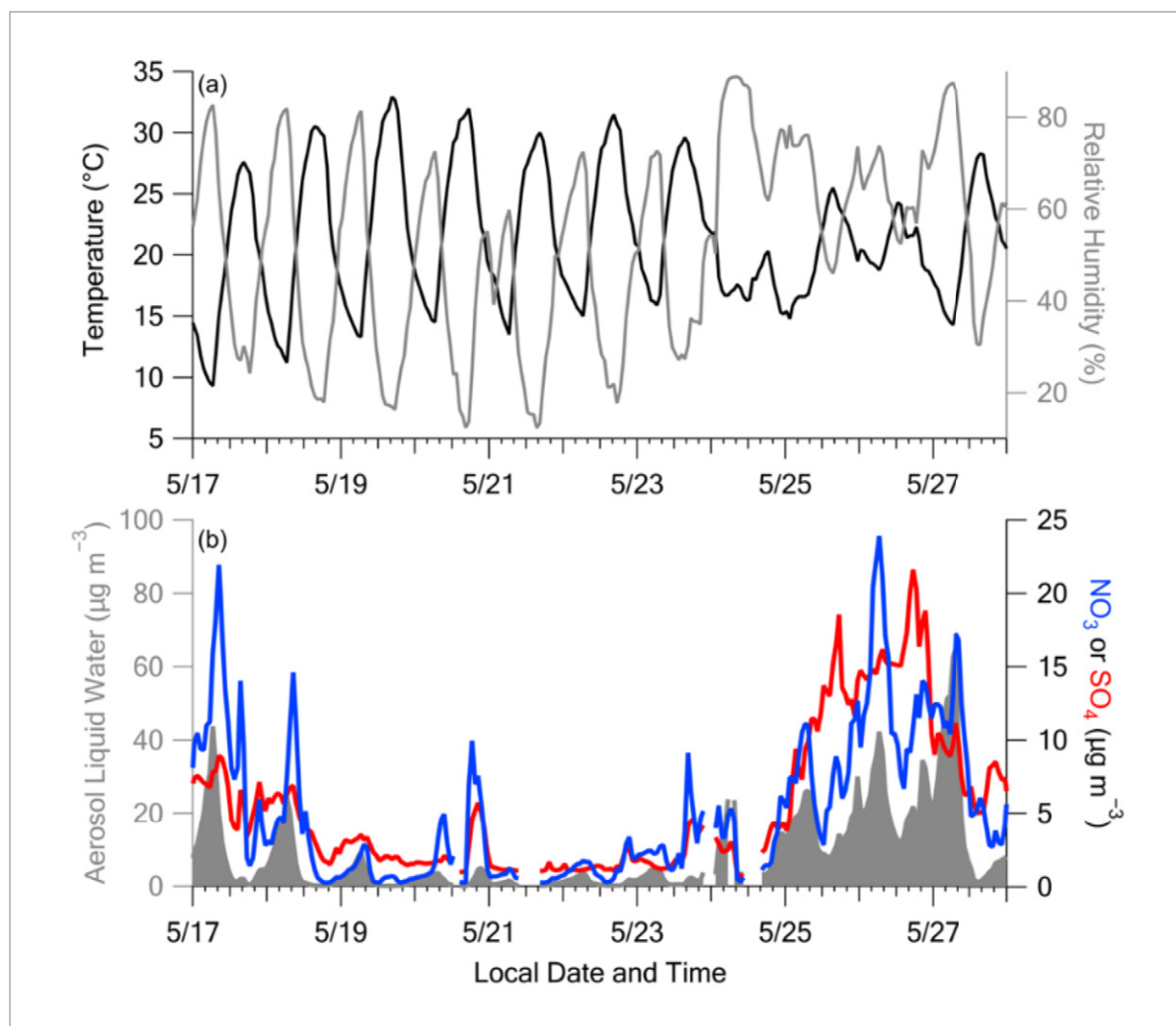


Figure 2-5. Time series of Olympic Park T and RH (top panel) and ALW with nitrate and sulfate (bottom panel) during the Stagnant and 1st half of Transport/Haze periods. ALW calculated from E-AIM thermodynamic model. Note the elevated RH throughout the day and night during Transport/Haze compared to Stagnant, along with the reduced daytime temperature for the Transport/Haze period. (Figure from Jordan et al., 2020)

The overcast/foggy conditions of the Transport/Haze period reduced the sunlight reaching the ground limiting the diurnal variability of the boundary layer (Fig. 2-6). The rapid heterogeneous production of aerosol in the humid boundary layer further reduces the sunlight reaching the ground, helping to stabilize the layer and allowing accumulation of aerosol throughout the day and night resulting in very high

concentrations and the poorest $PM_{2.5}$ air quality observed during KORUS-AQ (Fig. 2-6). Hence, the positive feedback loop driving the heterogeneous chemical production of SIA exists within another meteorological positive feedback loop that promotes the development of haze, stabilizing the boundary layer, reducing solar insolation, allowing for further accumulation of SIA.

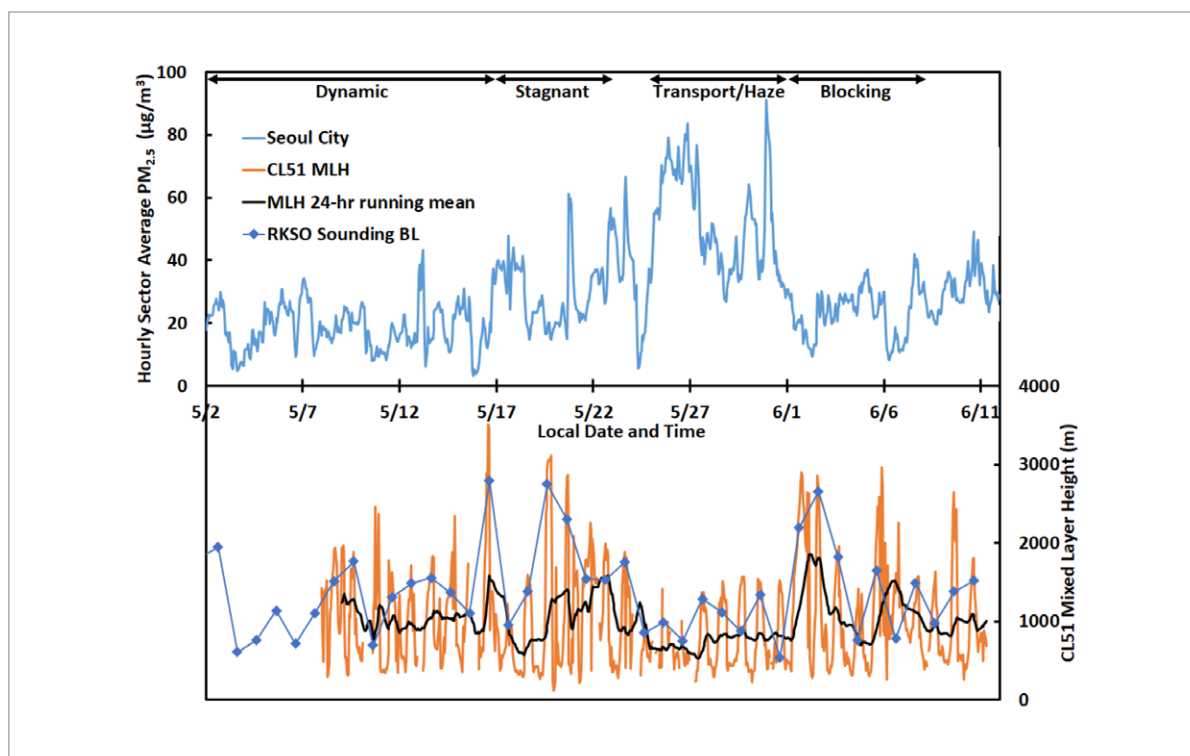


Figure 2-6. Time series of the hourly average $PM_{2.5}$ during the KORUS-AQ period for AirKorea sites in Seoul (top panel). Time series of hourly average mixed layer height (MLH) measured at Olympic Park in Seoul by a CL51 ceilometer (bottom panel) along with a 24-hr running mean showing MLH over the previous 24 hrs. BL depth based on daily soundings in the afternoon (3 p.m. local time) at Osan Air Base are also shown in the bottom panel. (Figure from Jordan et al., 2020)

Further, the stable boundary layer contributes to enhanced nocturnal nitrate formation by altering typical nighttime gas-phase reactivity. In Seoul at night, NO_x emissions in the shallow boundary layer usually remove nearly all of the near-surface O_3 (minima of a few ppbv). This reaction pathway ultimately produces aerosol nitrate, and when the O_3 is removed this process stops. However, during the Transport/

Haze period the nocturnal boundary layer did not collapse as usual, allowing greater vertical mixing with elevated O_3 (about 20 - 40 ppbv) throughout the night resulting in conversion of NO_x to nitrate at rates about three times faster than the rest of the campaign. Hence, while cloudiness limits the growth of the boundary layer during the daytime (limiting ventilation of the surface layer), the humid shallow layer retains heat at night limiting the nocturnal collapse of the layer resulting in greater nitrate production via enhanced gas-phase reactivity.

A confounding question during the Transport/Haze period was how much of this aerosol production ought to be attributed to upwind sources from China? Given its short lifetime, Nault et al. (2018) found only 10% of NO_x over Seoul could be attributed to transboundary sources. **Hence, nitrate during this period arises from local sources of NO_x .**

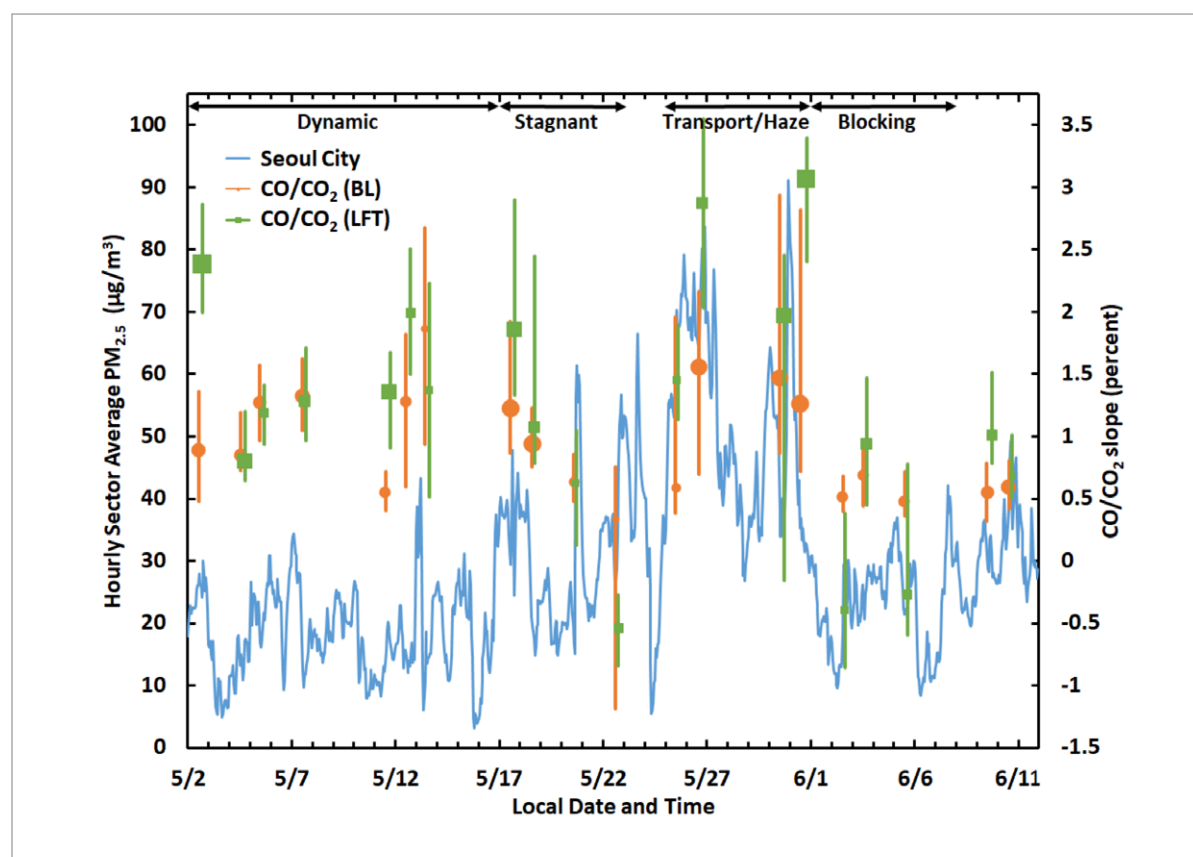


Figure 2-7. Time series of the hourly average $PM_{2.5}$ concentrations during the KORUS-AQ period for AirKorea sites in Seoul City. Median CO/CO_2 slopes are shown for DC-8 flight days and are taken

from descent profiles over Seoul. Statistics for the CO/CO₂ slopes (median and interquartile range) are shown for 1-minute data periods with slopes having a significant correlation ($R^2 > 0.5$). Symbol size is proportional to the fraction of data having significant CO/CO₂ correlation. Statistics are shown for both the boundary layer (BL, orange circles) and lower free troposphere (LFT, green squares). (Figure from Jordan et al., 2020)

Using a metric developed by Halliday et al. (2019) based on the different emission ratios of CO/CO₂ between China and Korea, aircraft data were used to assess transboundary transport throughout the campaign (Fig. 2-7). Inefficient combustion in China produces values as high as 4% compared to values closer to 1% in Korea. Negative values can occur when the air mass has been subject to strong biogenic uptake of CO₂. In the boundary layer (BL), the CO/CO₂ slope is comparable during the Dynamic, Transport/Haze, and early Stagnant periods. As the Stagnant period progressed and the atmosphere over Korea became more isolated, local sources became dominant indicated by the decreasing values of CO/CO₂ slope (Fig. 2-7). Similarly, local sources dominated throughout the Blocking period with CO/CO₂ slope values comparable to the late Stagnant period (Fig. 2-7). The separation in values between the BL and the layer of air above it (called the lower free troposphere, LFT) shows that the atmosphere was not as well mixed vertically during the weak frontal passages of the Transport/Haze period compared to that caused by the vertical lifting in the strong fronts of the Dynamic period. The difference in values between these two layers of air during Transport/Haze suggest that the influence of transported air from China was less in the stable BL air than that in the overlying LFT layer of air (Fig. 2-7). Nonetheless, transport likely contributed to the elevated SO₂ observed at the surface during this period, hence, the heterogeneous production of sulfate was probably due to both transboundary and local sources of SO₂. Unfortunately, CO₂ was not measured at a ground station in Seoul during KORUS-AQ to allow for a more quantitative assessment of the contributions of local and upwind precursors. ***For this reason, we recommend adding high quality measurements of CO and CO₂ to a ground site in Seoul to provide better statistics of the production of aerosols from local versus transboundary gas-phase precursors.*** Note, this metric will only be useful while there is a clear difference in emissions ratios of CO/CO₂ between Korea and China. Emissions are constantly evolving, so some care needs to be taken in evaluating this metric as time passes and emissions ratios shift due to changes in technology, combustion efficiency, and shifts in human activities.

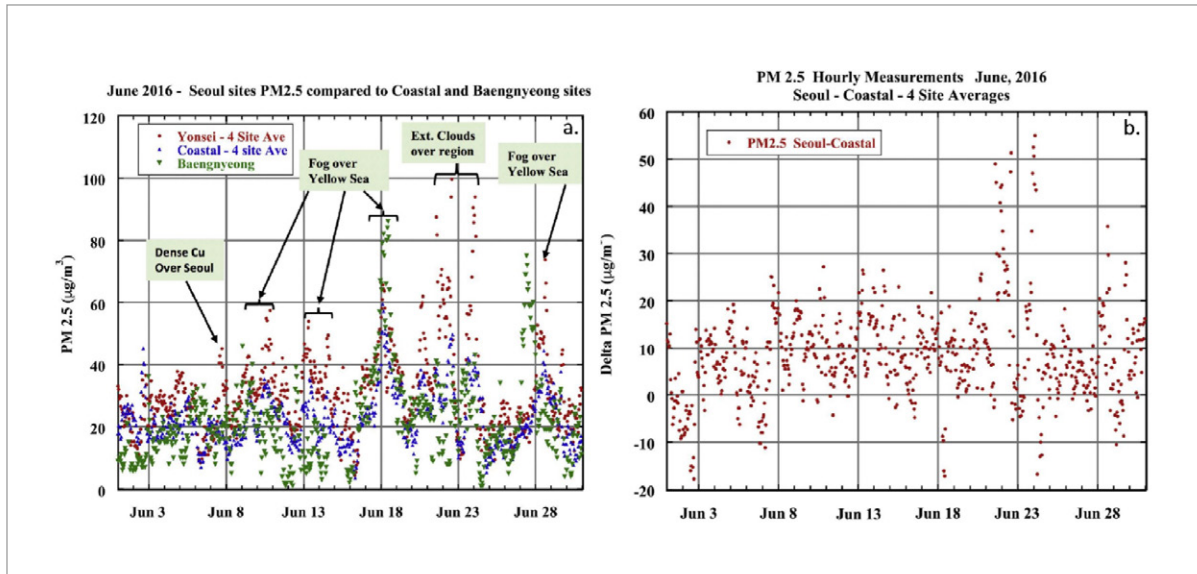


Figure 2-8. a) Time series of hourly PM_{2.5} measurements for Jun 01 through June 30, 2016 with the Baengnyeong site (~210 km NW of central Seoul) compared to measurements in central Seoul and the Yellow Sea coast. b) Time series of the differences in hourly PM_{2.5} between the central Seoul average and the coastal average. Note the much higher values in Seoul versus the coastal region for some of the days with highest PM_{2.5} levels, especially June 22–23 and June 28. (Figure from Eck et al., 2020)

Eck et al. (2020) examined the ground-based AErosol RObotic NETwork (AERONET) data throughout the KORUS-AQ study period and continued their evaluation through the end of June 2016 after the rest of the campaign activities had ended. They found that the peak PM_{2.5} events throughout June of 2016 were associated with cloudy and/or foggy conditions (Fig. 2-8), observing that foggy/cloudy conditions were not just associated with elevated PM_{2.5}, but also that the observed PM_{2.5} was greater at the Seoul sites than the coastal sites upwind. Their observations are consistent with the finding during the Transport/Haze period of local PM_{2.5} production associated with such meteorological conditions. These results suggest local heterogeneous aerosol production likely plays an important role in PM_{2.5}-related poor air quality in Korea in late spring and early summer.

2.6. Models do not yet fully represent various contributing factors to aerosol production

It is important to note that while we strive to improve models to more fully capture atmospheric observations and processes, it is the discrepancies between models and ambient observations that show us where to look to identify knowledge gaps. For example, the modeling study by J. Choi et al. (2019) revealed key discrepancies during the periods when $PM_{2.5}$ was most elevated during KORUS-AQ, i.e., late in the Stagnant period and early in the Transport/Haze period. These discrepancies were crucial in motivating our closer look at the $PM_{2.5}$ events during those periods.

As discussed in the preceding sections there are several areas where model improvements are needed. These include more work to identify gas-phase VOC precursors and/or atmospheric reaction pathways for known precursors to be able to reproduce SOA production under Stagnant conditions (see Choi et al., 2019; Nault et al., 2018; and H. Kim et al., 2018 for further details). The heterogeneous production of nitrate is often overestimated, while that of sulfate is underestimated in models such that the sum of fine aerosol mass may be well represented, but the individual reaction pathways are not (see Jordan et al., 2020, and references therein for more information). For example, heterogeneous production of sulfate in Asian haze events is an active area of research.

One factor that appears to be important in $PM_{2.5}$ events is the diurnal cycle of the height of the boundary layer of air. It is particularly challenging to measure the height of the nocturnal boundary layer as it pertains to the distribution and dynamics of aerosols, in part because of differing definitions of what is meant by the boundary layer height depending on the parameters used to measure it (e.g., meteorological definitions based on temperature and dynamics, or chemical definitions based on gas or aerosol distributions). We acknowledge the challenges of developing a suitable data product to capture both daytime and nighttime boundary layer dynamics relevant to aerosol production, accumulation, and ventilation. ***Nonetheless, we recommend the development of a boundary layer height product from the current network of ceilometers in Korea specifically to improve our ability to characterize the diurnal dynamics of the boundary layer relevant to aerosol dynamics at the surface.***

2.7. Ongoing research

The rich data set obtained through the KORUS-AQ study is continuing to be used in ongoing research across a wide variety of aerosol related topics and we anticipate more publications to appear in the international scientific literature as time goes on. Ongoing studies of which we are aware include work to improve our understanding of the mechanisms responsible for the SIA production in haze as noted above. A better understanding of aerosol acidity and the role of ammonia (NH_3) is expected to contribute to those efforts. For example, a study by T. Park et al. (in preparation) shows that Korea is an ammonia-rich region (Fig. 2-9). Figure 2-9 (left panel) shows that the relationship between the calculated concentration of $\text{H}^+_{(\text{aerosol})}$ and SO_4^{2-} depends on the form of SO_4^{2-} in the aerosol. The molar ratio of $[\text{NH}_4^+]/[\text{SO}_4^{2-}] \leq 2$ indicates some combination of the four forms of sulfate shown are present in the aerosol. Here, the submicrometer particles measured using an AMS on the DC-8 were fully neutralized by ammonium on average with that in excess of ammonium sulfate attributed to ammonium nitrate. “Excess ammonium” is defined as the amount in excess of that required for $[\text{NH}_4^+]/[\text{SO}_4^{2-}] = 1.5$. The nitrate/sulfate ratio was found to increase with the increase in excess ammonium (Fig. 2-9, right panel). Unfortunately, we did not have NH_3 measurements from the DC-8 during KORUS-AQ. **Hence, we recommend adding high quality NH_3 to the limited suite of targeted new measurements in Seoul for future studies.**

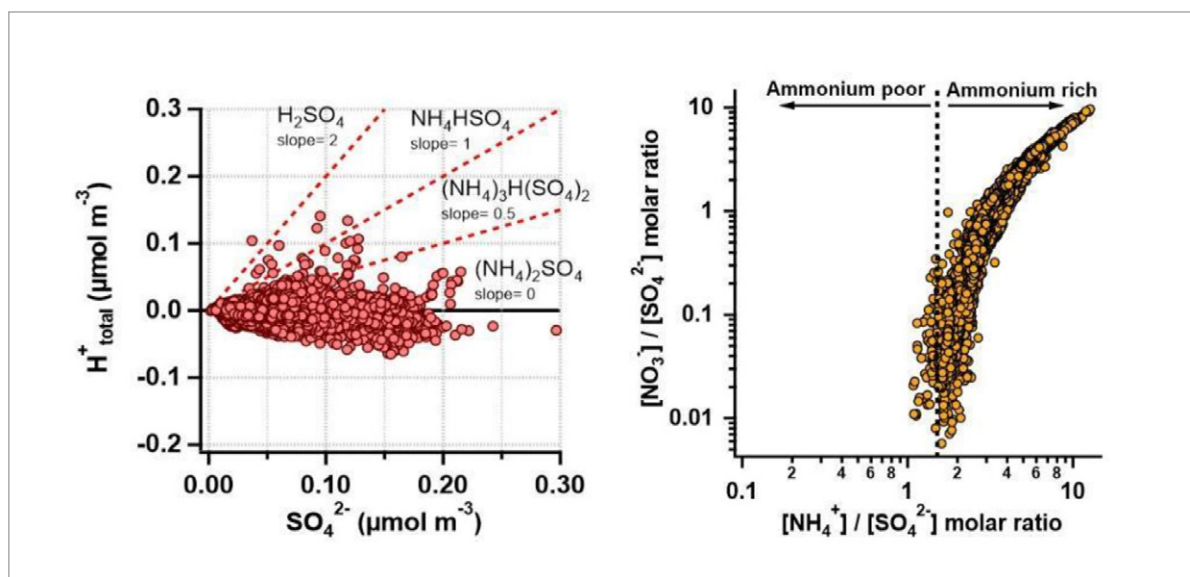


Figure 2-9. Observations from the DC-8 show that the relationship between the calculated concentrations of $H^+_{(aerosol)}$ and sulfate depend on the form of sulfate in the aerosol (left panel). The nitrate/sulfate molar ratio increases as a function of “excess ammonium” (right panel). (Figure from T. Park et al., in preparation)

2.8. Concluding remarks

We recommend targeted monitoring of additional parameters at one or a few sites within the AirKorea network that would greatly benefit future studies to address $PM_{2.5}$ air pollution mitigation. First, high quality measurements of CO and CO_2 to use as a metric to assess transboundary transport versus local sources. Second, high-time resolution aerosol composition to better document and evaluate the interplay between meteorology and secondary production of aerosols from gases. Third, humidified and dry aerosol scattering measurements from which aerosol liquid water can be calculated to better understand the coupled chemical and meteorological processes driving haze events. And fourth, high quality NH_3 measurements to fully constrain model assessments of inorganic aerosol formation, aerosol acidity, and related aerosol reaction pathways. Finally, we recommend the development of a product from current ceilometer measurements to characterize the diurnal cycle of boundary layer height relevant to aerosol dynamics to better understand the role of mixing and ventilation in $PM_{2.5}$ events.

Chapter 3: Ozone Pollution

Key Findings

- Daily variation of ozone over the Seoul Metropolitan Area demonstrates that local chemistry is driving ozone exceedances which can be well above 100 ppbv in the late afternoon during pollution episodes.
 - In addition to local production, there is a large and stable reservoir of background ozone with median abundances of 80 ppbv in the lower atmosphere that indicates a regional ozone problem also exists.
 - Calculations of ozone production rates based on observations indicate that C₇+ aromatic compounds play a dominant role with secondary contributions from alkenes and isoprene (see Chapter 4 for details in the source of these compounds).
 - Chemical Transport Model simulations demonstrate the expected sensitivity of ozone to emission reductions such that ozone can be expected to increase in urban areas and decrease across the rest of Korea if only NO_x is controlled. With additional VOC controls, urban increases could be avoided along with even greater benefit across Korea.
 - Observations of nitrous acid (HONO) at Olympic Park in the early morning show a relationship with peak afternoon ozone. This suggests additional chemistry that is not well represented in models and could signal additional benefit of NO_x reductions to control ozone in urban areas.
-

KORUS-AQ ozone study results complement those for PM_{2.5} by identifying the co-benefit of NO_x and VOC reductions with ozone being most sensitive to the same class of VOCs (C₇+ aromatics). Concurrent reduction of NO_x and VOCs is of particular importance as reduction in NO_x alone is expected to exacerbate ozone pollution in urban areas. Progress in reducing local ozone is limited by the high regional background for ozone (~80 ppbv) which calls for coordinated action by Korea and its neighbors to address ozone precursor emissions.

3.1. Ozone extremes are driven by local chemistry adding to an already large ozone background

Long-term monitoring in South Korea has shown a slow and steady rise in ozone pollution over the past three decades (Kim and Lee, 2018). KORUS-AQ enabled a detailed examination of the current drivers of ozone with a focus on the highly populated Seoul Metropolitan Area (SMA). Figure 3-1 shows the diurnal statistics of ozone with altitude taken from DC-8 spiral ascents conducted east of Seoul near the Taehwa Research Forest supersite. A distinct diurnal pattern is observed in the lowest kilometer with median ozone values ranging from 68 ppbv in the morning to 107 ppbv in the afternoon. This wide range is related to both low ozone in the early morning due to partitioning into NO_2 and late afternoon peak ozone resulting from photochemical production throughout the day. Moving up to 1-2 km, median ozone values cover a smaller range (72-90 ppbv) as the morning effects of NO_2 partitioning are reduced and boundary layer depths in the afternoon do not always bring polluted ozone conditions as high as 2 km. The effect of photochemistry in this layer is still quite large with ozone changing by almost 20 ppbv between morning and afternoon. Perhaps most striking are ozone values for the layers between 2-4 km, where median ozone values are in the vicinity of 80 ppbv and almost all ozone values exceed 60 ppbv, which equals the acceptable limit for 8-hr average ozone conditions under South Korea's air quality standard. This demonstrates that a substantial background ozone problem exists in addition to the local ozone production near the surface such that entrainment of air from the lower free troposphere alone is sufficient to violate the ozone standard. Whether the more modest daily ozone production rates (5-8 ppbv) in the lower troposphere (2-4 km) is locally or regionally driven does not alter the evidence that ozone can only be improved through a combination of measures taken locally and regionally by neighboring countries.

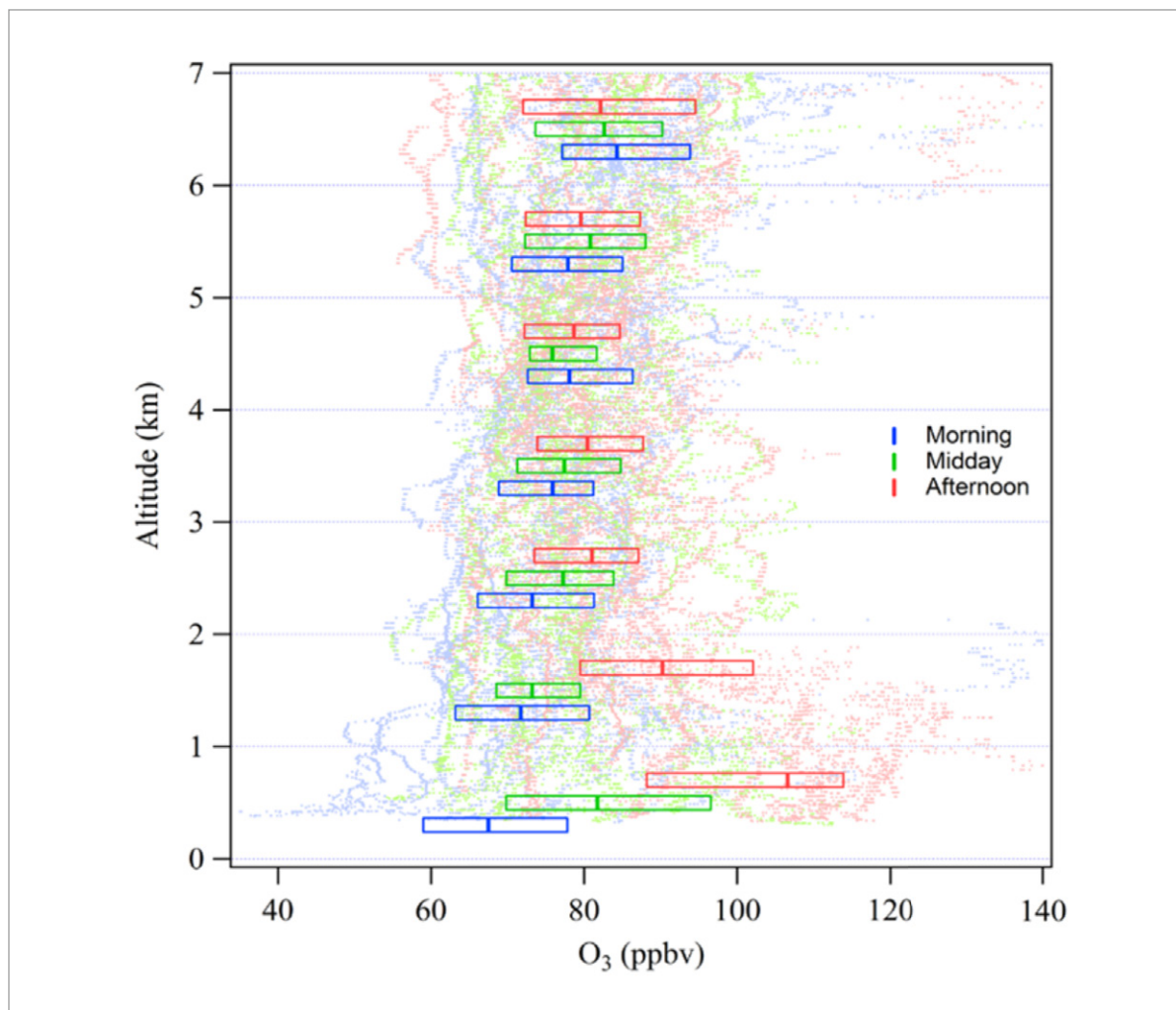


Figure 3-1. Vertical distribution of ozone observed by the DC-8 during fifty-two profiles conducted in the vicinity of the Taehwa Research Forest southeast of Seoul. Boxes showing median and interquartile values for 1 km increments of altitude are plotted over the individual measurements.

Investigation of the details governing ozone pollution in South Korea was conducted using both a 0-D box model (Schroeder et al., 2020) and a 3-D global chemistry transport model (Oak et al., 2019). These studies were complementary given the relative strengths of each approach. Box models have the distinct advantage of assessing chemical production rates directly from observed conditions; thus, they are ideal for examining the detailed sensitivity of ozone production to precursors. 3-D global chemistry transport models include full treatment of emissions, chemistry, transport, and physical processes; thus, they allow

assessment of ozone abundances and their response to changes in emissions. Both modeling studies provided careful scrutiny and evaluation of model performance through comparison with observations to provide confidence in their results. As discussed below, these evaluations provided valuable evidence for model improvements needed to properly represent ozone pollution chemistry.

3.2. Ozone sensitivity to different classes of VOCs

Schroeder et al. (2020) used a 0-D box model to calculate net ozone production rates for the Seoul Metropolitan Area based on the comprehensive DC-8 observations of precursors, photolysis frequencies, and photochemical products. Initial calculations revealed gross overpredictions of formaldehyde (CH_2O) and peroxyacetylnitrate (PAN) that were found to be related to the treatment of aromatic chemistry, specifically toluene and xylenes. These compounds typically play a minor role, even in polluted environments, but their abundance during KORUS-AQ led to careful updating of the model's chemical mechanism to reflect the most recent lab kinetics studies for these important compounds. Using the updated model to evaluate ozone production across the strong gradient in nitrogen oxides between Olympic Park and Taehwa Research Forest, Schroeder et al. demonstrated that NO_x -saturated (VOC-limited) conditions prevail in the Seoul Metropolitan Area. This assessment has been corroborated by others (S. Kim et al., 2018; H. Kim et al., 2020). Sensitivity calculations were then conducted by eliminating different types of VOCs from the model and assessing changes in ozone production rates (Figure 3-2). By far, the largest response was found for C_7+ aromatic compounds (e.g., toluene and xylenes) which accounted for a 32% reduction in mean ozone production when removed from the model. Significant response was also found for alkenes (14%), not including isoprene (15%) which was evaluated separately due to its biogenic source. These compounds far outweighed the impact of other VOC classes; thus, they represent the most important targets for ozone reduction strategies. These results are qualitatively similar to those presented in the RSSR (NIER & NASA, 2017), but these updated calculations offer a better quantification of ozone production and its sensitivity to precursors.

Recognizing that the regional extent of ozone production in the Seoul Metropolitan Area is still tied to NO_x emissions, Schroeder et al. also calculated responses in ozone production to reduced levels of NO_x . Given that NO_x -saturated conditions suppress the cycling of peroxy radicals responsible for ozone production,

these calculations demonstrated two effects. First, reductions in NO_x would lead to greater rates of ozone production, and second, the increase in chemical cycling under reduced NO_x conditions would shorten NO_x lifetimes and reduce the spatial extent of NO_x more rapidly than the simple rate of reduction in emissions. The interaction of these two effects, however, requires the use of a 3-D chemical transport model to fully quantify impacts on the NO_x distribution and resulting ozone abundances.

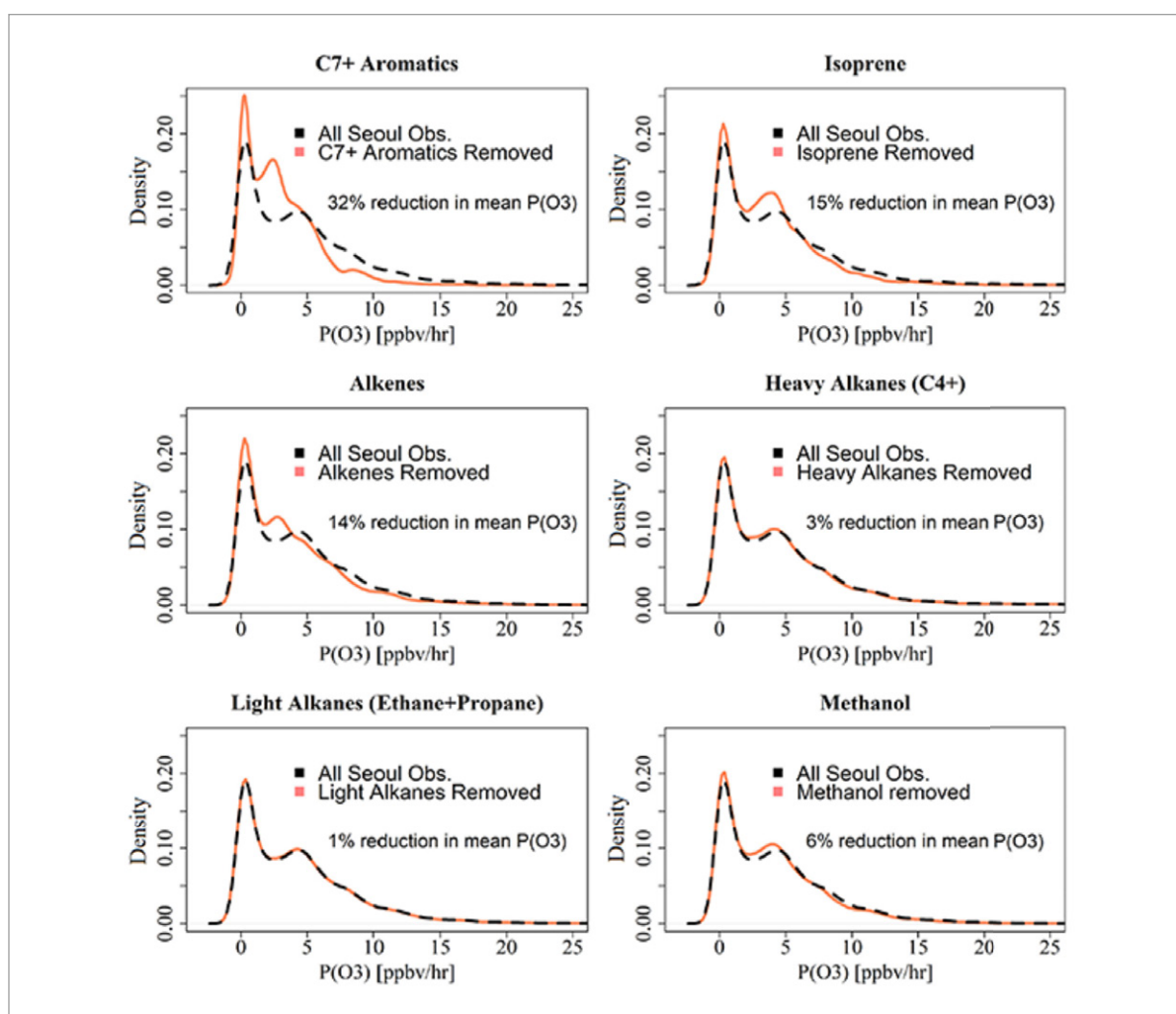


Figure 3-2. Modeled distributions of net ozone production, $P(\text{O}_3)$, over Seoul from the “base case” calculations (black dashed line in each panel) including all VOC precursors compared with calculations removing different VOC types (orange line in each panel). Each panel indicates the VOCs removed from the calculations and the integrated reduction in $P(\text{O}_3)$. (Figure from Schroeder et al., 2020)

3.3. Model assessment of ozone sensitivity to emission reductions

Oak et al. (2019) used the GEOS-Chem chemical transport model to examine ozone production efficiency and the expected response of ozone to NO_x and VOC emission controls. Three key adjustments to the model included updating the model with detailed aromatic chemistry, scaling the diurnal variation in PBL height based on lidar observations, and increasing NO_x emissions by 50% since it was based on the KORUS v2.1 inventory. These adjustments brought the model into better agreement with observations and also compared well with the observation-based box model results of Schroeder et al. (2020). With the larger regional perspective provided by the GEOS-Chem model, Oak et al. were able to show the gradients in ozone photochemistry between VOC-limited urban/industrial complexes and the greater South Korean peninsula. Sensitivity calculations were conducted to assess the response of ozone to emission controls (Figure 3-3). For a 30% reduction of NO_x emissions, ozone production efficiency increased across the peninsula, but this effect was partially offset by the reduced NO_x as well as the shorter NO_x lifetime. This was most evident in the Seoul Metropolitan Area, including industrial point sources along the northwest coast. Other coastal urban/industrial regions with VOC-limited conditions also stood out, including Busan, Pohang, and Ulsan in the southeast, Yeosu in the south, and Gangneung in the east. The overall impact when reducing NO_x alone was to increase ozone by 3-6 ppbv in these urban/industrial areas and slightly decrease ozone by a couple of ppbv in rural areas of the peninsula. This was improved for concurrent reductions in NO_x and VOC emission by 30%. Under this scenario, ozone in urban/industrial areas would be largely unchanged, but the rest of the peninsula would experience even more benefit as the NO_x reductions would outpace the more limited increases in ozone production efficiency due to VOC reductions. The average impacts integrated over urban/industrial and rural areas are summarized in Table 3-1 and reinforce the need for concurrent reduction of NO_x and VOCs to prevent ozone increases in urban industrial areas.

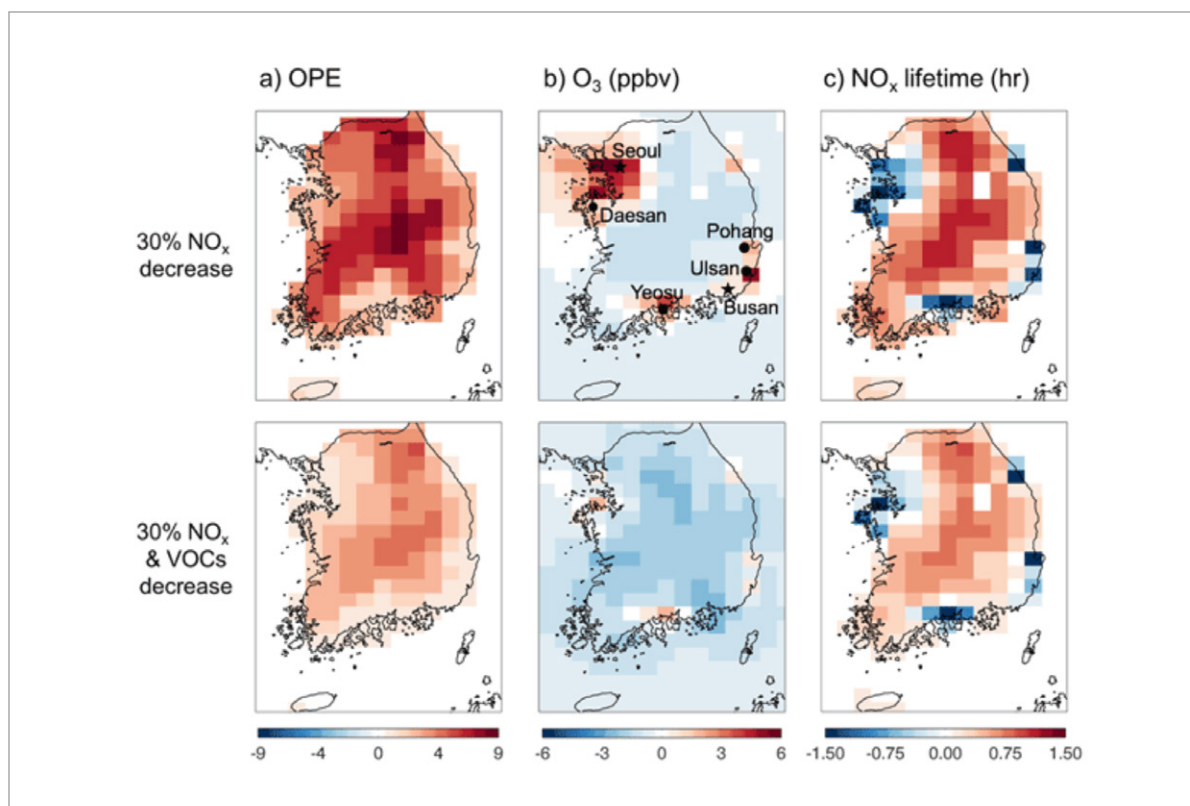


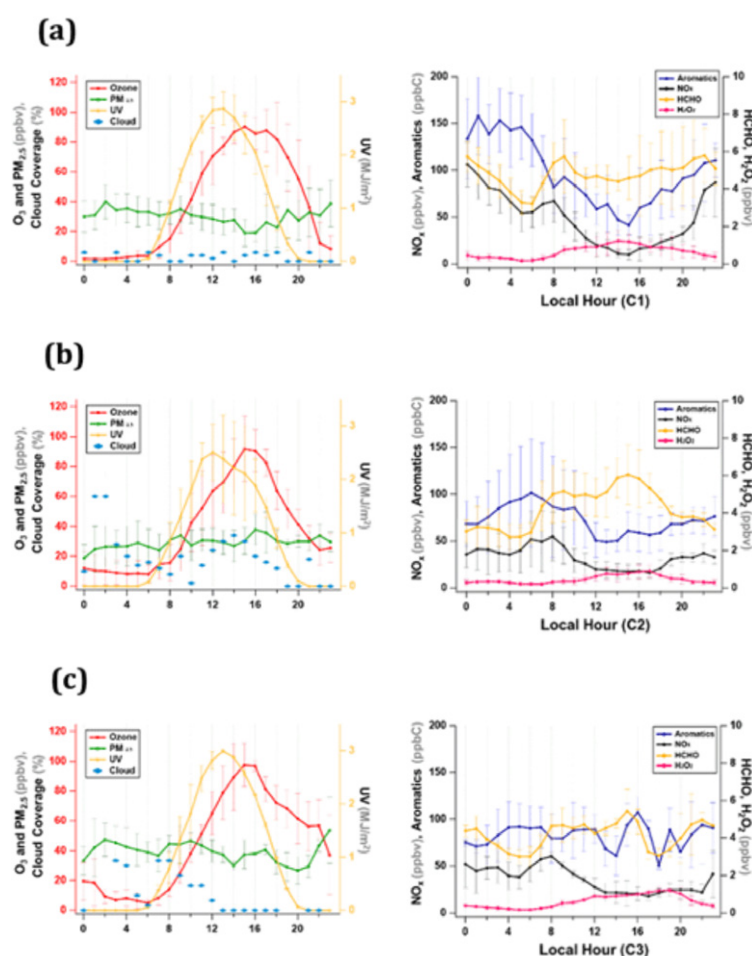
Figure 3-3. Spatial distributions of simulated OPE, O_3 , and NO_x lifetime changes. Spatial distributions of changes (modified emissions run minus base run) in simulated surface a) OPE, b) O_3 levels, and c) NO_x lifetime as a response to emission changes. Major metropolitan and industrial areas are indicated with stars and circles, respectively. (Figure from Oak et al., 2019)

Table 3-1. Ozone chemistry sensitivity to emission reduction scenarios in GEOS-Chem (Table from Oak et al., 2019)

	Urban/Industrial Areas		Rural Areas	
	30% NO_x decrease	30% NO_x & VOCs decrease	30% NO_x decrease	30% NO_x & VOCs decrease
O_3	+3%	0%	-1%	-2%
NO_x	-36%	-36%	-34%	-28%
$P(O_3)$	+13%	-8%	-15%	-18%
OPE	+40%	+18%	+32%	+17%

3.4. Observational indicators of precursors and conditions favorable for ozone production

While the average changes in ozone appear small, these emissions reduction scenarios represent only the initial steps in trying to reduce ozone pollution. They also represent average conditions rather than the extremes that can occur from day to day. H. Kim et al. (2020) provide a more detailed view of the factors controlling ozone through an analysis of the observations collected at the Olympic Park supersite. While meteorology was shown to play a role, high ozone episodes were observed across all meteorological regimes and were ultimately tied to conditions of high UV and greater precursor concentrations in the early morning compared to non-episode days (Figure 3-4). Thus, emission reductions may temper the severity and or frequency of episode days by limiting peak precursor concentrations.



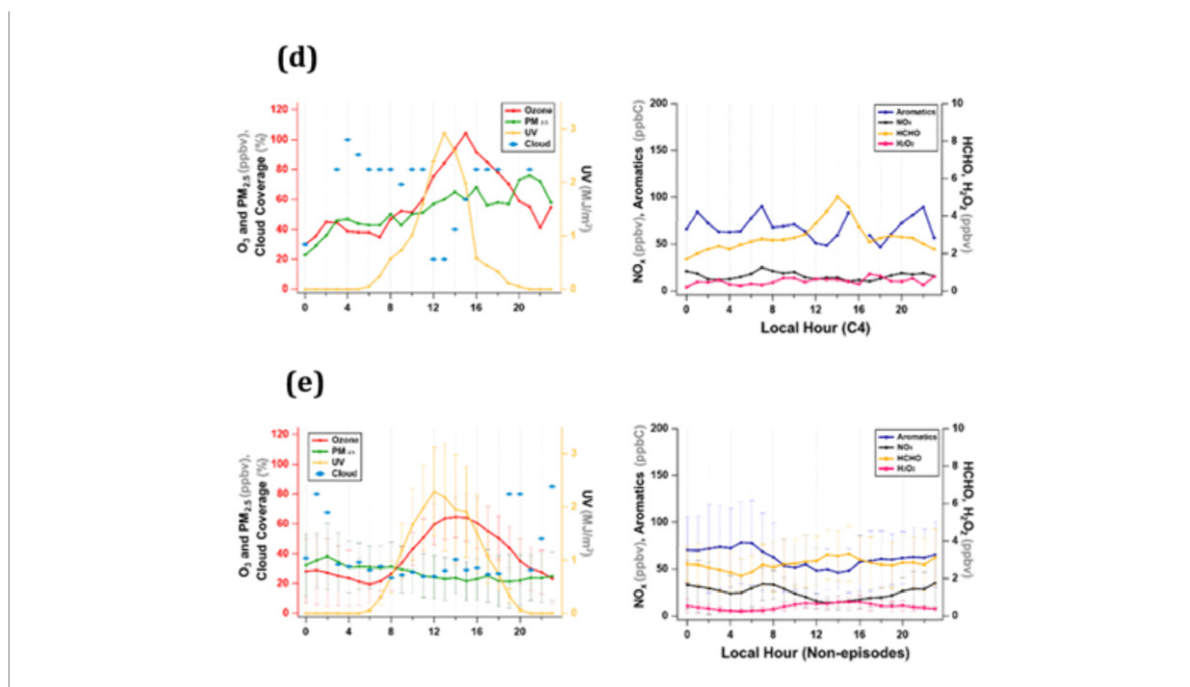


Figure 3-4. Diurnal variations of O₃, PM_{2.5}, cloud coverage, and UV (upper panel), and aromatics, NO_x, HCHO, and H₂O₂ (lower panel) for four high O₃ episodes associated with diverse meteorological conditions, e.g., (a) Stagnant period (C1), (b) Blocking period (C2), and (c-d) Transport period (C3 and C4). Non-episode conditions (e) are offered for comparison. (Figure from H. Kim et al., 2020)

Sensitivity calculations conducted on the Olympic Park observations by H. Kim et al. (2020) further corroborate the VOC sensitive regime and the anticipated increases in ozone in Seoul if only NO_x reductions are pursued. All of the simulations discussed thus far, however, are unable to fully account for the observed levels of HONO highlighted by Gil et al. (unpublished). Formed via poorly understood heterogeneous reactions, HONO was simulated by Gil et al. using an artificial neural network based on the correlation of HONO with eight chemical and meteorological variables. While HONO did not directly correlate with ozone, early morning peak values of HONO did appear to be a reliable indicator of afternoon peak ozone (Figure 3-5). This suggests that the additional source of radicals from HONO photolysis in the early morning could increase the morning rates of ozone formation and contribute substantially to peak ozone values in the afternoon. If the impact of HONO chemistry could be substantiated, this additional contribution to ozone production would render NO_x emission controls more effective for reducing ozone than indicated by conventional model predictions.

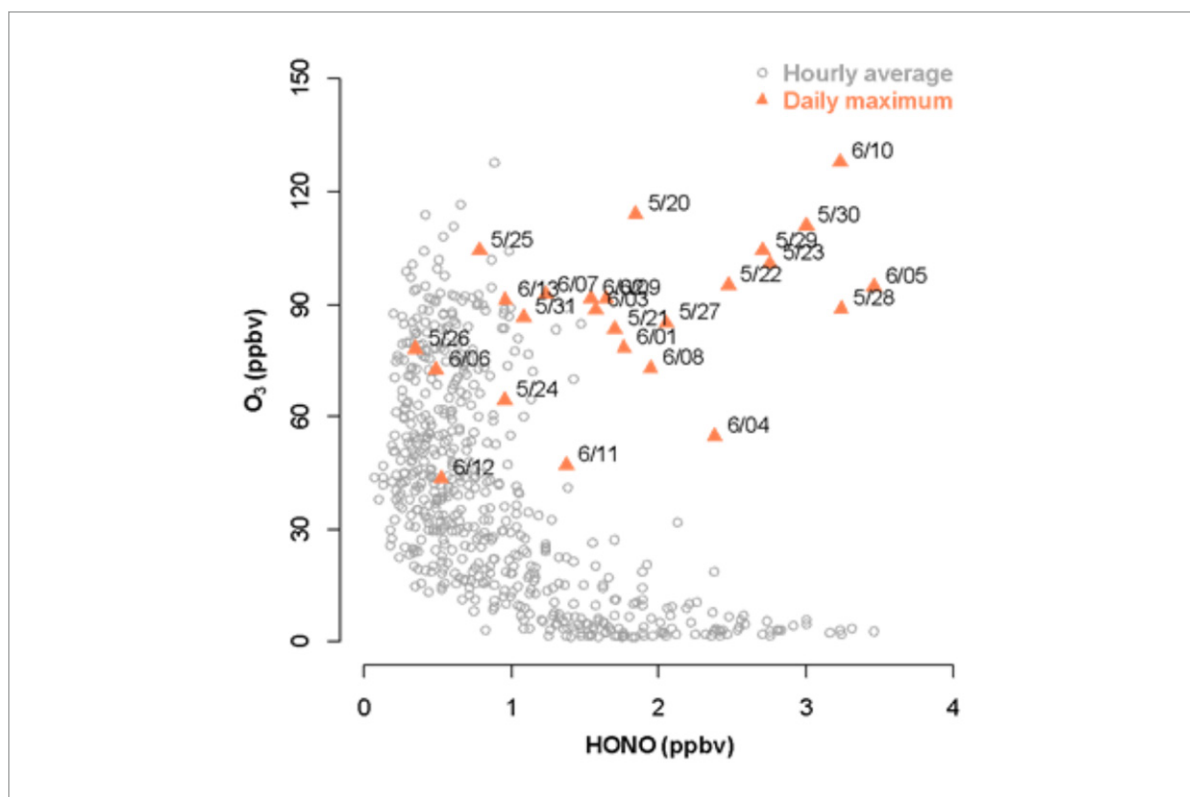


Figure 3-5. Correlation between ozone and HONO. Hourly average data (open circles) show a negative relationship. Triangles representing daily maximum levels of HONO (occurring in the morning) and ozone (occurring in the afternoon) have a positive correlation (Figure from Gil et al., unpublished).

3.5. Concluding remarks

A clear consensus message coming from the published analyses of ozone pollution in South Korea is the need for coordinated reductions in both NO_x and VOC emissions. NO_x reductions will be most effective at limiting the regional extent of ozone production, while VOC reductions will inhibit radical production and the efficiency of ozone production. The VOC-limited conditions present in the most populated areas call for initial reductions to be more aggressive for VOCs. This will minimize the potential for degraded ozone conditions in densely populated areas that could occur before reductions of 30% or more in both NO_x and VOCs can be achieved. Also, ozone and fine particle pollution share overlap in their sensitivity to NO_x and VOC emissions, with aromatic VOCs being of particular importance to both types of pollution. This

encourages joint mitigation strategies that address ozone and $PM_{2.5}$ together. Such efforts will serve to limit pollution extremes, but regional cooperation with neighboring countries will remain a high priority for reducing high background conditions.

Chapter 4: Emissions

4.1. Introduction

Primary pollutant emissions associated with human activity include trace gases such as nitrogen oxides (NO_x), volatile organic compounds (VOCs) and sulfur dioxide (SO_2). Understanding the source and magnitude of these emissions is important because they impact air quality and human health directly as well as through the formation of secondary pollutants (e.g. $\text{PM}_{2.5}$ and ozone). Emission inventories provide an accounting of the distribution and amount of each pollutant emitted into the atmosphere and are compiled annually by region and source category. While emission inventories are usually developed to understand national emissions statistics for policy use, they are also a critical component of scientific assessments supported by air quality modeling. Emissions exhibit complex variations on daily, seasonal, and annual scales. Even when based on the best knowledge, field observations are needed to assess the accuracy of emission estimates. Discrepancies are common due to the difficulty in identifying all sources. Hence, underestimation is a common occurrence when model forecasts driven by emission inventories are compared with observations. KORUS-AQ provided an opportunity for improving emission inventories and evaluating them extensively with observations. This included providing model-ready emissions for participating groups. Using the KORUS-AQ observations to assess and improve emissions was critical to understand the relationship between current emissions and air quality conditions and effectively predict what might be expected from further strategies to reduce emissions. Observations also provide detailed speciated VOC measurements, which can inform specific policy recommendations to help control ozone and SOA. In the following sections, we address Bottom-Up Emissions Development and Evaluation, Observation-Based Analysis of VOC Emissions, Evaluation of Point Source Emissions, and Recommendations for Ongoing Assessments.

4.2. Bottom-up Emissions Development and Evaluation

Key points

- KORUS-AQ research led to the development of multiple versions of the KORUS emission inventory (v1, v2.1, and v5) based on feedback from the observation and modeling communities. The version updates were prompted by scientific findings from KORUS-AQ, but changes were strictly implemented based on bottom-up information, such as new energy information, temporal allocation surrogates, or chemical speciation profiles to maintain connectivity to policy.
- An ensemble of models using KORUSv5 emissions compares well with DC-8 observations of SO₂, NO_x, and toluene (an aromatic VOC) over Seoul. These three compounds test important emissions sectors including point sources for power generation, transportation, and broad use of solvent-based products.

4.2.1 Emissions inventory development process

KORUS emission inventories were developed mainly based on CREATE (Comprehensive Regional Emissions inventory for Atmospheric Transport Experiment; Woo et al., 2020a), in support of the KORUS-AQ field campaign. Since the KORUS emission inventory geographically covers the entirety of Asia as defined in Streets et al. (2003), a mosaic of regional inventories was used, including, CREATE for the entirety of Asia, CAPSS (Clean Air Policy Support System) for Korea, MEIC (Multi-resolution Emission Inventory for China) for China, and additional inventories for Japan, Southeast Asia, and India (Woo et al., 2020b, in-preparation).

For anthropogenic emissions, there are 54 fuel classes, 201 sub-sectors and 13 pollutants including SO₂, NO_x, CO, VOCs, NH₃, PM₁₀, and PM_{2.5}. The KORUS emission inventory maintains the framework of the CREATE emission inventory, which includes an integrated policy assessment modeling framework and the comprehensive emission processing/modeling system, named Sparse Matrix Operator Kernel Emissions-Asia (SMOKE-Asia; Woo et al., 2012a). It, therefore, can be used to support science-driven atmospheric field campaigns and policy implications as well. Emissions for use in air quality modeling were created with the SMOKE-Asia emissions processing using the SAPRC-99 chemical mechanism (Carter, 2000) and

monthly temporal allocations. The final modeling emissions products were generated at grid resolutions of 0.1 degree for Asia and 3 km for Korea, respectively (Figure 4-1).

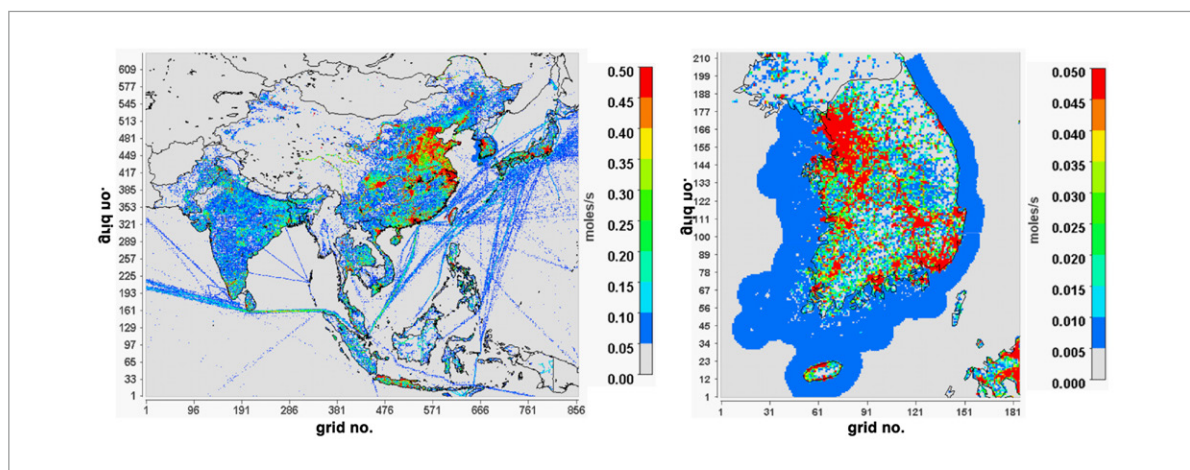


Figure 4-1. KORUS v5 modeling NO_x emissions for Asia (left) and South Korea (right) domains

Distributing standard emission products in model-ready form for the KORUS-AQ campaign is a unique accomplishment. Previously, the processing of emissions data, such as chemical speciation and temporal allocation, was the responsibility of the individual modeling groups who were free to make different decisions. For KORUS-AQ, the modeling community could make direct use of emissions that were provided in a standard gridded, monthly, and speciated form with little additional processing necessary to fit specific model needs (R. Park et al, 2020). This additional transparency in the implementation of emissions in models is useful to understanding how differences in emission processing contribute to differences in model simulations.

4.2.2 Changes in emissions inventory and modeling emissions

Even though the aircraft field campaign occurred in May-June of 2016, comprehensive studies relating to emissions, chemical evolution, trans-boundary contributions, and satellite application were conducted over a much longer period, from 2015 to 2020. During 5 years of KORUS-AQ research, multiple emission inventory versions (from Version 1 to Version 5) were developed based on energy information updates and

feedback from the observation and modeling communities.

The KORUSv1 emission inventory was developed in 2014 based on CREATE ver2.3 (2010 inventory projected to 2015) in support of MAPS-Seoul and KORUS-AQ pre-mission modeling (Woo et al., 2020b, in-preparation). The version 2.1 inventory was subsequently developed in 2016 based on the projected CAPSS 2015 (3-year projected emissions from CAPSS 2012) for Korea and CREATE version 3.0 (year 2015) for the rest of Asia. Emissions due to the construction of new power plants between 2013-2015 were also included, as well as the more comprehensive database of Large Point Sources (LPSS) for China (Jang et al., 2019, Oak et al., 2019).

A major upgrade in KORUSv2.1 was the creation of 19 new chemical speciation profiles, based on recent research efforts which were mainly conducted in China and Korea. Those profiles provided important details on the chemical composition specific to different sectors of importance, e.g. solvent use, mobile sources, residential sources, and industrial processes (Woo et al., 2020b, in-preparation).

KORUSv5 was developed in 2019, taking advantage of the updated national emission inventories that became available in 2018 for Korea (CAPSS 2015), China (MEIC 2016), and Japan (PM2.5 EI 2015). The KORUSv5 emission inventory was initially developed based on these updated emissions, with subsequent adjustments based on feedback from the observation and modeling communities (Woo et al., 2020b, *in-preparation*).

Emission changes across the different versions of KORUS modeling emissions are shown in Figure 4-2. Since these amounts are annual estimates, effects of monthly variations are not included. Overall the evolution of the KORUS emissions can be described as follows. The NO_x emission increased by 37% in KORUSv5 emissions compared to KORUSv1 to reflect the findings of top-down analyses by Goldberg et al. (2019) and Miyazaki et al. (2019). This change is corroborated by the more recent CAPSS inventory for 2016 (not available until 2019) showing that NO_x emissions for the on-road mobile sector in Seoul had increased by 30% due to the application of Portable Emissions Measuring Systems (PEMS)-based emission factors. Even though this update was not available to include in the KORUSv5 emissions, the top-down emissions modification, which was based on the KORUS-AQ measurement and modeling, was found to be in the right direction. For the changes in organic particle precursors (i.e. VOCs) for China, modeling emissions in KORUSv2.1 are increased due to the inclusion of new speciation profiles which

allocate more mass to reactive VOCs (e.g., alkanes, aromatics, and alkenes) than non-reactive VOCs. Further increases in KORUSv5 were derived from increases of VOC emission mass in the reference inventory (MEIC 2016) in China. For Korea, the VOC emission mass is increased in KORUSv2.1, and the large increase of aromatics and alkenes (and reduction of alkanes) from the new speciation profiles are maintained in KORUSv5.

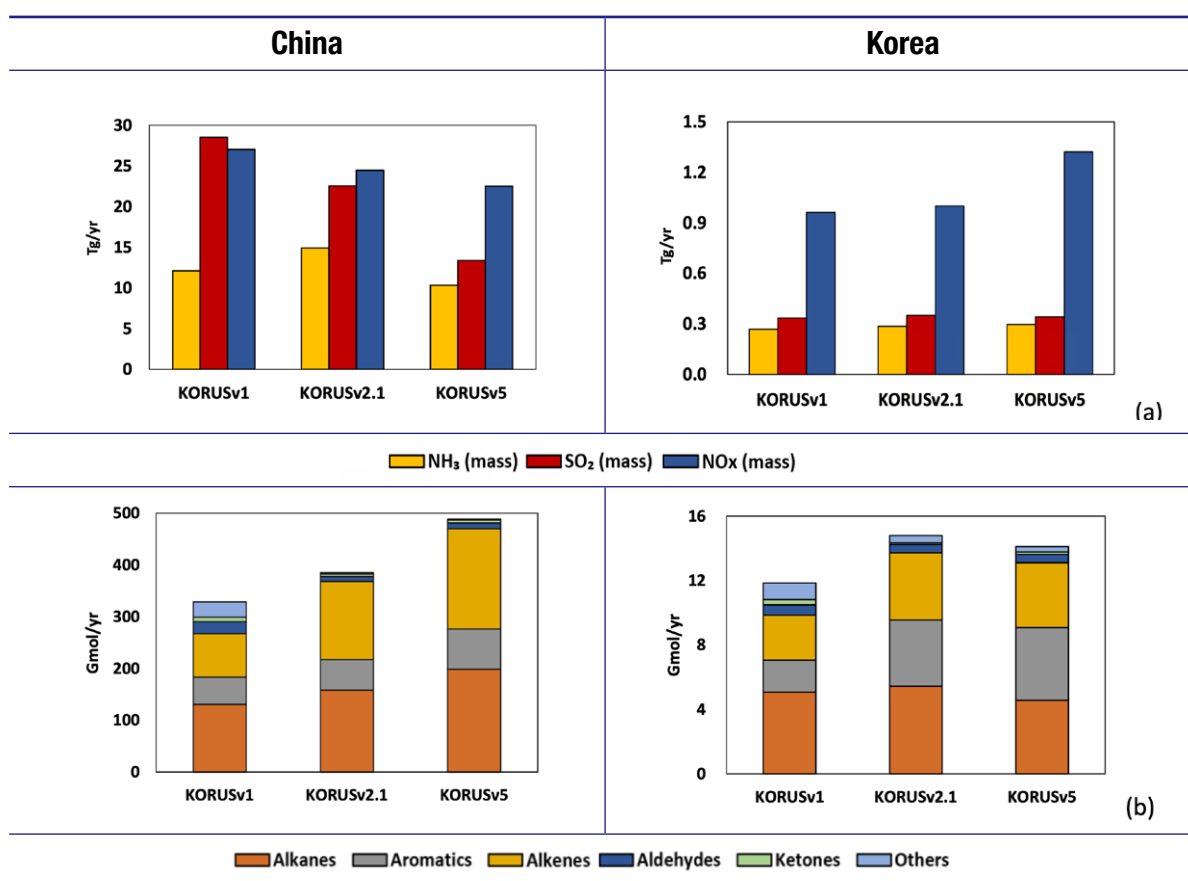


Figure 4-2. Annual average emission changes for China (left) and Korea (right) based on subsequent versions of the KORUS modeling emissions for (a) Inorganic precursors and (b) Organic precursors (Woo et al., 2020b, in-preparation).

4.2.3 Evaluation of bottom-up emissions using multiple air quality models

The best practice for evaluating modeling emissions is to compare the performance of multiple air quality models versus observations for several chemical species. During and after the field campaign, the KORUS

modeling emissions were provided to participating air quality models, such as CMAQ, WRF-Chem, CAMx, GEOS-Chem, and CAM-chem, for forecasting and post-campaign analysis. The early modeling analyses revealed the underestimation of NO_x and VOC emissions through comparison with observations (RSSR, 2017). Top-down assessments of emissions (e.g., NO_x) using satellite observations corroborated these underestimates (Goldberg et al., 2019; Miyazaki et al., 2019).

In R. Park et al. (2020), an inter-comparison of multiple air quality models using the KORUSv5 emissions and KORUS-AQ observations was conducted. Figure 4-3 shows comparisons for SO_2 , NO_x , and an aromatic VOC (toluene) between DC-8 observations and several models using KORUSv5 emissions. It is important to note that each of these compounds come from a range of different sources. SO_2 emissions are heavily influenced by point sources. NO_x also comes from point sources but is more heavily affected by transportation. Toluene comes from a large number of solvent-based products as discussed in the following section on VOC sources. Thus, the comparison in Figure 4-3 broadly tests the various source sectors in the KORUSv5 emissions inventory. There is substantial variation between the models, with the ensemble averages tending to fall slightly above observations in the lowest layer and showing good agreement or slight underestimation in the layers just above. It is quite common for the ensemble result to provide the best overall answer, while individual models can be better or worse depending on the pollutant and its distribution. This reflects the varying strengths and weaknesses of the individual models. The importance of ensemble analyses is further emphasized and discussed in Chapter 5.

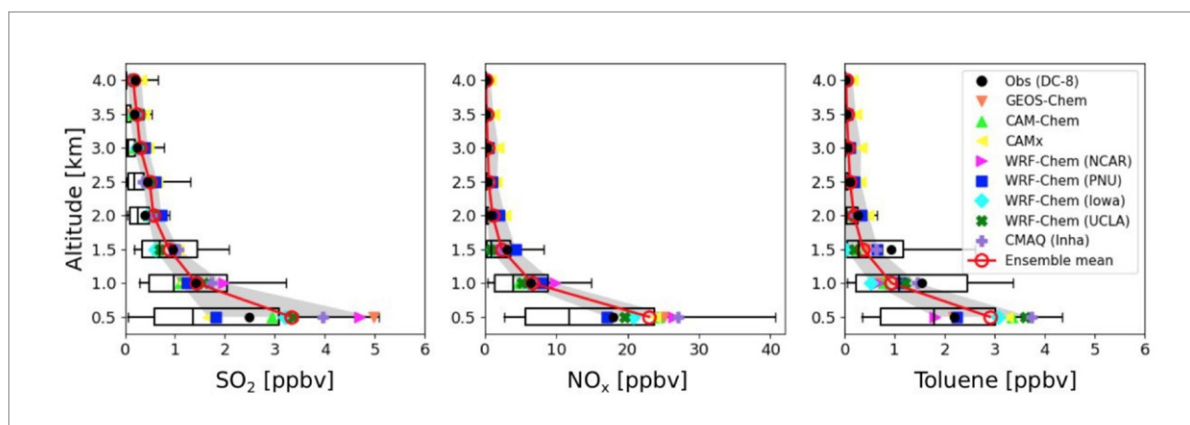


Figure 4-3. Comparison of DC-8 observations with model simulations for SO_2 (left), NO_x (center) and toluene (right) in the lower atmosphere over the Seoul metropolitan area during KORUS-AQ. Symbols indicate mean values. The full range of DC-8 observations at each altitude are also shown using a box-whisker format (center line = median, box = interquartile range, lines = 10th to 90th percentiles). The number of values contributing to the statistics for each altitude bin are shown on the right. Gray shading indicates the spread in model values.

The evolution of the KORUS emission inventory emphasizes the value of providing modeling emissions (i.e. emissions ready for use in models) and the feedback gained by using observations to assess current understanding of emissions. The process was more iterative and fostered closer collaboration between emissions and modeling/analysis researchers. This enabled the early identification of discrepancies that could later be understood in term of improved bottom-up information. For instance, initial findings of underestimation of NO_x emissions was found to be consistent with results of an independent effort of national inventory development revealing that the deficit of NO_x emissions, at least in part, was due to non-PEMS emission factors. The newer speciation profiles for VOC emissions effectively addressed the initial deficit of aromatic species over the SMA but still might underestimate other source regions that received more limited sampling during KORUS-AQ. While these efforts provided a better understanding of emissions in general, there are several issues still remaining for further investigation. The following sections provide more details specific to VOCs and point source emissions.

4.3. Observation-Based Analysis of VOC Emissions

Key points

- Seoul has a mix of biogenic and anthropogenic VOC sources. Solvents, mobile sources and industry are among the major anthropogenic VOC sources in Seoul, based on both measurements and emission inventories. Observations during KORUS-AQ suggest that gasoline evaporation, natural gas and biomass burning were less important VOC sources in Seoul.
 - Detailed VOC measurements and analysis during KORUS-AQ has provided critical information on the relative importance of specific VOCs (e.g., aromatics and alkenes) to local ozone chemistry in Seoul, especially toluene, xylenes, ethene, and the biogenic compound isoprene.
 - Additional analysis has identified sources of these reactive VOCs in Seoul. Solvents are the main source of aromatics in Seoul, and both paint and non-paint sources of aromatics are particularly important targets for VOC reductions. Traffic is the main source of alkenes such as ethene.
 - The VOC mixture at the Daesan petrochemical facility is different from Seoul. For example, Seoul is toluene-rich whereas Daesan is benzene-rich. Ethene, *n*-hexane, propane and benzene were major VOC species emitted from the Daesan facility. These plumes may reach Seoul under certain wind directions, and research on this topic is ongoing.
-

4.3.1 VOC background and measurements during KORUS-AQ

Volatile organic compounds (VOCs) are important components of air pollution. VOCs react with nitrogen oxides (NO_x) to form ozone, a component of smog, and VOCs also produce secondary organic aerosol (SOA). As well as forming secondary products, some VOCs may pose health risks if concentrations in the atmosphere exceed recommended limits. The Korean Ministry of Environment (KMOE) has ongoing policies to tighten environmental standards and reduce the emissions of major pollutants, including VOCs. During KORUS-AQ, more than 80 speciated VOCs were measured aboard the NASA DC-8 using both fast-response instrumentation and more than 2500 canister-based whole air samples (WAS). The measurements were used to (1) characterize the VOC composition in Seoul and surrounding regions, (2) determine which VOCs are major ozone precursors in Seoul, and (3) identify the sources of these reactive VOCs.

4.3.2 VOC composition in Seoul

VOCs measured during KORUS-AQ showed distinct signatures depending on their source origins (Simpson et al., 2020). The composition of air measured over Seoul in 2016 during KORUS-AQ was similar to that measured a year earlier during the ground-based MAPS-Seoul campaign in 2015 (Kim, Choi et al., 2018), with abundant ethane, propane and toluene in both cases (Figure 4-4a-b). By comparison, plumes from the Daesan petrochemical complex had a different VOC composition, and were rich in ethene, light alkanes and benzene (Figure 4-4c). Air from China sampled over the Yellow Sea was characterized by long-lived gases such as ethane, propane, ethyne and carbonyl sulfide (COS), which is emitted from sources including coal combustion (Figure 4-4d).

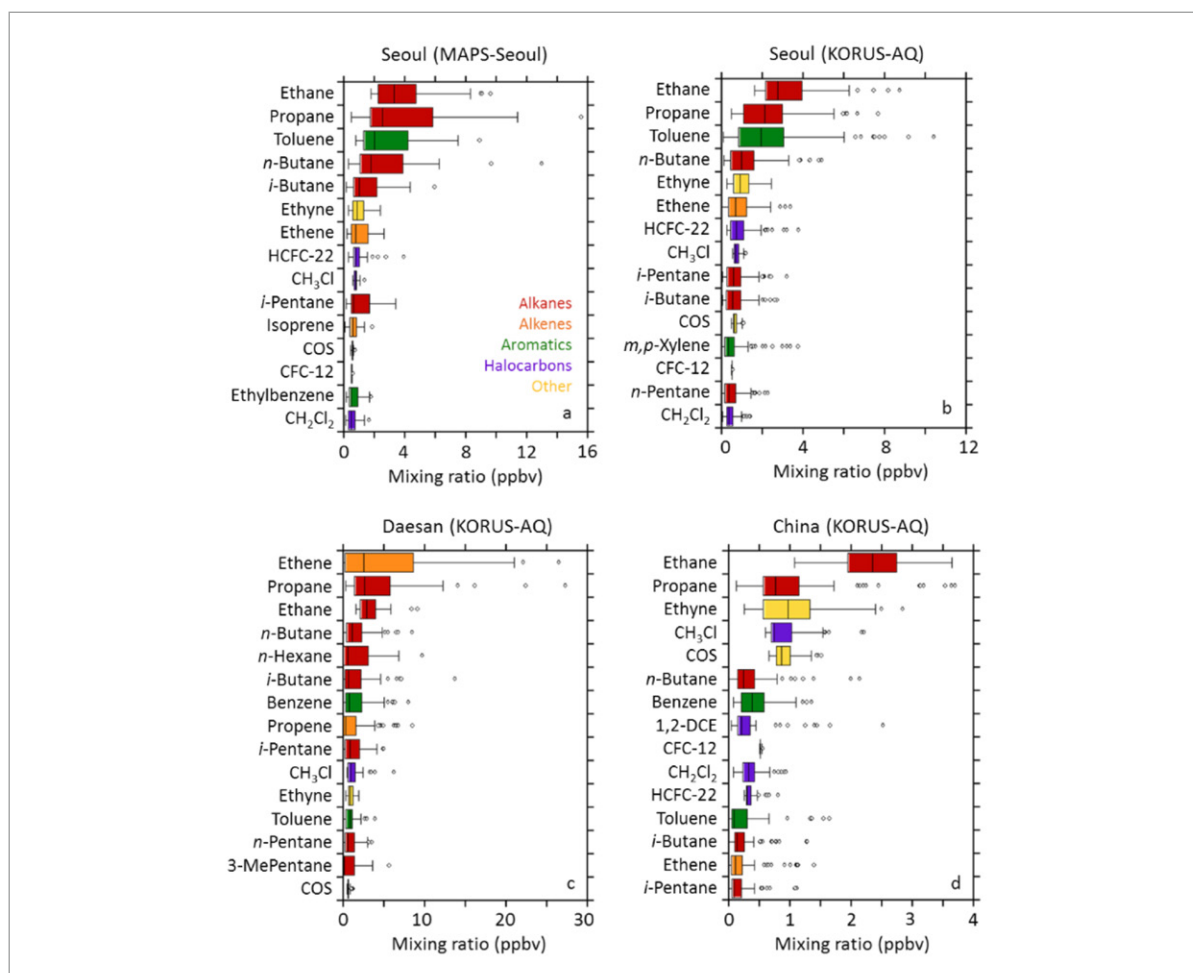


Figure 4-4. Top 15 most abundant VOCs measured during the MAPS-Seoul and KORUS-AQ campaigns,

plotted in descending order based on average mixing ratio. (a) Ground-based data at KIST in May 2015 during MAPS-Seoul ($n = 23$). Low-altitude airborne samples (< 0.5 km) during KORUS-AQ over (b) Seoul ($n = 177$), (c) Daesan ($n = 63$), and air sampled over the Yellow Sea downwind of (d) China ($n = 68$). A maximum Daesan propane value of 62.5 ppbv is not shown. (Figure from Simpson et al., 2020)

Examples of the influence of different source regions on VOC concentrations can be seen in Figure 4-5, which shows high concentrations of toluene over Seoul, and high levels of carbonyl sulfide in air arriving from China, which was sampled over the Yellow Sea during periods of meteorological transport from the west.

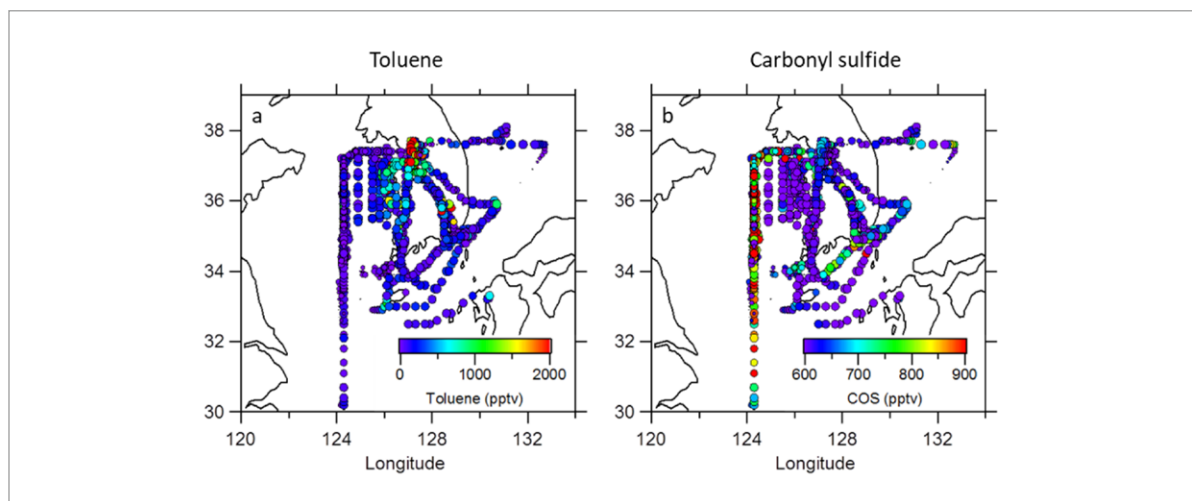


Figure 4-5. Spatial distributions of (a) toluene and (b) carbonyl sulfide (COS) during KORUS-AQ. Toluene was most elevated over the Seoul Metropolitan Area (red points), while carbonyl sulfide was most enriched in air arriving from China. Each graph is color-coded by VOC mixing ratio. We note that the KORUS-AQ campaign targeted Seoul, and we recognize that other major urban centers in Korea are also impacted by VOC emissions and ozone pollution. (Figure from Simpson et al., 2020)

4.3.3 Impact of VOCs on ozone production

Most VOCs react in the atmosphere with the hydroxyl radical (OH), and VOCs that react quickly with OH have a greater potential to form O_3 than those that react more slowly. The potential of individual VOCs to form O_3 in Seoul was estimated using different types of calculations, including OH reactivity (Simpson et

al., 2020) and photochemical box modeling (Schroeder et al., 2020). The OH reactivity calculation is the product of VOC concentration and how quickly that VOC reacts with OH (OH rate constant) (Figure 4-6).

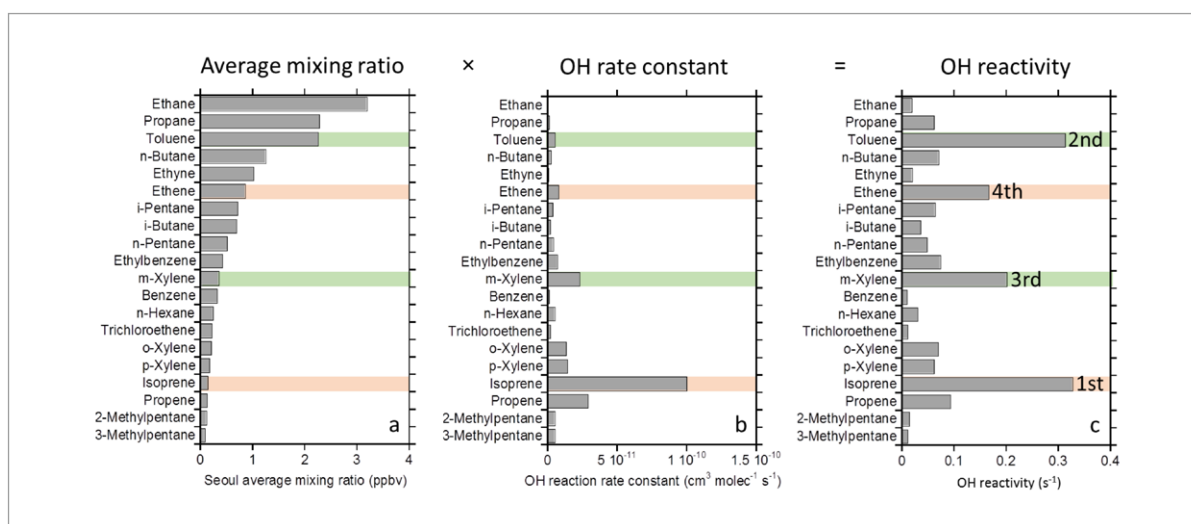


Figure 4-6. (a) Top 20 most abundant VOCs measured at low altitude (< 0.5 km) over Seoul during KORUS-AQ, (b) their OH reaction rate constants, and (c) their OH reactivity. Selected aromatics are colored in green and selected alkenes in orange. The top 4 OH reactivity rankings are labeled in panel (c). (Figure from Simpson et al., 2020)

As shown in Figure 4-6, VOCs can have a high OH reactivity (and therefore high potential to form O₃) based primarily on their abundance (e.g., toluene), their OH rate constant (e.g., isoprene), or a combination of both (e.g., *m*-xylene). Overall, the OH reactivity calculations show that isoprene, toluene, *m*-xylene and ethene are individual VOCs that were most likely to form O₃ in Seoul during KORUS-AQ. This is consistent with ground-based WAS measurements made a year earlier during the MAPS-Seoul campaign (S. Kim et al., 2018).

Photochemical box modeling is a more sophisticated way of calculating O₃ formation potential, because the model better accounts for complex chemistry. However, unlike OH reactivity calculations, the model treats the VOCs as groups (aromatics, alkenes, etc.) rather than as individual VOC species (toluene, ethene, etc.). Figure 4-7 compares the relative potential of different VOC groups to form O₃ on the basis

of OH reactivity versus detailed box model calculations. Note that these relative numbers are not the same as the sensitivities shown in Chapter 3, which account for overall O_3 production from oxidation of other important precursors such as CO and methane. As a group, aromatics contributed most to VOC OH reactivity in Seoul during KORUS-AQ (44%), followed by non-isoprene alkenes (19%), isoprene (17%), heavy alkanes $\geq C_4$ (16%) and light C_2 - C_3 alkanes (5%) (Figure 4-7a). Similarly, the photochemical box modeling was most sensitive to ozone production by aromatics (49%), followed by isoprene (23%), other alkenes (22%), heavy alkanes (5%) and light alkanes (2%) (Figure 4-7b). The overall good agreement between the two techniques suggests that the speciated VOC results from the OH reactivity calculations can reasonably be used to determine which anthropogenic VOCs are most likely to form O_3 in Seoul and could be targeted for VOC emission reduction strategies (i.e., toluene, xylenes, ethene).

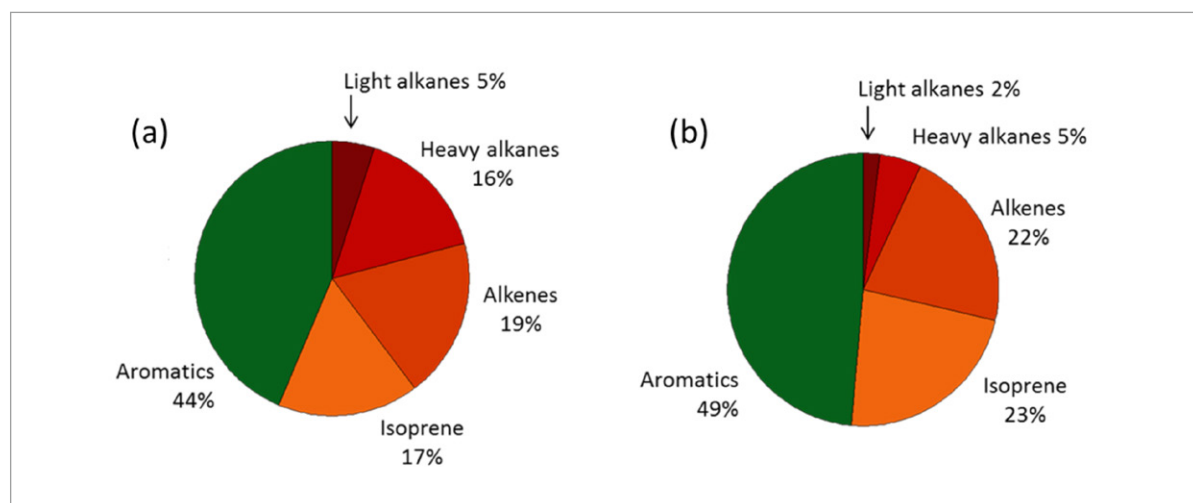


Figure 4-7. Relative potential of different VOC groups to form O_3 in Seoul during KORUS-AQ based on (a) OH reactivity calculations (Simpson et al., 2020) and (b) photochemical box modeling calculations (Schroeder et al., 2020). Light alkanes are C_2 - C_3 and heavy alkanes are C_4 and higher. (Figure from Simpson et al., 2020)

4.3.4 VOC sources in Seoul

VOC source influences in Seoul were diagnosed using a combination of techniques, as described in Simpson et al. (2020). For example, the ratio of toluene-to-benzene (T/B) is a sensitive indicator of the influence of solvents versus traffic: a T/B ratio of 1-2 indicates traffic while > 2 indicates solvent influence. Here the average T/B ratio over Seoul was 7.6 ± 4.9 , with ratios of 10-19 for toluene levels greater than 6 ppbv, suggesting a prominent influence of solvents on toluene in Seoul. Tunnel sampling of traffic in Seoul on June 2, 2016 found a T/B ratio of 2.2, compared to 8.4 ± 1.5 measured at the same time during a missed approach by the DC-8 over the Seoul Air Base. This analysis clearly shows the additional impact of solvents on toluene levels in Seoul.

VOC sources were further investigated using a technique called source apportionment, which finds correlations within complex data sets, as described in Simpson et al. (2020). As shown in Figure 4-8, five major sources were found for VOCs in Seoul using this analysis. VOCs of interest are highlighted with their strongest source in orange (alkenes) and green (aromatics).

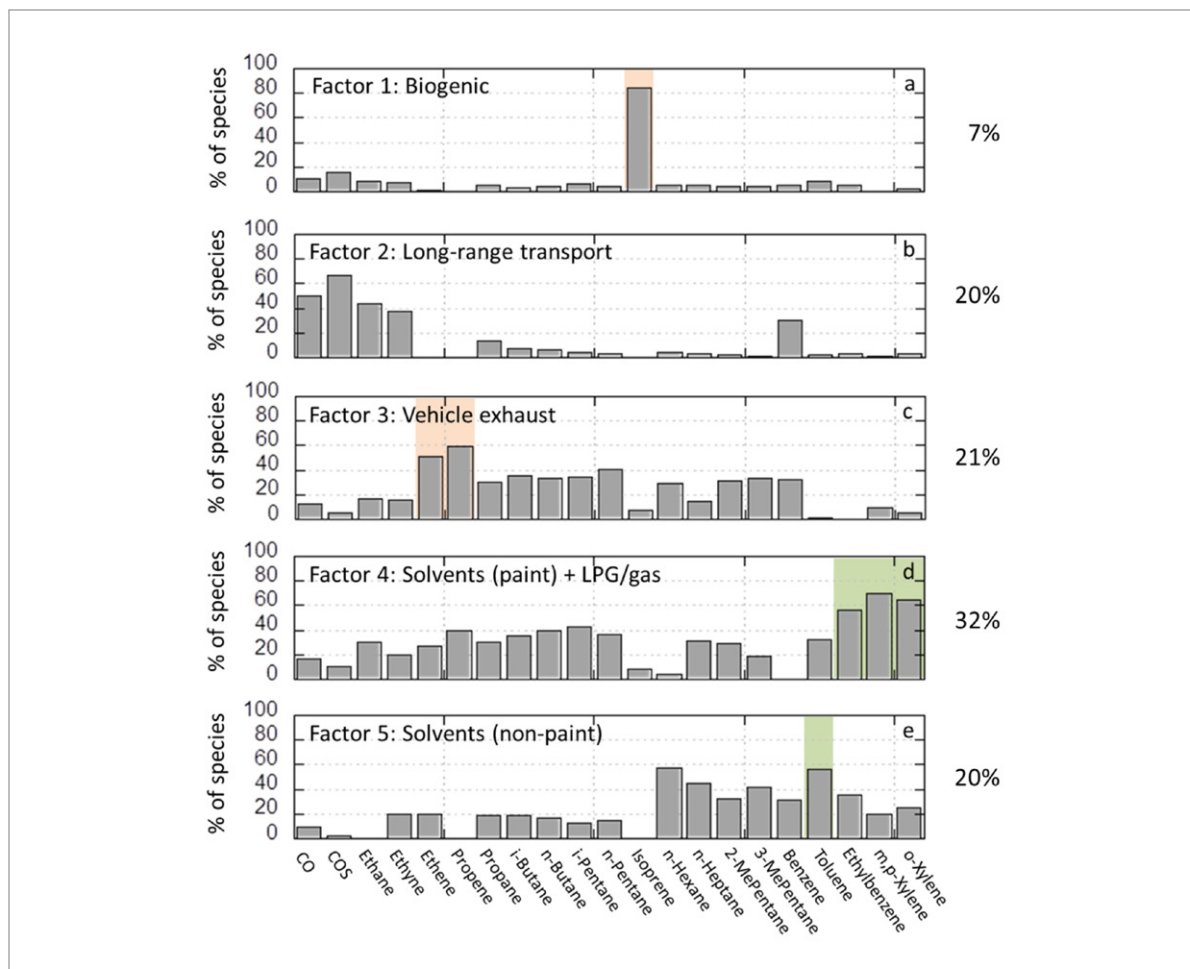


Figure 4-8. Source apportionment results for selected VOCs measured over Seoul during KORUS-AQ. Colored bars show major sources of reactive alkenes (orange) and aromatics (green). (Figure from Simpson et al., 2020)

The five major VOC sources are as follows. (1) A biogenic source, characterized by the biogenic tracer isoprene, accounted for 7% of source apportionment results. (2) A long-range transport source, characterized by the China tracer carbonyl sulfide (COS) and long-lived combustion tracers such as CO, ethyne and benzene, accounted for 20% of the source apportionment. (3) A vehicle exhaust source, characterized by the traffic tracers ethene and propene, accounted for 21% of the source apportionment. (4) A mixed paint-solvent and clean fuel source, characterized by the paint tracers xylenes and ethylbenzene, the gasoline tracer *i*-pentane, and the liquefied petroleum gas (LPG) tracers propane and butanes, accounted for 32% of the source apportionment. A substantial portion of toluene (32%) is

also associated with this factor. (5) A non-paint solvent source, characterized by toluene, *n*-hexane, and *n*-heptane, accounted for 20% of the source apportionment.

In summary, the VOCs measured in Seoul during KORUS-AQ were calculated to be a mix of biogenic sources (7%), long-range transport (20%), vehicle exhaust (21%), a mix of paint solvents and cleaner fuels (32%), and non-paint solvents (20%). It is important to note that there are uncertainties in this analysis, as discussed in Simpson et al. (2020), including the selection of CO and 20 VOCs, but the results still provide helpful guidance for attributing the sources of important reactive VOCs in Seoul.

4.3.5 Recommendations for VOC reductions in Seoul

Toluene, xylenes and ethene are major precursors to ozone in Seoul (Simpson et al., 2020), and aromatics also contribute to SOA formation (Nault et al., 2018). Because NO_x reductions in South Korea have been faster than VOCs and because air pollution in Seoul may worsen under increasing ratios of VOC/NO_x (Kim and Lee, 2018), aromatics and alkenes are attractive targets for VOC emission reduction strategies. Vehicle exhaust was found to be the main source of ethene and propene emissions in Seoul, and solvents were the main sources of aromatics—primarily paint solvents for ethylbenzene and xylenes, and non-paint solvents such as consumer products and printing for toluene (Simpson et al., 2020). This indicates that aromatic reductions can be best achieved by targeting solvents, with a focus on multiple solvent products including both paint and non-paint solvents. This step would complement and expand on existing strategies to limit VOC content in paints, in addition to long-established policies in South Korea to limit emissions from vehicle exhaust.

A similar strategy has been successfully applied in Hong Kong, a city where toluene used to be the most abundant VOC and where policies that regulate the VOC content in solvent products have led to a decline in toluene levels (Guo et al., 2006; Lyu et al., 2017). Specifically, the Hong Kong government prescribed VOC content limits for 172 types of regulated products including architectural paints, printing inks, consumer products, vehicle refinishing coatings, vessel and pleasure craft coatings, adhesives and sealants, fountain solutions, and printing machine cleansing agents (Simpson et al., 2020). Source sampling in Seoul and other urban centers of Korea may help to identify the specific VOC products that are top priorities to target.

4.4. Evaluation of Point Source Emissions

Key Points

- Top-down estimates of the VOC emissions from the Daesan petrochemical complex by three independent approaches indicate that present bottom-up inventories are underestimated by a factor of 2.5 to 4.0.
 - Likewise, top-down Daesan estimates of the sum of formaldehyde and its 4 major precursors (ethene, propene, 1,3-butadiene, and 1-butene) are underestimated by a factor of 4.3 ± 1.5 relative to bottom-up inventories.
 - In contrast, top-down estimates of sulfur dioxide and nitrogen oxides emissions are in agreement with the bottom-up inventory, ranging from 0.8-1.3 and 0.7-1.0 for NO_x and SO_2 , respectively.
 - Underestimated emissions from Daesan fail to adequately constrain Hazardous Air Pollutants that pose health risks to local workers, and under onshore wind conditions, present additional risk to local populations. Efforts to better monitor and reduce these emissions are encouraged.
-

4.4.1 VOC sources in Daesan

Measurements of emissions from the 4 largest west coast facilities (Taean power plant, Dangjin thermal power plant, Hyundai Steel, and the Daesan petrochemical complex) were measured from the DC-8 over 3 sampling days (Thursday June 2, Friday June 3, and Sunday June 5, 2016) during the KORUS-AQ study. Because of the dominance of emissions from the Daesan petrochemical complex, airborne sampling was focused more heavily on isolated plumes directly attributable to Daesan. The KORUSv5 emissions inventory also provided the latest Daesan bottom-up emissions estimate for comparison with a top-down analysis based on DC-8 observations.

Top-down emission rates for 33 individual VOCs measured by the WAS sampling system, their sum, as well as the rates for HCHO were determined employing the mass balance approach, which is schematically shown in Figure 4-9 for measurements on June 5, 2016.

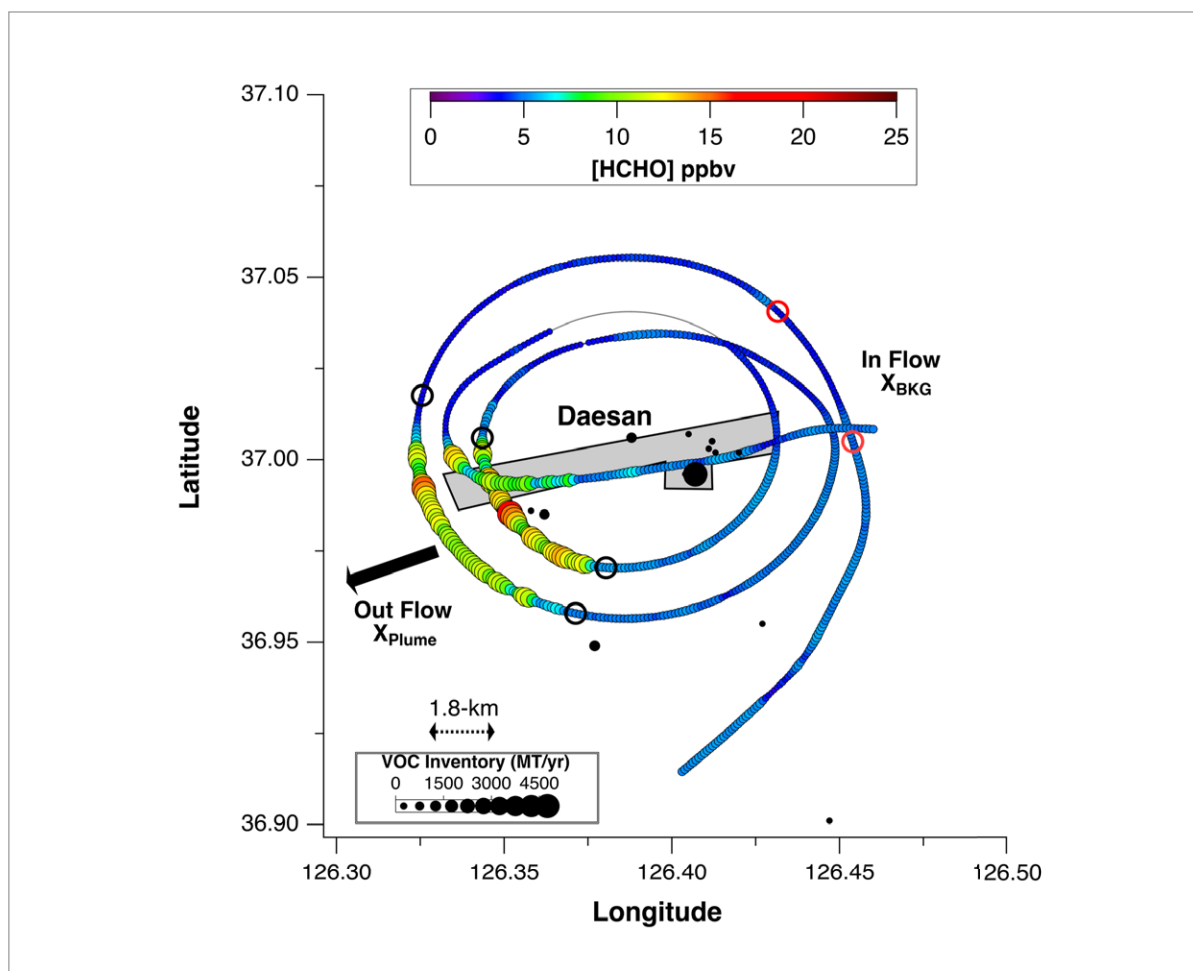


Figure 4-9. Flight tracks at altitudes around 300-m in the morning around 10:50 (local) on June 5, 2016. The Daesan complex is shown as the gray shaded region along with the largest individual VOC emission sources sized by their yearly emissions in MT/year. The flight legs are colored and sized by the HCHO concentrations measured on the DC-8. The large black arrow shows the average wind direction ($70.7^\circ \pm 13.5^\circ$) and wind speed (4.5 ± 0.7 m/s) from analysis of DC-8 wind measurements. The plume outflow boundaries are indicated here by the \bullet symbols, and the upwind inflow period by the \circ symbols. (Figure adapted from Fried et al., 2020)

In the mass balance approach, one integrates mixing ratio differences between plume outflow (X_{Plume}) and inflow (X_{BKG}) over the full plume width and over the depth of the mixed layer (from the surface to the altitude where pollutants are mixed) and uses the wind speed to estimate instantaneous emission

rates for each of the measured constituents. The 33 WAS measurements in these determinations encompass the major families of VOC compounds, including: C₂-C₁₀ alkanes, methyl substituted alkanes, cycloalkanes, alkenes, and aromatics.

Continuous fast measurements of HCHO, ethane, benzene, toluene, SO₂, and CO were used to define the plume boundaries and provide correction factors necessary to apply to the WAS VOC measurements collected at coarser time resolution. Fried et al. (2020) provides extensive details of this analysis, the underlying assumptions, and detailed estimates of uncertainties.

Panel (a) of Figure 4-10 shows the final top-down Daesan emission results in MT/year (megatons per year) based upon the mass balance approach for the 3 sampling days of this study. The top down measurements reflect the sum of the 33 VOCs from this study extrapolated to yearly estimates. This panel also shows the latest bottom-up VOC emission inventory (KORUSv5, Woo et al., 2020b, in-preparation) for comparison. The top-down estimates from the various plumes studied yield consistently higher values, ranging between 44,800 to 82,000 MT/year, and result in a grand average of $61,400 \pm 13,700$ MT/year. The top down estimate for the VOC sum is a factor of 2.9 ± 0.6 times higher than the 21,400 MT/year from the bottom-up inventory. The uncertainties in both panels of Figure 4-10 were derived from the 1σ standard deviations of the mean for the 3 sampling days. If one further considers systematic uncertainty estimates, which fold in conservative upper limits for systematic biases in the various terms in the mass balance approach, the (top down/bottom up) ratio becomes 2.9 ± 1.0 . The same approach is taken in Figures 4-11 and 4-12, with uncertainties that include possible systematic biases included in the text.

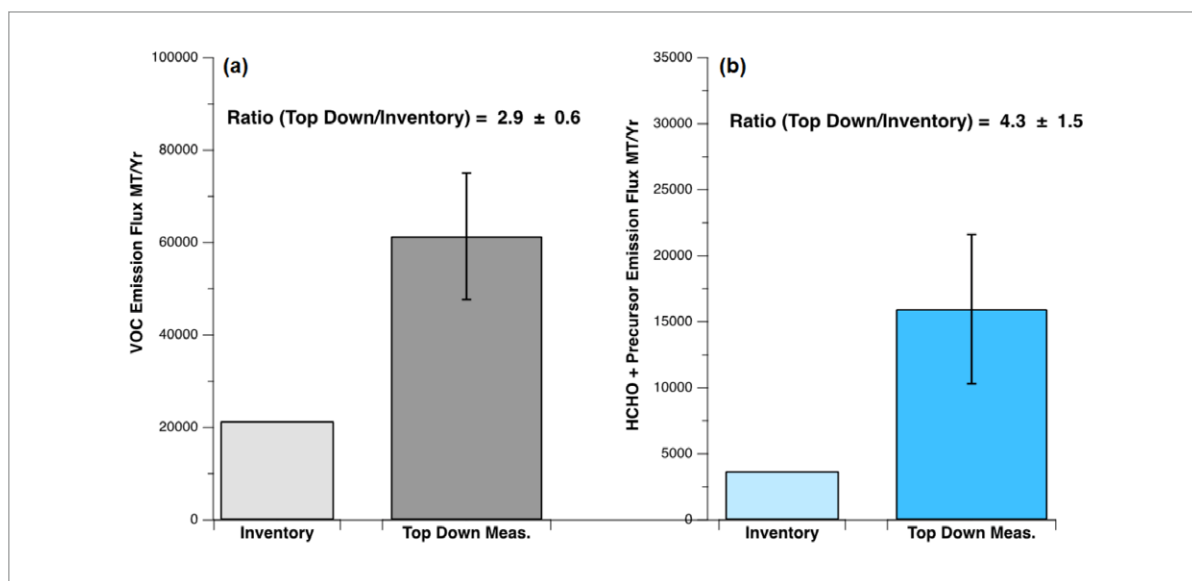


Figure 4-10. (a) Top-down total Daesan VOC yearly emission estimate with error bars reflecting the measurement imprecision (1σ level) and comparison with the bottom-up inventory estimate. (b) Similar analysis for HCHO and its four major precursors (Figure adapted from Fried et al., 2020).

Panel (b) of Figure 4-10 shows the results for a similar mass balance analysis of Daesan for HCHO and its four major precursors (ethene, propene, 1,3-butadiene, and 1-butene). The resulting top down emission estimate for HCHO and its four major precursors averages $16,000 \pm 5,700$ MT/year. This estimate is a factor of 4.3 ± 1.5 times the bottom-up estimate of 3,700 MT/year. Considering conservative upper limits for systematic biases, this ratio is 4.3 ± 1.9 .

Figure 4-11 shows two additional top down Daesan VOC flux comparisons with the bottom-up inventory based upon studies by Kwon et al. (2020) and Cho et al. (2020). Kwon et al. (2020) carried out top-down VOC emission estimates over several regions of South Korea, including the Daesan facility. This approach employed HCHO vertical column densities measured on the NASA B200 aircraft from the GeoTASO instrument, in conjunction with GEOS-Chem simulations for the total HCHO net production per unit time and with assumed HCHO yields from the various organic precursors. Using this approach, Kwon et al. (2020) determined that the Daesan VOC emission inventory is too low by a factor of 4.0 ± 2.3 , which compares well with the factor of 2.9 ± 0.6 by Fried et al. (2020) within the mutual error bars.

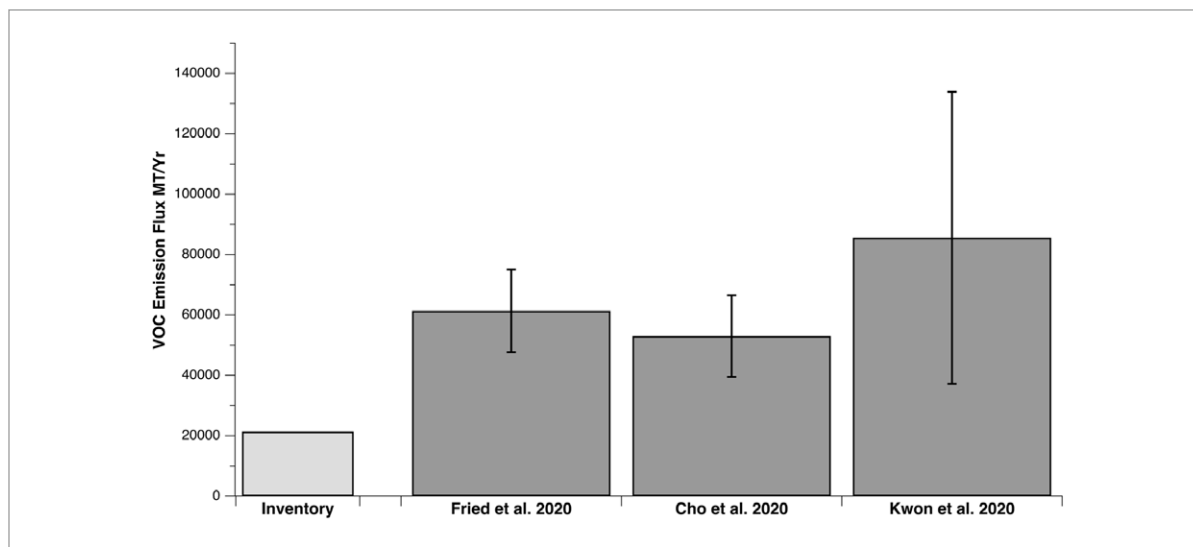


Figure 4-11. Summary of Daesan VOC emission inventory determinations in MT/year during the 2016 KORUS-AQ study. The inventory value is from Woo et al. (2020b, in-preparation), and the 3 measurements are: 1) Fried et al. (2020) from DC-8 VOC measurements employing mass balance analysis for June 2, 3, 5, 2016 plumes; 2) Cho et al. (2020) from Hanseo King Air measurements of HCHO on May 22, 2016 coupled with a 0-D box model analysis of HCHO build-up and loss; and 3) Kwon et al. (2020) from HCHO vertical column density measurements from the GeoTASO instrument on the NASA B-200 coupled with GEOS-Chem simulations for HCHO net production assuming yields from various organic precursors. The error bars represent the estimated 1σ total uncertainties for each top-down determination.

A similar top-down Daesan VOC emission effort was carried out by Cho et al. (2020) for downwind Daesan plumes captured around 2 pm local time on May 22, 2016 employing an indirect method based upon HCHO build-up and loss rates from measurements on the Hanseo King Air, a limited set of DC-8 WAS measurements acquired ~ 4.5 hours earlier, and a box model. This study deduced a lower limit of $31,000 \pm 4,750$ MT/year for Daesan VOC emissions when only parent HCHO precursors were considered. Including all Daesan VOC emissions for May 22, 2019, Cho et al. (2020) deduced a top-down value of $53,000 \pm 9,000$ MT/year, which is in remarkable agreement with the grand average of $61,400 \pm 16,600$ MT/year from Fried et al. (2020).

Collectively, all 3 studies employing different approaches indicate that the Daesan bottom-up inventory is underestimated by a factor of 2.5 to 4.0.

Fried et al. (2020) and Cho et al. (2020) also analyzed plumes from Daesan and other west coast facilities that were transported tens of km downwind over the Yellow Sea. Fried et al. (2020) report transported HCHO and benzene mixing ratios of 29.4 ppb and 4.6 ppb 44-km downwind over the Yellow Sea on June 5. Hence, under onshore wind conditions, elevated levels of these compounds and other Hazardous Air Pollutants (HAPs) such as 1,3-butadiene and their oxidation products put local communities at greater risk than the emission inventory would indicate. Thus, for the protection of local workers, their families, and nearby populations, efforts to reduce and verify ongoing changes in these emissions from west coast industrial facilities and those in other locations are strongly encouraged.

4.4.2 SO₂ and NO_x from West Coast point sources:

Unlike VOC emissions, there is greater confidence in the bottom-up SO₂ emissions inventory since it is based on actual measurements. VOC emissions at a facility like Daesan come from a wide range of sources, including fugitive emissions from a multitude of facility components and activities such as: storage tanks, transport lines throughout the complex and to/from the nearby shipping port, petroleum production and handling, as well as combustion and flaring operations. By contrast, Daesan SO₂ emissions are based on actual measurements of SO₂ inside the facility stacks acquired on a several minute time base and averaged over a year-long time period. These measurements are based on the CleanSYS, the Continuous Emissions Monitoring System (CEMS), and the resulting year-long measurements from the Korean Environmental Corporation are used to derive the 2016 CAPSS SO₂ emission inventory for the Seosan Province. Emissions of SO₂ in the Seosan Province occur primarily from 3 major categories: 1) Daesan industrial processing (sulfur recovery, petroleum production and manufacturing); 2) Daesan combustion processes associated with power generation, industrial boilers; and 3) from ship emissions. Figure 4-12 shows the SO₂ emission inventory compared to top-down estimates from six plume intercepts by the DC-8. The grand average of the top-down SO₂ emissions yields a mean and standard deviation of 13,000 ± 3,800 MT/year, which is excellent agreement with the inventory. This result lends confidence to the application of the mass-balance approach to the VOC measurements and finding that VOC emissions are underestimated in the inventory. As with the previous plots, if one folds in conservative upper limits for systematic uncertainties, the top down measurement with its total uncertainty is 13,000 ± 5,400 MT/year.

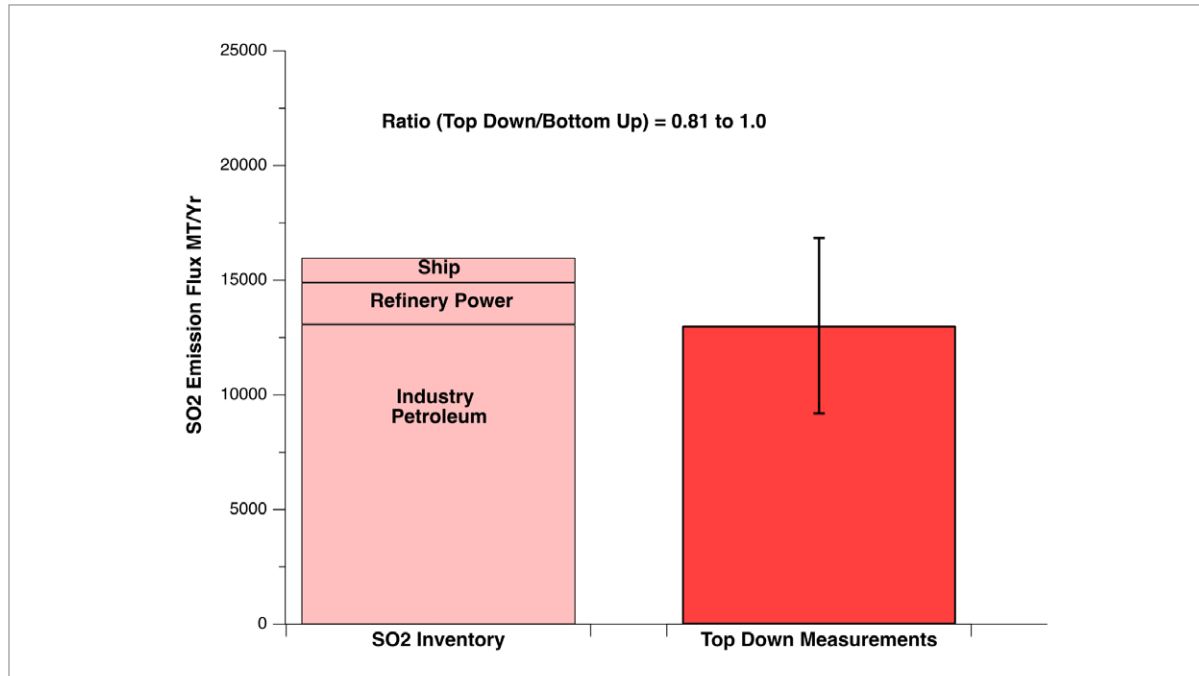


Figure 4-12. Top-down SO₂ yearly emission estimate based on the Daesan plumes sampled by the DC-8 on the 3 sampling days. The grand average of six measurements is 13,000 ± 3,800 MT/Yr (1σ standard deviation). The 2016 CAPSS SO₂ emission inventory for the Seosan Province (the province where Daesan is located) includes 3 different categories, which comprise 97% of the SO₂ emissions in this province (Figure adapted from Fried et al., 2020).

The SO₂ and NO_x emissions of five major large point sources were evaluated by comparing the emissions-based concentrations from a Gaussian plume dispersion model with aircraft-based measurements from the NASA DC-8 “around-the-stack” flights (Figure 4-13). In this example, the stacks of Dangjin Power Plant (PP) are aligned with the wind direction as in Figure 4-13b. Since the magnitude of dispersion in a Gaussian plume model only varies along the major wind direction, the model concentrations are only affected by the distance from each source stack to the measurement points. In the initial modeling of these point sources, results for Dangjin PP stood out as anomalous. This was due to the additional capacity that was not included in the official CleanSYS (i.e. Continuous Emissions Monitoring System; CEMS) emissions data. This additional capacity (increase from 4 to 6 stacks), improved model estimates from 0.36 to 0.74 times the observed DC-8 measurements for SO₂ and 0.41 to 0.83 for NO_x. Additionally, the shape of the concentration profiles from the model also matched better with DC-8 measurements when the additional stacks were added (see Figure 4-14).

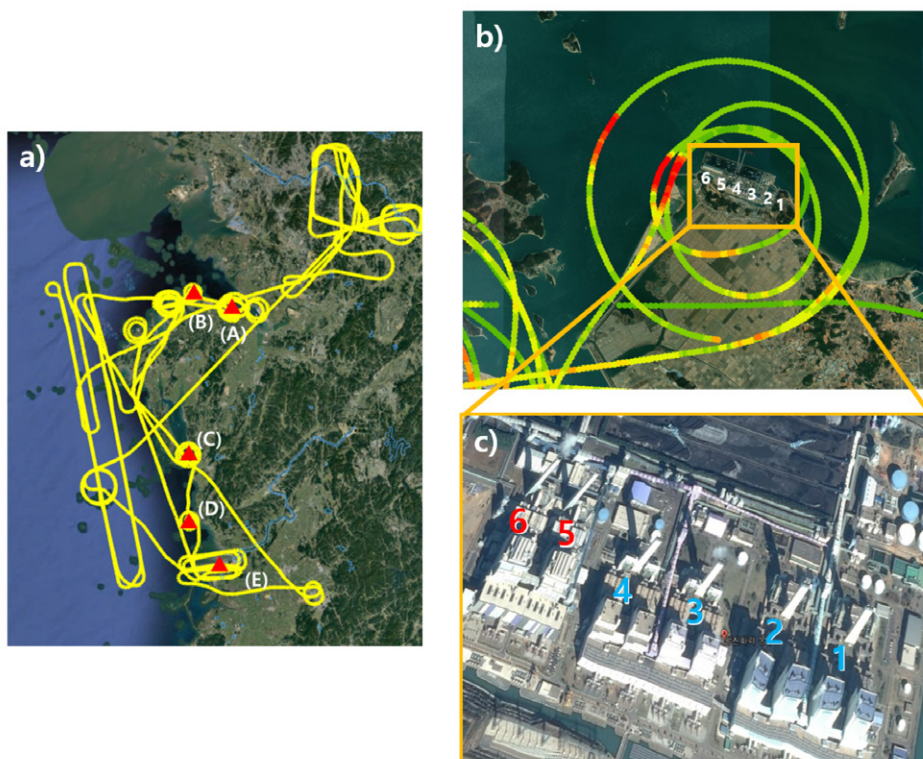


Figure 4-13. (a) Point sources sampled by the DC-8 along the west coast of Korea (A: Hyundai Steel, B: Dangjin PP, C: Boryeong PP, D: Seocheon PP, E: Gunsan IC); (b) DC-8 flight track around Dangjin PP colored by SO₂ concentration (red dots: over 70ppb); (c) Close-up of the Dangjin PP stacks. 1-4 (blue) indicate original stacks and 5-6 (red) indicate newly added capacity.

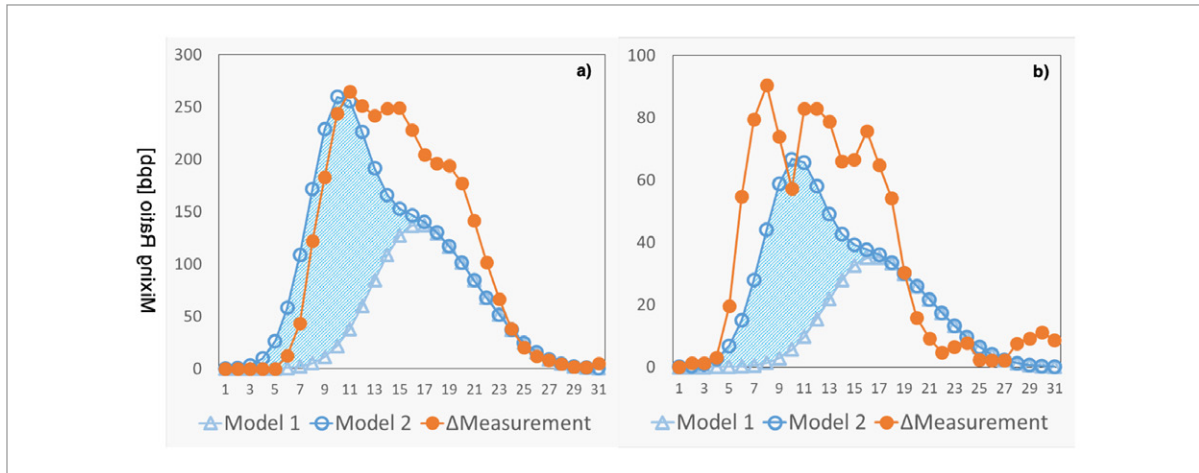


Figure 4-14. Inter-comparison between model and Δ measurement for (a) NO_x and (b) SO_2 concentration at Dangjin PP. ‘Model 1’ shows model calculations that include only stacks 1-4, and ‘Model 2’ show calculations for all six stacks. ‘ Δ Measurement’ means difference between upwind and downwind locations of DC-8 measurements. The x-axis indicates sequential DC-8 measurement points across the plume. The blue shaded part of the graphs indicates the amount of additional emissions from stacks 5-6 (i.e. Model 2 – Model 1) (M. Park et al., 2020, submitted).

After correcting the capacity at Dangjin PP, the agreement between modeled and measured concentrations for all five large point sources were in the range from 0.83 - 1.26 for NO_x and 0.74 - 0.91 for SO_2 (Figure 4-14). NO_x concentrations were overestimated by 4-26% compared to the Δ Measurement (i.e. concentration difference between upwind and downwind locations) at Hyundai Steel, Boryeong PP and Gunsan Industrial Complex (IC). NO_x concentrations of Dangjin PP and Seocheon PP were underestimated by 13-17%. Modeled SO_2 concentrations were underestimated by 9-26% (M. Park et al., 2020, submitted).

These results lend confidence to CAPSS emissions that are based on direct observations of point source emissions. However, the case for Dangjin PP emphasizes the need for the most current information. VOC estimates will remain a challenge given their diverse sources and lack of sufficient measurements.

4.5. Recommendations for Ongoing Assessments

KORUS-AQ provided an excellent opportunity to test and improve understanding of the role that emissions play in determining air quality outcomes in Korea. Observations and analysis placed particular emphasis on the highly populated Seoul Metropolitan Area. From the body of KORUS-AQ work on emissions, the following themes emerge: 1) any attempt to reduce VOC emissions must prioritize aromatic compounds, specifically, toluene and xylenes; 2) VOC emissions from industrial point sources may be grossly underestimated based on the analysis of Daesan emissions; and 3) top-down analysis of emissions using both satellite (see also Chapter 6) and in situ observations is an effective means for identifying errors in emissions inventories.

The prevalence of highly reactive aromatics in Korea play a prominent role in the chemical processes for production of both fine particle pollution and ozone. This is borne out directly in observation-based modeling. Even though these compounds are identified, their treatment in the emissions inventory does not pinpoint their specific origin. As noted earlier, control of VOCs in Hong Kong targeted 172 types of products responsible for VOC emissions. Controlling these compounds requires one to identify their commerce and the volume of products sold and used that are responsible for their emissions. **Thus, we recommend a targeted in situ source sampling program for VOCs in Seoul along with product testing to identify the many sources of aromatic compounds to enable the formulation of a strategy to address limiting their abundance.**

Industrial VOC emissions from Daesan were shown to be grossly underestimated by three independent analysis methods, while power plant emissions were largely verified by observations. This suggests that industrial point source emissions could be underestimated. The composition of these emissions is unique and can be fingerprinted based on the mix of compounds coming from the chemical processes in these facilities. As noted above, many of these compounds are toxic, such that exposures to workers and local communities are a concern and the potential for transport of industrial emissions into more populated areas deserves attention in light of underestimated emissions. The recent establishment of the Seosan research site on the Taean peninsula was an important step in enabling long-term observations to determine how Daesan and other nearby point sources affect local communities. **Based on the results of the Daesan analysis, we recommend top-down assessments of other industrial point sources employing airborne in situ observations and mass balance methods. This will help to**

determine if emissions from these types of facilities are consistently underestimated and in need of additional reduction efforts.

Top-down estimation of emissions based on remote sensing proved to be an effective complement to bottom-up methods through KORUS-AQ analyses. Both satellite observations of NO_x and airborne remote sensing of HCHO with GeoTASO were used to effectively diagnose discrepancies in emission inventories for NO_x and VOCs. The launch of GEMS will provide unprecedented spatial and temporal resolution for top-down emissions assessments across the peninsula as well as over neighboring countries (see Chapter 6 for additional discussion). Coupled to flights of opportunity for airborne in situ or remote sensing, specific targets identified by GEMS could be targeted for more detailed sampling. **We recommend a robust research program to conduct regular top-down emissions assessments with GEMS as a primary source of data to both track and verify efforts to reduce emissions of NO_x and VOCs into the future.**

Chapter 5: Air Quality Modeling

Key Points:

- Air quality models have become an essential tool for developing an efficient strategy to reduce pollutant levels. Models can account for the integrated impacts of emissions, dynamics, and chemistry; thus, they allow quantitative assessment of how local air quality is affected by local, regional, and global influences as well as the sensitivity to changes in emissions sources across these scales.
 - Recent advancements in both scientific understanding as well as modeling techniques allow us to better predict temporal evolution of air quality in local, regional, and global scales for a few hours to several days.
 - A hierarchy of models of varying scale (regional-to-global), resolution, and complexity is needed to place bounds on quantitative assessments rather than a specific answer.
 - An ensemble of model results, incorporating individual models with differing strengths and weaknesses, performs better than most individual models at representing observed atmospheric composition.
 - Ongoing model development and evaluation, in close collaboration with emissions inventory development, are needed to improve air quality forecasting.
-

During the KORUS-AQ campaign, a number of 3-D atmospheric chemistry models were used to produce 5-day air quality forecasts for aircraft observations in the peninsula and nearby oceans. The forecasts were valuable for identifying pollution plumes and other features targeted for observational sampling. These models are being used in conjunction with the KORUS-AQ observations to understand the sources of observed pollution and its variation and to identify where models and emissions can be improved. Accurate prediction of PM and ozone pollution requires accurate representation of the emissions driving the model, the representation of meteorology in the model, as well as chemical processes to produce secondary pollutants such as aerosols and ozone. Models are also the primary means of attributing the source contributions of pollution.

5.1. Evaluation of emissions

One of the important questions raised in the RSSR is “How well do KORUS-AQ observations support current emissions estimates by magnitude and sector?” Modeling analyses, combined with remote sensing and in-situ measurements, were applied to evaluate the anthropogenic emissions in Korea. Miyazaki et al. (2019), Goldberg et al. (2019), and Gaubert et al. (2020) used a top-down method integrating satellite retrievals and CTMs to evaluate the emission inventory in Korea. Oak et al. (2019) conducted a model evaluation against aircraft observations to constrain bottom-up emission estimates for Korea. These studies suggested 40-50% and 83% increases in NO_x and CO emissions, respectively, are needed for the KORUSv5 inventory in Korea. For example, Figure 5-1, taken from Goldberg et al. (2019), shows an improved agreement of WRF-Chem results with the DC-8 observations for NO_x and NO_y concentrations after doubling NO_x emissions in the KORUSv1 emission inventory. Updates in the KORUSv5 emissions were in part based on these studies. Model results using the KORUSv5 also show improved comparisons with observations in surface air for both ozone and $\text{PM}_{2.5}$ concentrations during the campaign (Figure 5-2). Note that model ensemble results incorporating individual models, each with specific strengths and weaknesses, perform better in representing observed atmospheric composition. Point sources, such as power plants, are a specific emissions category that may have a significant impact on SMA air quality. The conditions and observations during KORUS-AQ, however, were not conducive to quantifying this impact. Future work, combining observations near the point sources with model simulations will be required to study the contributions of point sources on air quality.

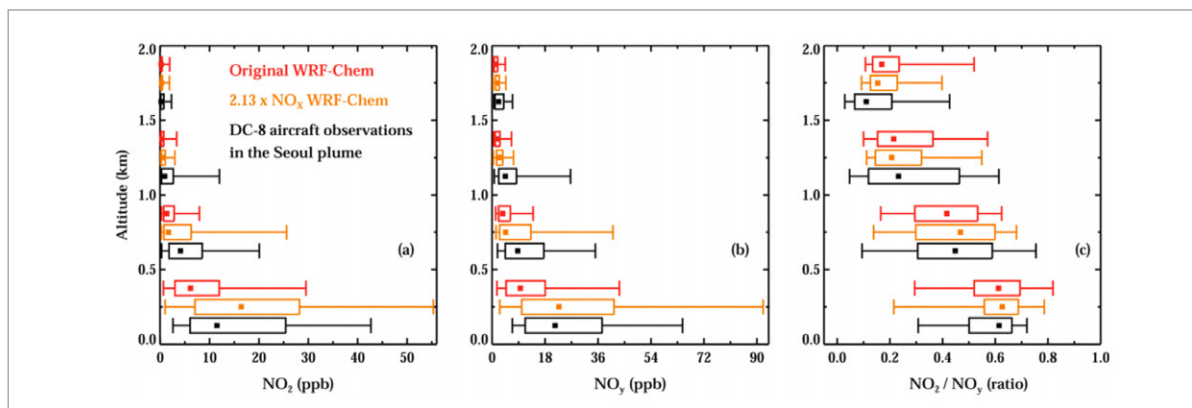


Figure 5-1. Measurements from the DC-8 aircraft binned by altitude in black for the Seoul plume (SW corner: 37.1 °N, 127.05°E; NE corner: 37.75°N, 127.85°E). Co-located WRF-Chem within the same altitude bin as the aircraft observations are plotted (vertically offset from the observations) in red for the original and in orange for the $2.13 \times \text{NO}_x$ emissions simulation. Square dots represent the median values. Boxes represent the 25th and 75th percentiles, while whiskers represent the 5th and 95th percentiles. Comparisons are for (a) NO_2 , (b) NO_y , and (c) the NO_2 – NO_y ratio when coincident NO_2 and NO_y measurements are available. (Figure from Goldberg et al., 2019)

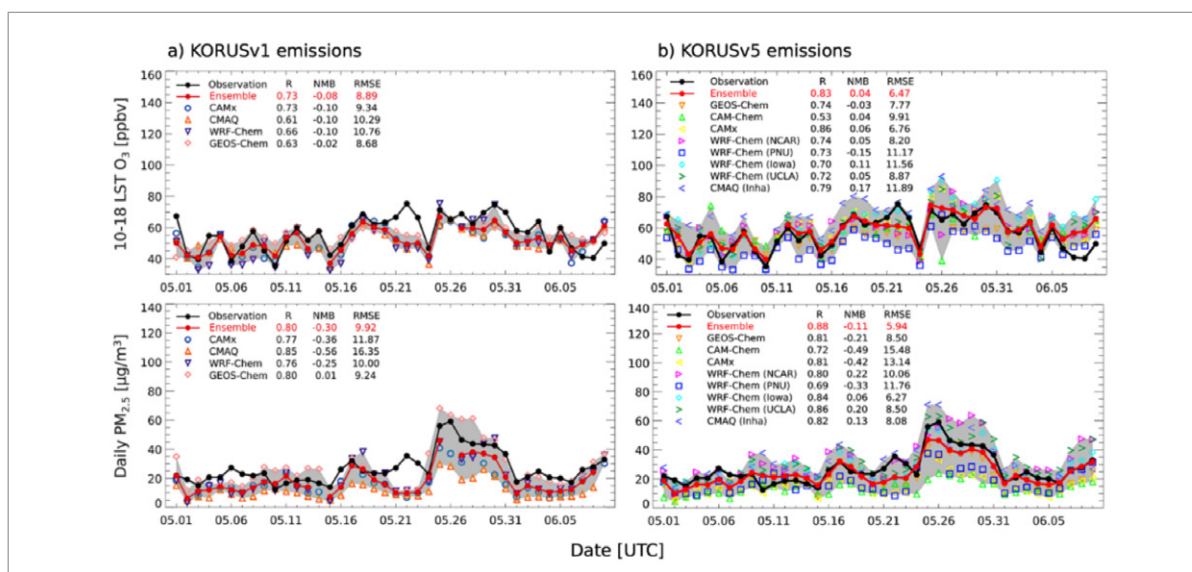


Figure 5-2. Simulated and observed daytime (8-hour average) O_3 (top) and daily $\text{PM}_{2.5}$ (bottom) concentrations averaged at AirKorea surface sites located in Seoul, Busan, Incheon, Gwangju, Yeosu, and Gangwon. Observations are in black solid lines and individual models are in different colors with the

ensemble model mean in red solid lines. Model ranges are shown in gray shades. The Pearson correlation coefficient (R), normalized mean bias (NMB), and root mean square error (RMSE) of each model and the ensemble model are denoted in the upper-left corners. (Figure from R. Park et al., 2020).

5.2. Role of modeling in synthesizing ozone observations

Chemical transport models (CTMs) with constraints based on observations from in situ and remote sensing measurements were used to identify the NO_x or VOC dependence of O_3 production throughout the country. Schroeder et al. (2020) used an observationally constrained photochemical box model to quantify O_3 production sensitivities to various precursor VOCs. They identified aromatics as the dominant VOC contributors to O_3 production, with isoprene and anthropogenic alkenes making smaller but appreciable contributions as shown in Figure 3-2 in Chapter 3. Oak et al. (2019) investigated the O_3 production sensitivity to changes in NO_x and VOCs emissions in South Korea using a 3-D CTM and emphasized the importance of concurrent reduction of both NO_x and VOC emissions to alleviate O_3 pollution especially in the major metropolitan areas (see Chapter 3 Figure 3-3).

5.3. Role of modeling in synthesizing aerosol (PM) observations

Observed $\text{PM}_{2.5}$ concentrations during KORUS-AQ reflected distinct temporal characteristics determined by synoptic meteorology (Peterson et al., 2019), with high $\text{PM}_{2.5}$ concentrations occurring during the transport period and relatively low $\text{PM}_{2.5}$ concentrations during the dynamic weather across the peninsula (Jordan et al., 2020). This observed temporal variability of $\text{PM}_{2.5}$ concentrations averaged across the AirKorea network was well captured by the models as shown in Figure 5-2, indicating the models' capability in reproducing large-scale synoptic influences.

Not only the mass concentrations but also the chemical composition of $\text{PM}_{2.5}$ differed depending on the synoptic regimes. Referring back to Figure 2-2 (Chapter 2), the enhancements of major inorganic ions concentrations mainly contributed to high PM_1 concentrations observed at the KIST site in Seoul during the transport period. Organic aerosols also contributed to high PM_1 concentrations during the transport period, but their relative contribution to PM_1 is highest during the stagnant period especially due to secondary organic aerosols (SOA) (H. Kim et al., 2018). Nault et al. (2018) used a box model with an

observational constraint to calculate SOA production from each VOC class during KORUS-AQ and showed the dominant SOA production was from the reactive aromatic species and semi-volatile and intermediate-volatility organic compounds (S/IVOCs) (see Chapter 2 Figure 2-4). Although the emission estimate of the latter needs further in-depth investigation, the two classes of compounds with a short lifetime (< 4 hr) during the day, comprise ~ 70 % of the total simulated SOA over Seoul, most of which originates from local emissions (Nault et al., 2018).

Differences in PM concentrations and its chemical composition depending on the synoptic regimes offered an insight for understanding the determining factors for PM air quality in South Korea. Using air quality models, a few studies conducted a quantitative estimation of source attribution for PM exposure in South Korea, which is discussed below. However, the use of a single or few models is subject to large uncertainty associated with quantitative estimates. In order to overcome this limitation, the use of multi-model ensembles is highly recommended, as shown in Figure 5-2.

R. Park et al. (2020) used the observations from aircraft platforms and surface networks during the campaign to evaluate and inter-compare air quality simulations for the campaign. Models were extensively examined to determine their capability for reproducing observed chemical composition for the KORUS-AQ campaign. Figure 5-3 shows a comparison of the observed versus simulated PM_{10} chemical composition at the KIST ground site in Seoul during the campaign. First of all, the temporal variability of the observed PM_{10} mass concentrations, being high in the transport period and low in the dynamic weather period, was well captured by the model ensemble but with large inter-model variability. In addition, the simulated enhancement of SOA concentrations during the stagnant period was not as large as that of the observations, resulting in an underestimate of PM_{10} concentrations in the model ensemble, which typically overestimated the observations for other regimes. The large contribution from the major inorganic ions to PM_{10} during the transport period was well reproduced by the models.

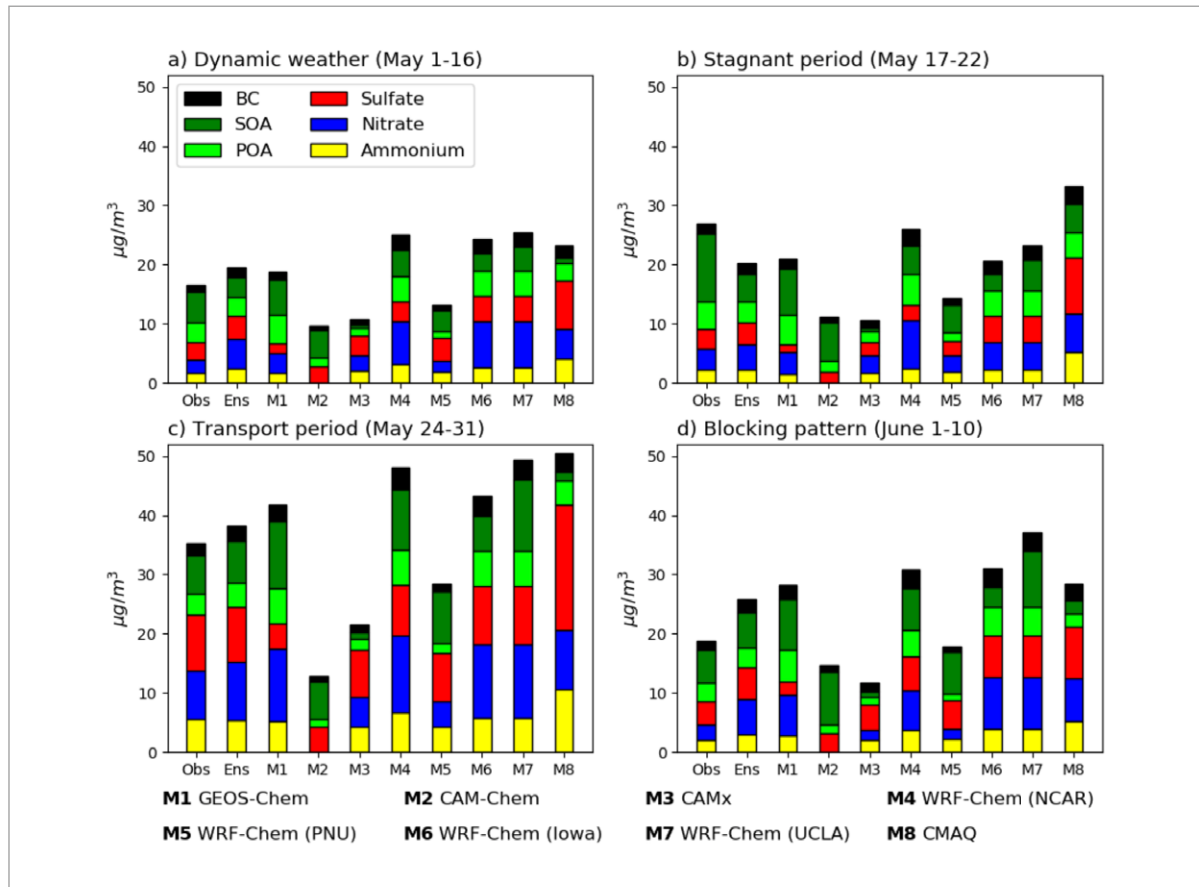


Figure 5-3. Comparison of simulated and observed mean PM_{10} chemical compositions in surface air for different synoptic regimes during the campaign. Each chemical component is indicated in different colors and the observations are from AMS at the KIST ground site (127.045°E, 37.601°N). Model results from the lowest model layer were sampled coherently with the observations. (Figure from R. Park et al., 2020)

5.4. Attribution of source contributions

One of the main scientific questions that the KORUS-AQ campaign aimed to resolve was the quantification of transboundary and local impacts on regional air quality. Several studies conducted source attribution analyses using global CTMs, back-trajectory analysis, and satellite remote sensing to identify source regions, from which air pollutants affecting air quality in South Korea originated. Several of these studies are summarized in Table 5-1, however each study used a single model or technique and looked at different parameters. In addition, none of these studies used the final KORUSv5 emissions inventory.

This summary shows that there can be significant variation in source contribution due to meteorological conditions and also depending on which parameter ($PM_{2.5}$, BC, CO, ozone) is studied.

J. Choi et al. (2019) used an adjoint model (based on KORUSv2 emissions) to calculate regional source contributions to $PM_{2.5}$ in Korea for different synoptic patterns. Their results indicated that contributions from emissions in China amounted to 68% during the extreme pollution event (May 24-31), which was accompanied with rapid eastward transport, while domestic contributions were more important (up to 57%) during the blocking period (June 1-10), showing the important role of synoptic meteorology in determining transboundary transport of air pollutants (Table 5-1). Tang et al. (2019) used a tagged CO simulation and found that Chinese contribution to CO in Korea was 44-64% during a plume event on May 31 (transport period) and 11-20% on June 5 (blocking period). Miyazaki et al. (2019) ran a model experiment setting to zero the NO emissions in China to approximate the contribution of ozone from China. The results for one strong transport day (May 25) show approximately 25 ppb of ozone over Seoul could be attributed to emissions in China. Lamb et al. (2018) identified regional contributions to vertically resolved BC (black carbon) concentrations using a back-trajectory model. Similar to the CTM-based studies, the dominant contribution between 400-900 hPa during the transport period was from China. Geostationary satellite observations of AOD (aerosol optical depth) over East Asia during the transport period showed supporting evidence of the large contribution of air pollutants that were generated in east-central China (Lee et al., 2019).

The quantitative estimates of CO, ozone and PM source attribution using a single 3-D air quality model are subject to large uncertainties because of inaccurate representation of meteorological, chemical, and physical processes in the model. As shown above, the model ensemble always outperforms individual models in reproducing observations and thus, the use of a multi-model ensemble for estimating regional source contributions to PM and ozone concentrations in South Korea is needed to quantify source contributions more accurately.

Table 5-1. Source contributions [%] to South Korea pollution for a variety of pollutants and metrics during KORUS-AQ.

Pollutant or metric	Korea	E. Asia (no Korea)	Method, Reference
Pop. exposure to PM _{2.5}			
Dynamic Weather:	50	46	Adjoint model (using KORUSv2.1 emissions), J. Choi et al., 2019
Stagnant:	34	63	
Extreme Pollution:	26	71	
Blocking:	57	37	
CO over Korea for DC-8 track over Seoul below 850 hPa (all days):	11-24	39-71	3D model tagged CO from an ensemble of emissions, Tang et al., 2019 (Table 2)
GOCI AOD and back trajectories	16-64	30-61	GOCI, Figure 10 (Seoul R1 vs R2+R3+R4) of Lee et al., 2019
O ₃ on May 25	n/a	25	Model with zeroed NO emissions Figure 3 of Miyazaki et al., 2019

5.5. Concluding Remarks

The modeling of air quality and atmospheric composition depends strongly on the accurate representation of reality, including meteorology, chemistry, and emissions. The varying weather patterns encountered during KORUS-AQ highlight their impact on pollutant amounts and distributions. On a finer scale, land-sea breezes were seen to rapidly change ozone and PM_{2.5} amounts across Seoul. The complex terrain around Seoul also contributes to the challenges in simulating meteorology and consequently air quality. Our understanding of anthropogenic emissions in South Korea was improved based on the scientific findings from KORUS-AQ, resulting in an improved model agreement with the observations for ozone and PM. However, some precursor species (e.g., NH₃, S/IVOCs) contributing to high PM formation still need further investigation to obtain quantitative emission estimates. PM concentrations in South Korea were still largely contributed by major inorganic ions but the importance of SOA is growing especially by local emissions of its precursors. SOA formation is governed by complex chemistry, which is still poorly parameterized in air quality models. Ongoing model development and evaluation, in close collaboration with emissions inventory development and improved scientific understanding of chemistry and meteorology, are needed to improve air quality forecasting.

Chapter 6: Satellite Remote Sensing

Key Findings

- Airborne mapping spectrometer observations of NO_2 and HCHO during KORUS-AQ are prototypes for GEMS observations and highlight the revolutionary air quality information that will be provided by routine hourly high spatial resolution GEMS data.
- The ratio of tropospheric column HCHO to NO_2 , often used as an indicator of the sensitivity of ozone formation to column VOC or NO_x reductions, varies significantly among the different measurement and modeling perspectives.
- High spatial resolution airborne remote sensing observations clearly identify large point source emissions of SO_2 and NO_x and the spatial extents of their resulting downwind plumes. Long-term averaging of GEMS observations within different meteorological regimes should also allow such sources to be characterized.
- Geostationary satellite observations with back-trajectory analysis provide valuable evidence for the long-range transport (LRT) of aerosols. LRT cases originating from the boundary layer of east-central China usually contribute to the high AODs in Korea, while air masses coming from above the boundary layer in north China and Mongolia did not relate to the high AODs in Korea.
- Satellite remote sensing by GOCI and AHI provides a broader view of the aerosol spatial distribution and plume movement tracking with high temporal resolution. GeoTASO successfully demonstrated the capability of GEMS to observe pollutant gases. However, remote sensing provides columnar information lacking surface concentration, and full interpretation requires in situ measurements and chemistry-transport models as a complement.

Remote sensing observations from many different perspectives were part of KORUS-AQ, including satellite, airborne, and ground-based instruments. An objective was to prototype the integrated observing and modeling system that will begin with the GEMS era. GEMS is a UV-Visible spectrometer measuring the radiance spectrum of 300-500 nm with a

spectral resolution of 0.6 nm (J. Kim et al., 2020). While it is clear that the high-resolution observations from GEMS many times per day will provide revolutionary information, it is also clear that interpreting the observations using complementary surface measurements and, whenever possible, vertical profile measurements, will be necessary to make full use of the GEMS observations. Studies using airborne GEMS-like measurements during KORUS-AQ have demonstrated the potential for systematic GEMS observations to provide improved top-down emission constraints for NO_2 , HCHO , and SO_2 across the GEMS field of regard. Aerosol observations from current sensors including AHI, AMI, and GOCI show ability to help distinguish aerosol pollution from transported and local sources.

6.1. Prototype GEMS observations from airborne mapping spectrometer measurements

The NASA King Air carrying the Geostationary Trace gas and Aerosol Sensor Optimization (GeoTASO) instrument was flown in a regular grid pattern to provide first-ever continuous high-spatial-resolution maps up to 4 times per day of NO_2 and HCHO , two key species that will be measured by GEMS. These data illustrate for the first time the tremendous spatial and temporal variability of the distributions of important precursors to ozone and aerosol formation across the SMA. KORUS-AQ provided SMA diurnal mapping observations on two different days.

June 9 was a unique measurement day as the northern portion of the SMA was mapped four times from early morning through late afternoon (Figure 6-1). The observations span a similar range of times of day as GEMS observations but are only half as frequent as hourly GEMS observations because the aircraft required 2 hours to cover the area shown on each map. This day was late in the KORUS-AQ campaign and followed the passage of a weak cold front that terminated a meteorological blocking pattern and is considered a weak transport period, characterized by moderately high O_3 and PM levels (Peterson et al., 2019). White arrows in Figure 6-1 show 6-hourly archived winds averaged through the lowest 500m above ground level from the Global Data Assimilation System (GDAS) at 00:00 UTC (09:00 LT) and 06:00 UTC (15:00 LT). As described by Judd et al. (2018), relatively light winds during the morning hours resulted in NO_2 patterns that reflect emission sources in localized industrialized regions and transportation corridors. NO_2 levels generally increase from early morning to late morning, reflecting ongoing emissions

at a faster rate than NO_2 removal processes. By early afternoon, as the planetary boundary layer heights increase and surface NO_2 is mixed through a deeper layer, the NO_2 distribution appears as a broader enhancement over much of the SMA instead of reflecting localized source regions, while overall column amounts continue to increase. Wind speeds have increased and shifted to westerly, beginning to generally transport this broad pollution plume to the east, as reflected by decreased NO_2 values near the west coast and increased values over the central SMA. By late afternoon the largest NO_2 amounts have shifted still further east over the SMA, reaching the Taehwa Research Forest site.

HCHO, often used as an indicator of total VOC abundance, shows a diurnal behavior on June 9 with some similarities to that of NO_2 but also important differences. HCHO abundances in the early morning are relatively uniform across the entire SMA domain, although there are some isolated enhancements in the western SMA (e.g. Incheon and Gimpo areas) that are collocated with NO_2 enhancements, indicating anthropogenic emission sources. As the day progresses, column HCHO values increase by factors of up to 4 in an increasingly homogeneous SMA plume. This is similar to the NO_2 diurnal behavior although the largest HCHO amounts are farther to the south and do not coincide with the largest NO_2 amounts. By late afternoon the peak HCHO amounts have decreased but are farther east, including the Taehwa area. Because HCHO is dominated by photochemical production resulting from many VOC precursors, it is more difficult to attribute local enhancements to individual sources. Its distribution is clearly influenced by emissions, meteorology, and chemistry, like NO_2 , however the differences in diurnal evolution of the two species complicate the inference of resulting ozone production.

May 17 was the other day in which SMA was mapped by GeoTASO in both morning and afternoon. The flights on this day covered a much larger area, extending farther to the western, eastern, and southern portions of SMA, thus a single mapping occurred during the morning hours and a single mapping occurred during the afternoon hours (Figure 6-2). This day, approximately one-third of the way through the KORUS-AQ campaign, was during the meteorological period of stagnant conditions under a persistent

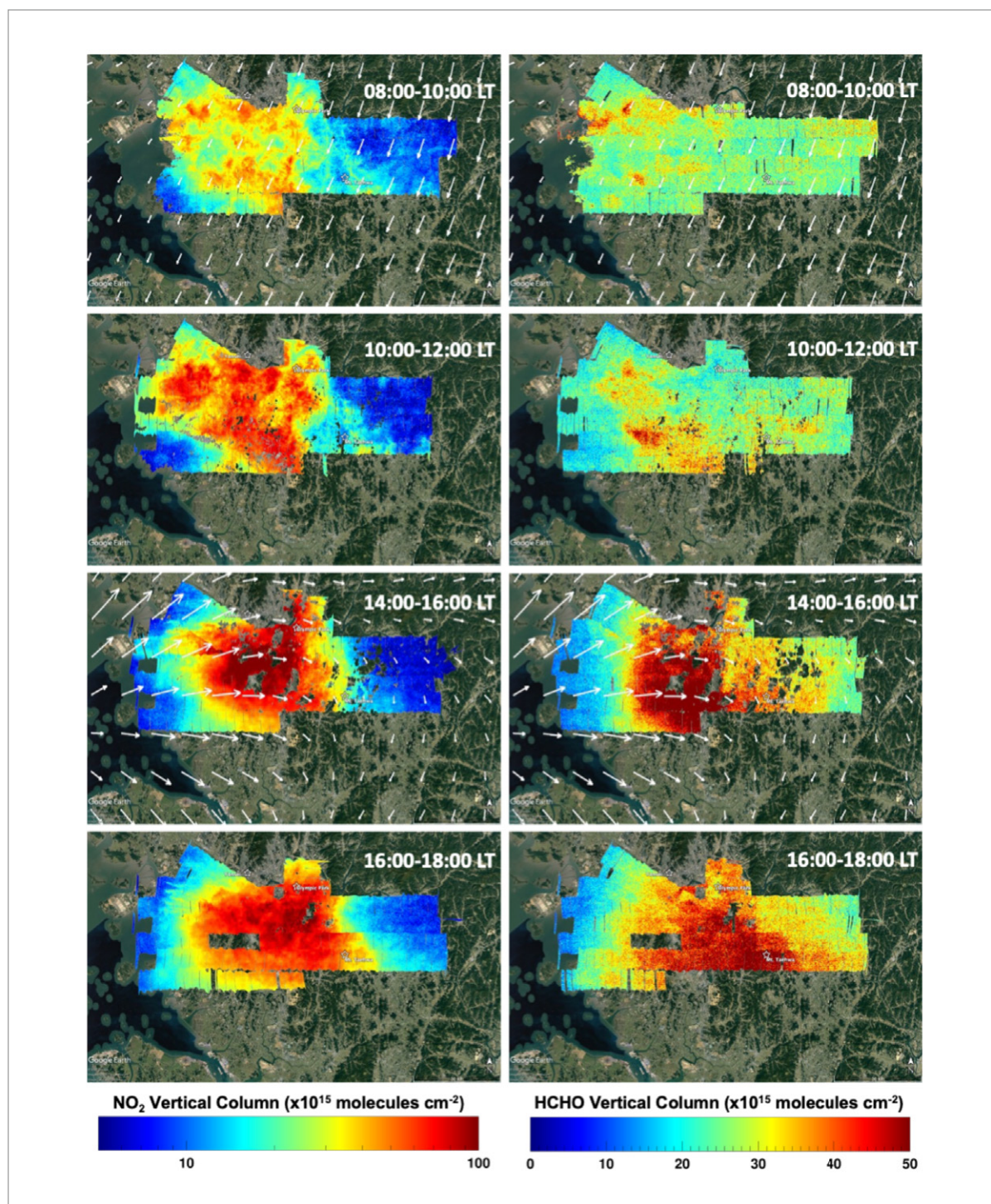


Figure 6-1. GeoTASO observations of tropospheric vertical column NO_2 (left) and HCHO (right) on June 9, 2016, acquired at 4 times of day progressing from early morning (top) through late afternoon (bottom). (Figure adapted from Judd et al., 2018).

anticyclone, leading to some of the highest ozone levels of the study period (Peterson et al., 2019). Light near-surface winds in the morning were southerly over the western part of the domain, and near the coast NO_2 plumes emanating from large point sources are clearly evident flowing to the north. (See also Figures 6-4(b) and 6-4(c) for additional information on these large point sources as observed in SO_2 .) In the central part of the domain the morning winds were essentially stagnant such that the highest NO_2 amounts occur very close to sources. By afternoon the winds have shifted to northwesterly and the NO_2 distribution has increased dramatically and become more homogenous, with an urban plume extending from the center of Seoul southeast past Taehwa. Another notable feature is the isolated plume emanating from a location southeast of Taehwa, very near the location of a large chemical manufacturing facility.

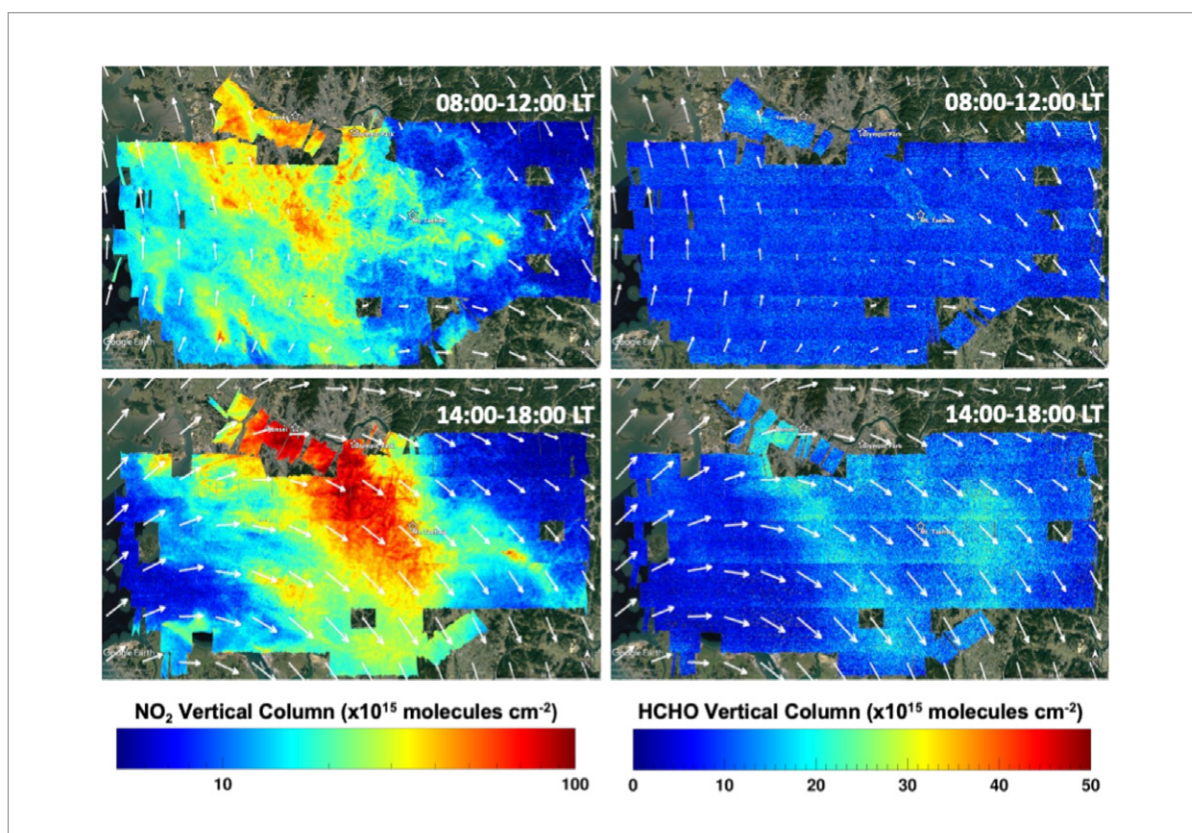


Figure 6-2. GeoTASO observations of tropospheric vertical column NO_2 (left) and HCHO (right) on May 17, 2016, acquired over a large SMA domain in the morning (top) and afternoon (bottom). (Figure adapted from Judd et al., 2018).

The behavior of HCHO is very different on May 17 than on June 9. In the morning, column amounts are uniformly 2-3 times lower all across the SMA than on the morning of June 9. By the afternoon of May 17 there are moderate broad enhancements of up to a factor of two to the southeast of Seoul that are not coincident with the peak of the NO₂ plume (which actually corresponds to a minimum in HCHO).

The much lower “baseline” HCHO values observed in May than in June are believed to be, to first order, a temperature or length-of-daylight effect in which emissions of biogenic VOC precursors to HCHO increase with temperature or actinic flux. GeoTASO observations over the Olympic Park and Taehwa Forest sites (not shown) indicate monotonic increases in HCHO from May 1 through June 10 (by factors of ~3 at Olympic Park and ~4 at Taehwa). Both May 17 and June 9 were ozone exceedance days in Korea, with similar ozone values observed on each day (Peterson et al. 2019, Figure 3). These large-scale similarities in ozone are notable given that similar NO₂ amounts were observed on each day but the VOC amounts, as indicated by HCHO, were very different.

6.2. Ozone formation in Seoul: NO_x-limited or VOC-limited

Ozone formation sensitivity was one of the key questions of the RSSR. The patterns of column HCHO and NO₂ over Taehwa Research Forest, located in the southeastern part of SMA (~ 55 km distance), were investigated to evaluate the sensitivity of ozone production as observed by remote sensing. Schroeder et al. (2020) reported that the Seoul and Taehwa regions belonged to the VOC-limited regime during KORUS-AQ, which was supported by model calculations constrained by observations. However, in the absence of detailed in situ observations, the ratio HCHO/NO₂ has been posited to be a proxy for the non-linear sensitivity of ozone to VOC and NO_x precursor emissions.

Previous studies have used column HCHO/NO₂ ratio as an indicator of surface ozone sensitivity and the threshold values of the photochemical regime were estimated differently depending on the study area and the observation data (Tonnesen and Denis, 2000; Martin et al., 2004; Duncan et al., 2010; Choi et al., 2012; Jin and Holloway., 2015; Chang et al., 2016). Martin et al. (2004) analyzed the GEOS-Chem and OMI observations in North America, East Asia, and Europe and estimated that the ozone sensitivity transition point is when the column HCHO/NO₂ ratio is 1. Subsequent work has shown this transition point to actually be a transition range with values that can be quite variable depending on conditions. Additionally, Schroeder et al. (2017) showed that the transition range also changes when assessing in situ

observations (values of 0.9 to 1.8) versus column amounts (values of 1.1 to 3.0). Schroeder et al. also emphasized that the ratio can change substantially with time of day, raising questions about the viability of using satellite observations at a single time of day to diagnose sensitivity.

Figure 6-3 explores the variations of tropospheric HCHO and NO₂ columns and their column ratios (HCHO/NO₂) across a range of perspectives from in-situ observations, ground and satellite remote sensing, modeling outputs, and GeoTASO remote sensing at the suburban Yeosu/Taehwa Research Forest (TRF) site. While most HCHO/NO₂ values fall within the ambiguous transition range of ~1-3, values occurring outside this range are almost exclusively on the low side, below 1, indicating VOC-limited conditions. DC-8 measurements indicated varying amounts of VOC-limited conditions with the strongest shift towards values below 1 at midday. By contrast, Pandora column measurements fell almost exclusively in the transition range with values trending toward the NO_x-limited regime with time of day. By afternoon, the upper quartile of values were greater than 3 and clearly in NO_x-limited conditions. The inconsistency of photochemical regimes is due to Pandora HCHO column being 16% larger than DC-8 integrated column density during hot afternoons in particular (Spinel et al., 2018, 2020). GeoTASO measurements showed an opposite trend towards more VOC-limited conditions as the day progresses. For GeoTASO, roughly half of the values were less than 1, firmly in the VOC-limited regime. For satellite observations, OMI data at midday fell entirely in the transition range while morning data from GOME-2B

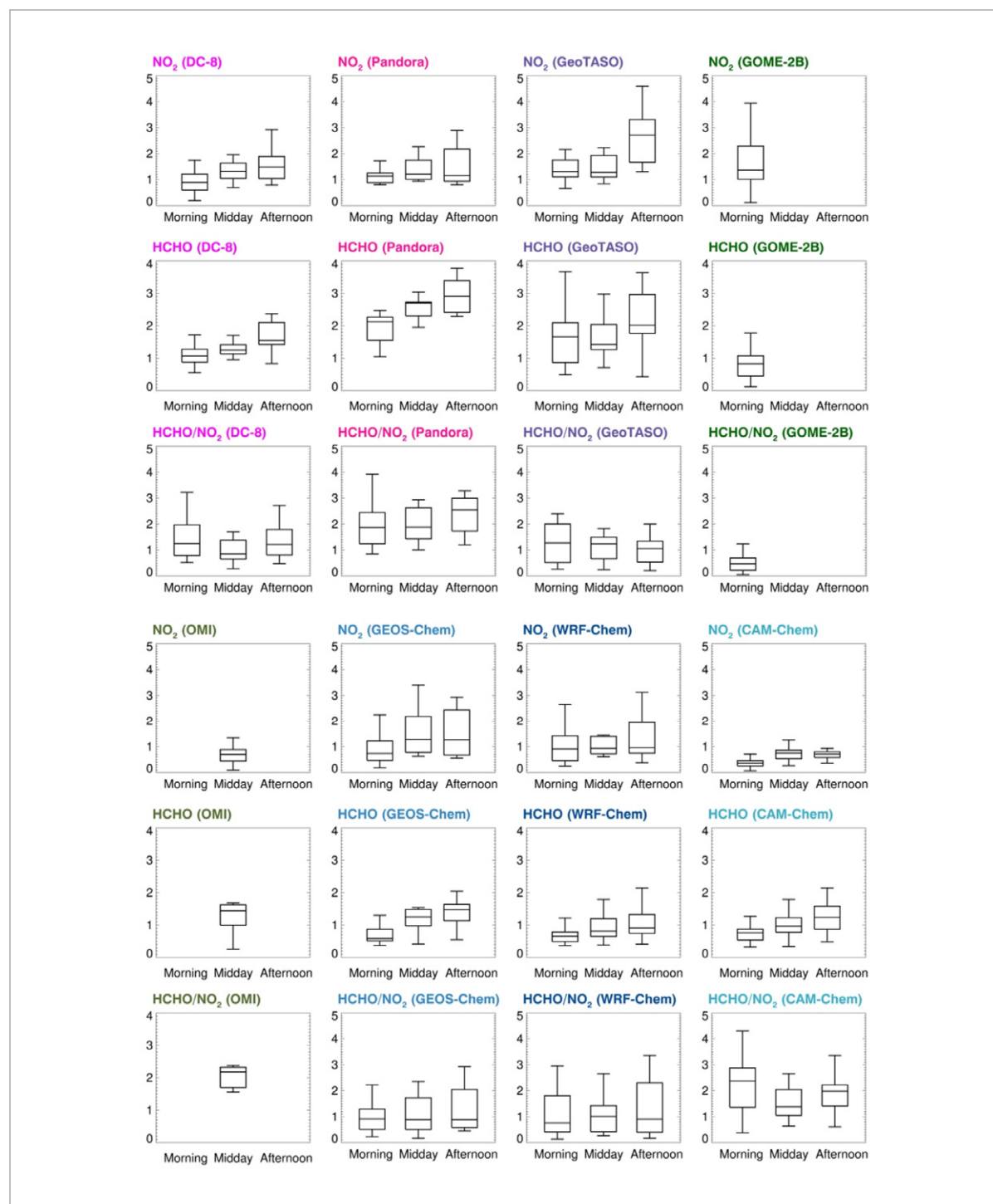


Figure 6-3. Comparison of DC-8 observations, ground and GeoTASO and satellite remote sensing, and model simulations for column NO_2 , HCHO, and HCHO/ NO_2 over Taehwa Research Forest according to the measurement time. Upper three rows show NO_2 , HCHO and HCHO/ NO_2 ratio from DC-8, Pandora,

GeoTASO and GOME-2B measurements, and lower three rows show the same from OMI measurements and model results from GEOS-Chem, WRF-Chem and CAM-Chem. (Figure taken from Koo et al., in preparation)

showed a VOC-limited regime. Both the differences in observation time and pixel size between OMI and GOME-2B may influence their results. GEOS-Chem, WRF-Chem, and CAM-Chem showed similar results for HCHO column as it increased from morning to afternoon. However, HCHO/NO₂ ratio values were different for each model due to their very different NO₂ behaviors. GEOS-Chem and WRF-Chem trended toward a VOC-limited regime, but WRF-Chem data were shifted more heavily into the transition range and into a NO_x-limited regime for some data. During the KORUS-AQ period, HCHO tropospheric columns increased gradually over time as temperature also increased. Observations and model results for HCHO were generally consistent. However, the variations of NO₂ tropospheric columns between the observations and the models are much larger than the variations of HCHO tropospheric columns. The inconsistency of the NO₂ tropospheric column patterns drives the differences in column HCHO/NO₂ between the various observational and modeling perspectives. Different sampling characteristics is one cause of the apparent NO₂ differences. While model output can be uniformly sampled at all times through the period, the aircraft data are only available on flight days and times and the Pandora data and satellite data are continuous, though may have gaps due to clouds or quality screening. Nevertheless, differences between models were just as large as between observations.

These differences in what has been one of the more common remote sensing approaches to evaluating ozone production sensitivity illustrate how the column observations must be assessed within a broader integrated strategy that includes models and surface measurements.

6.3. The detection of the large point sources along the west coast

The capability of high-resolution remote sensing to detect SO₂ emission sources was demonstrated successfully by generating SO₂ maps from GeoTASO airborne measurements during KORUS-AQ (Chong et al., 2020). GeoTASO measurements with the high spatial resolution of 250 m x 250 m can detect small SO₂ emission sources and emitted plumes even from a single overpass, without merging many

observations. SO₂ column retrievals from GeoTASO provide 2-dimensional snapshots of SO₂ emissions from point sources along the west coast, particularly in the northern area of South Chungcheong Province (Chungnam) (Figure 6-4). In general, the largest SO₂ column amounts were observed around industrial facilities at which Stack Tele-Monitoring (TMS) devices measured high SO₂ emission rates. GeoTASO observations demonstrate that the spatial distribution of SO₂ concentrations around the point sources can largely vary with wind conditions, implying that SO₂ emissions from these sources can affect the air quality in the vicinity. For instance, in the morning of 17 May (Figure 6-4b), the SO₂ plume reached close to southern Gyeonggi Province, but the SO₂ columns decayed by a factor of 1/e at ~1 km away from source number 6. More frequent and long-term observations from nadir-viewing airborne remote sensing instruments can provide useful information for assessing the impact of those point sources on the air quality of SMA. As discussed in Chapter 4 of this report, long-term GEMS observations will provide useful top-down constraints for emissions inventory evaluations over time.

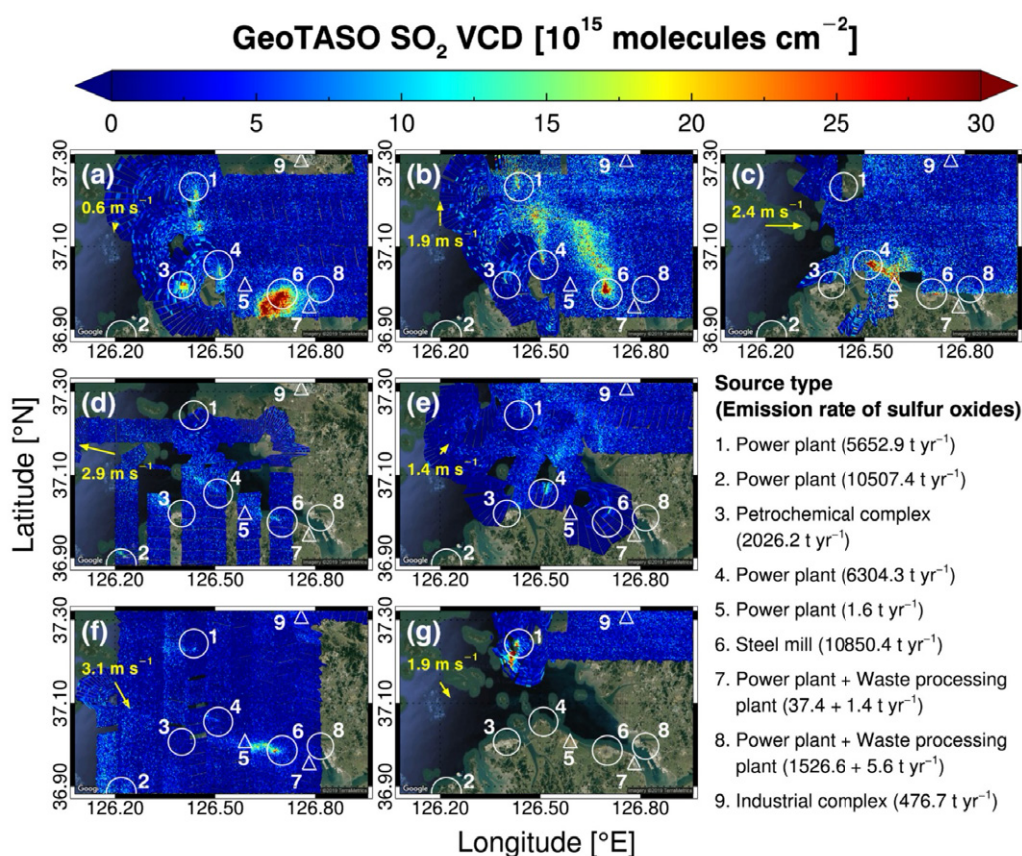


Figure 6-4. Enlarged views of GeoTASO SO₂ observations over the northern Chungnam area. The seven flights shown covered this region on (a) 11 May 08:58-11:23 LT; (b) 17 May 08:39-11:05 LT; (c) 17 May 14:10-16:31 LT; (d) 22 May 09:52-11:52 LT; (e) 2 June 10:19-11:47 LT; (f) 5 June 13:26-16:55 LT; and (g) 9 June 07:48-11:51 LT. Mean wind speed and direction obtained from the ERA5 data during each GeoTASO flight over this area is indicated in yellow. Nine SO₂ emission sources listed in the Stack Tele-Monitoring (TMS) reports for this region are numbered and marked with circles and triangles. The circles indicate SO₂ sources with SO_x emission rates of >1 kt yr⁻¹ on average during 2015-2017, while the triangles represent the sources with mean SO_x emission rates lower than 1 kt yr⁻¹ for the same period. A radius of each circle is proportional to the logarithm of a mean SO_x emission rate measured by Stack TMS devices at each facility in 2015-2017. The emission type of each numbered source and the corresponding 3-year mean SO_x emission rate from the Stack TMS reports are indicated (Maps were created using Google Earth Imagery.) (Figure taken from Chong et al., 2020).

6.4. Transport of aerosol air pollution from sources across regional to continental to hemispheric scales

The issue of how Seoul is affected by transport of air pollution from sources across regional to continental to hemispheric scales was another key RSSR question that can be partially addressed by satellite observations. Geostationary satellites have the advantage of monitoring the diurnal variation of aerosols and trace gases.

During KORUS-AQ, multiple satellite sensors provided AOD products with high accuracy, which enables monitoring of the spatio-temporal aerosol distribution in East Asia (M. Choi et al., 2019; Gupta et al., 2019). Satellite data fusion can be considered as a way of obtaining accurate aerosol optical properties with high spatio-temporal resolution (Lim et al., 2018; M. Choi et al., 2019; Lim et al., 2020). A Level-2 satellite fusion product can improve estimates of Aerosol Optical Depth (AOD) and aerosol type by using multiple products from different instruments and algorithms. During KORUS-AQ, Advanced Himawari Imager (AHI) and Geostationary Ocean Color Imager (GOCI) data were used as proxies for a fusion product from Advanced Meteorological Imager (AMI) and GOCI-2 data, respectively.

The utility of the fusion product for assessing transport is illustrated in Figure 6-5, according to the four representative meteorological situations during the campaign defined by Peterson et al. (2019). First, during the blocking period case (right-bottom), higher AODs were observed over eastern China than in the other meteorological regimes. On the other hand, during the stagnant period case (right-top), wildfire aerosol transported from Russia to the Hokkaido region in Japan was stagnated, leading to high AOD. While the majority of the wildfire aerosol plume continued to move eastward over the Pacific Ocean, a portion of the plume was entrained into the broad anticyclone to head back to the Korean Peninsula. However, when considering the distance traveled and relatively weak low-level wind speeds, any residual smoke particles reaching the study region were diffused and well mixed with local pollutants. The case of the transport period (left-bottom) shows that the AOD observed over China was being transported through the Korean Peninsula to Japan, consistent with the meteorological wind fields (black arrows). By improving the accuracy of AOD measurements in Northeast Asia through this fusion process, more accurate input can be used for data assimilation.

During the transport period, airborne LIDAR measurements of vertical extinction profiles by DIAL/HSRL combined with GOCI AOD observations revealed the 3-D structure of long-range transported aerosols

on May 25th, 2016 as shown in Figure 6-6. Vertical profiles of aerosol extinction across the North-South cross section along the longitude of 124°E over the Yellow Sea show a transported aerosol plume confined within the boundary layer height of 1.5 km. GOCI AODs shown by the map also indicate aerosol plumes transported from China to the Korean Peninsula during this meteorological transport period.

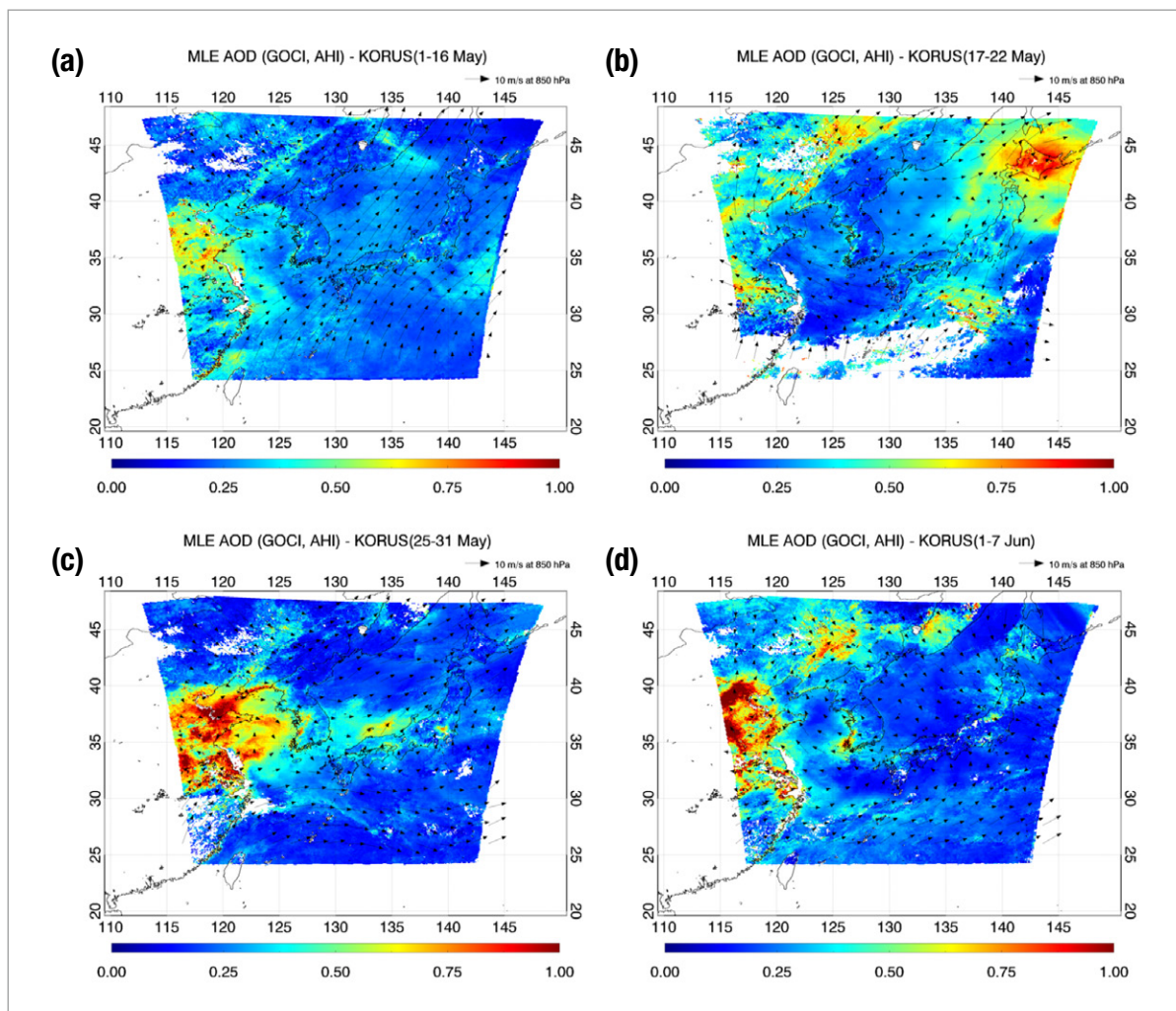


Figure 6-5. Average of AHI fusion AOD during the KORUS AQ campaign ((a): Dynamic period, (b): Stagnant period, (c): Transport period, (d): Blocking period). (Figure taken from Kim, Al-Saadi et al., in preparation)

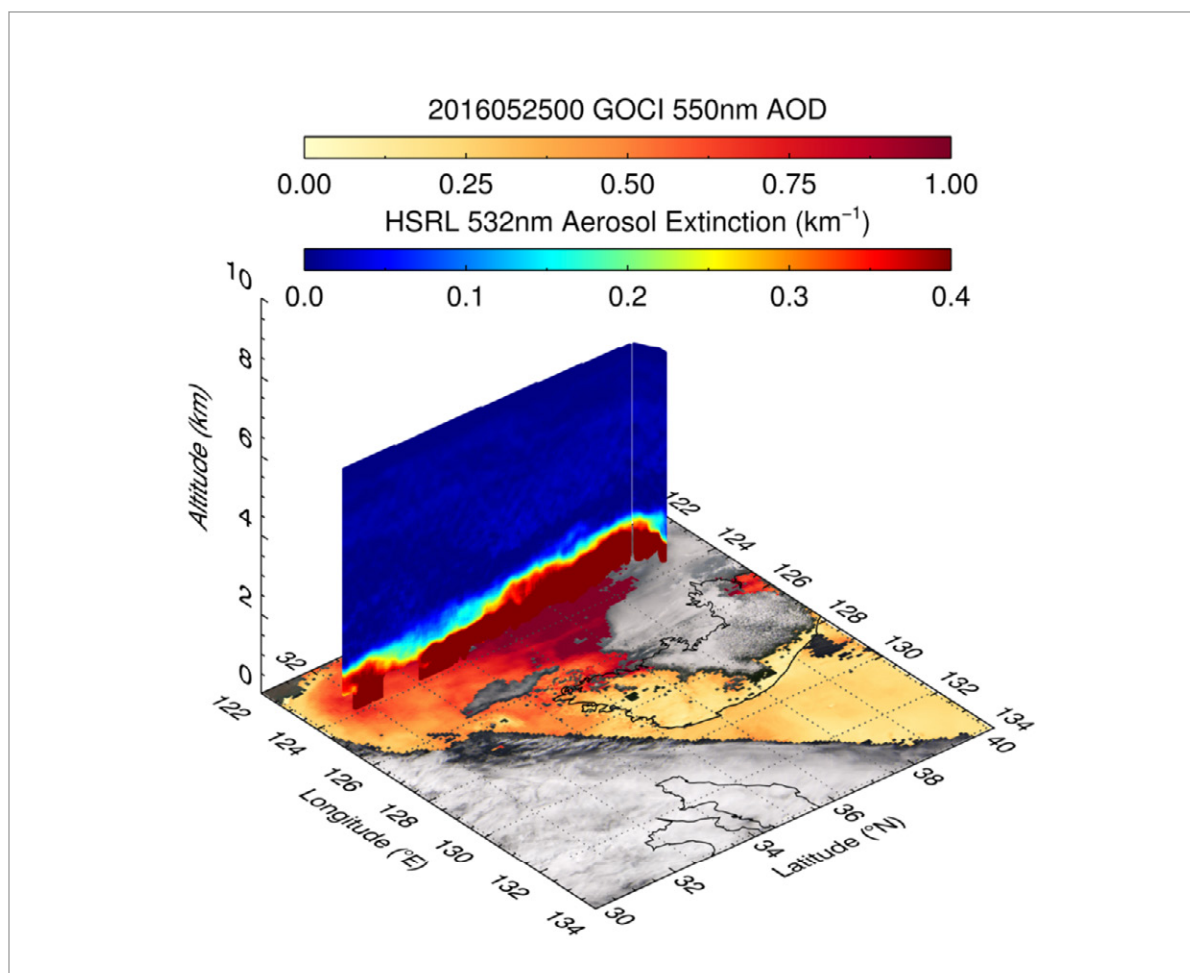


Figure 6-6. Airborne LIDAR measurements of vertical extinction profile through the N-S cross section over the Yellow Sea with GOCI observations of daily average AODs on May 25th, 2016. (Figure taken from Kim, Al-Saadi et al., in preparation)

The characteristics of long-range transport of aerosols during the KORUS-AQ campaign were investigated using GOCI satellite AOD with meteorological data and backward trajectories from the Korean Peninsula (Lee et al., 2019). Figure 6-7 indicates that composite images of GOCI AOD with the wind field clearly show significant differences in high and low aerosol loading cases. For the 5 highest AOD days, heavy aerosol plumes over the Yellow Sea were advected from east-central China by westerly winds. In contrast, GOCI AOD composites for the 5 lowest AOD days do not describe the evolution and progress of transboundary transport over the Yellow Sea. Long-range transport of aerosol cases through the inside

of the boundary layer at east-central China usually contribute to high AODs in Korea, while air masses above the boundary layer in north China and Mongolia do not relate to the high AOD cases in Korea in general. It is important to note that these observed transport cases can also be accompanied by local effects on aerosol formation that further exacerbate fine particle pollution in Korea (see Chapter 2 for this discussion).

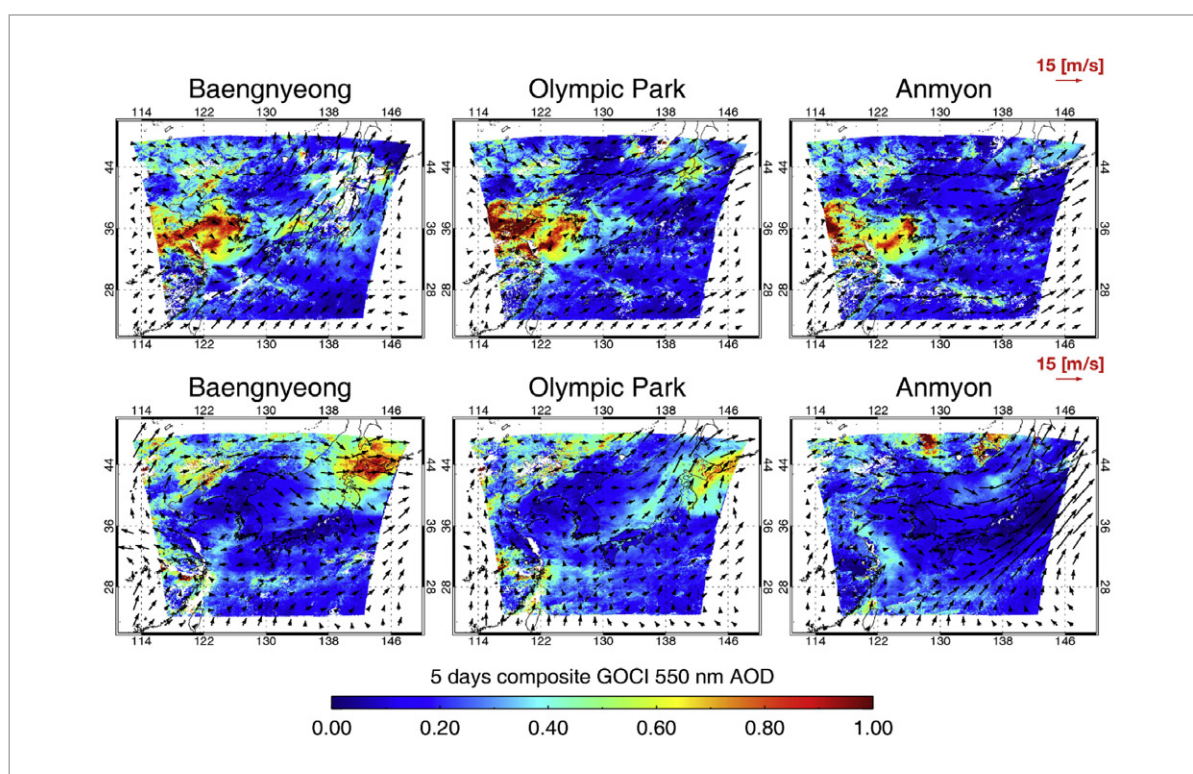


Figure 6-7. GOCI AOD composites and wind vectors at 850-hPa pressure level for the 5 highest AOD days (upper) and 5 lowest AOD days (bottom) at Baengnyeong, Olympic Park and Anmyon during KORUS-AQ (Figure taken from Lee et al., 2019)

Hovmöller diagrams of the GOCI AOD product for the western half of the Korean peninsula and Yellow Sea (35–38 °N, 123–128 °E) were constructed by averaging meridionally at a 0.2 deg longitude interval to evaluate the temporal aerosol transportation quantitatively, as shown in Figure 6-8 (M. Choi et al., 2019). On 25 May, during the meteorological regime of low-level transport, the peak at 09:30 LT

was located at 123.5 °E and moved continuously eastward to 126.3 °E until 16:30 LT. This transport corresponds to westerly zonal wind direction at 850 hPa, as derived from the fifth generation of European Centre for Medium-Range Weather Forecasts (ECMWF) atmospheric reanalyses of the global climate (ERA5; Copernicus Climate Change Service, 2017). As aerosols were transported over the Yellow Sea, the AOD over the Korean Peninsula (126–129.5 °E) increased gradually, particularly over 127 °E in the western Korean Peninsula where it increased from 0.3 to 0.8. In contrast, the evolution on 5 June 2016, during the meteorological blocking pattern, was very different. The overall AODs on 5 June 2016 over the Yellow Sea and Korean Peninsula were low (0.1–0.2) and the AOD over the Seoul Metropolitan Area (SMA) near 37 °N, 127 °E was about 0.4–0.6 from GOCI in the morning. The focus here is on SMA AOD, which increased up to 1.0 and dispersed out to surrounding areas to the west of SMA in the afternoon. Lennartson et al. (2018) also revealed the existence of persistent diurnal variations of aerosol concentrations from GOCI, ground-based AERONET, and the WRF-Chem model. Diurnal variations of AODs show early morning and late afternoon AOD maxima and noontime AOD minima, which were attributed to traffic, site location, land classification and long-range transport. These trends were similar for the coastal sites and for the inland sites. Angstrom exponent also showed diurnal variation with maxima (i.e. fine particles) at around 2 pm at most sites, except for coastal rural sites at Anmyon, Baengnyeong, and Gosan which showed opposite tendencies. Angstrom exponent decreased (i.e. coarser) in early morning and late afternoon.

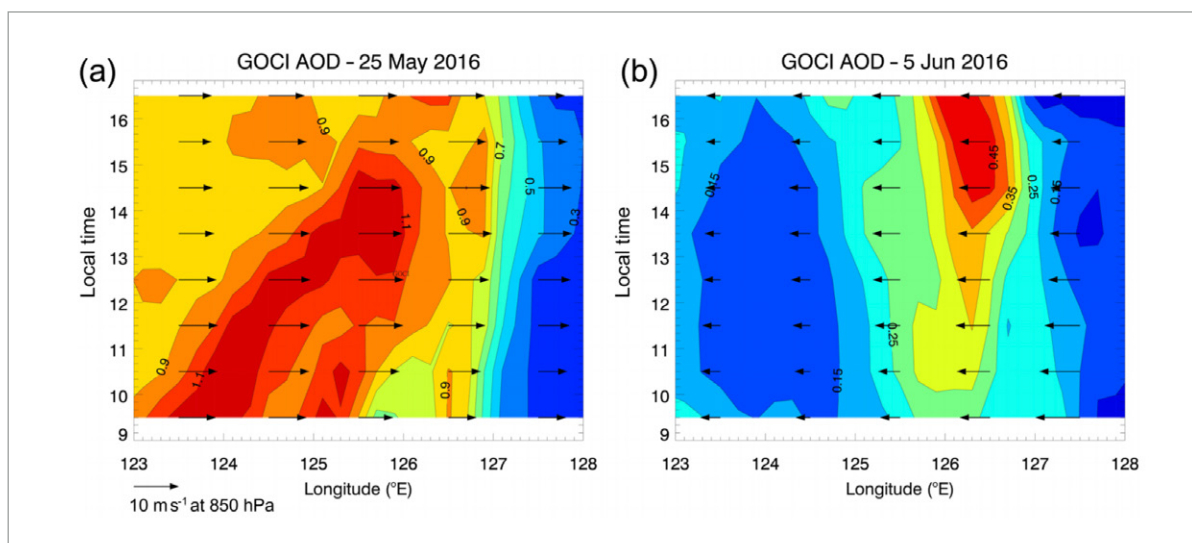


Figure 6-8. Meridional mean GOCI AOD over the Yellow Sea and the Korean Peninsula (35–38 °N, 123–128 °E) at 0.2 longitude intervals on (a) 25 May and (b) 5 June 2016. Overlaid arrows represent meridionally averaged zonal wind at 850 hPa. (Figure taken from M. Choi et al., 2019)

A time series of the AERONET measured AOD at 675 nm and the retrieved fine mode volume median radius at the Yonsei University site (central Seoul) for the KORUS-AQ field campaign period is shown in Figure 6-9(a). The stagnation period of May 17–23, 2016, is shaded in gray, while the major transboundary transport intervals in late May are shaded in blue. During transport dates, cloud fraction was high over much of the peninsula, associated with a weak frontal passage and advection of pollution from China. Both AOD and volume median radius showed sharp increases during the transport periods. Particle volume was at least 10 times larger on pollution transport days due to hygroscopic growth at high RH (Figure 6-9(b)). As discussed in Chapter 2, this hygroscopic growth also likely led to faster gas-to-particle conversion of local emissions that further exacerbated fine particle pollution during the transport episode. These changes in aerosol size and AOD related to hygroscopic growth also have important implications for model assimilation of AOD from satellites to forecast fine particle pollution. Saide et al. (2020) showed that AOD assimilation could lead to overprediction of $PM_{2.5}$ by a factor of 2 or more. This was related to model deficiencies in representing aerosol optical properties which are related to particle size distribution, chemical composition, and hygroscopicity. This adds emphasis to the need for in situ observations to ensure that the translation of information between satellites and models is done correctly.

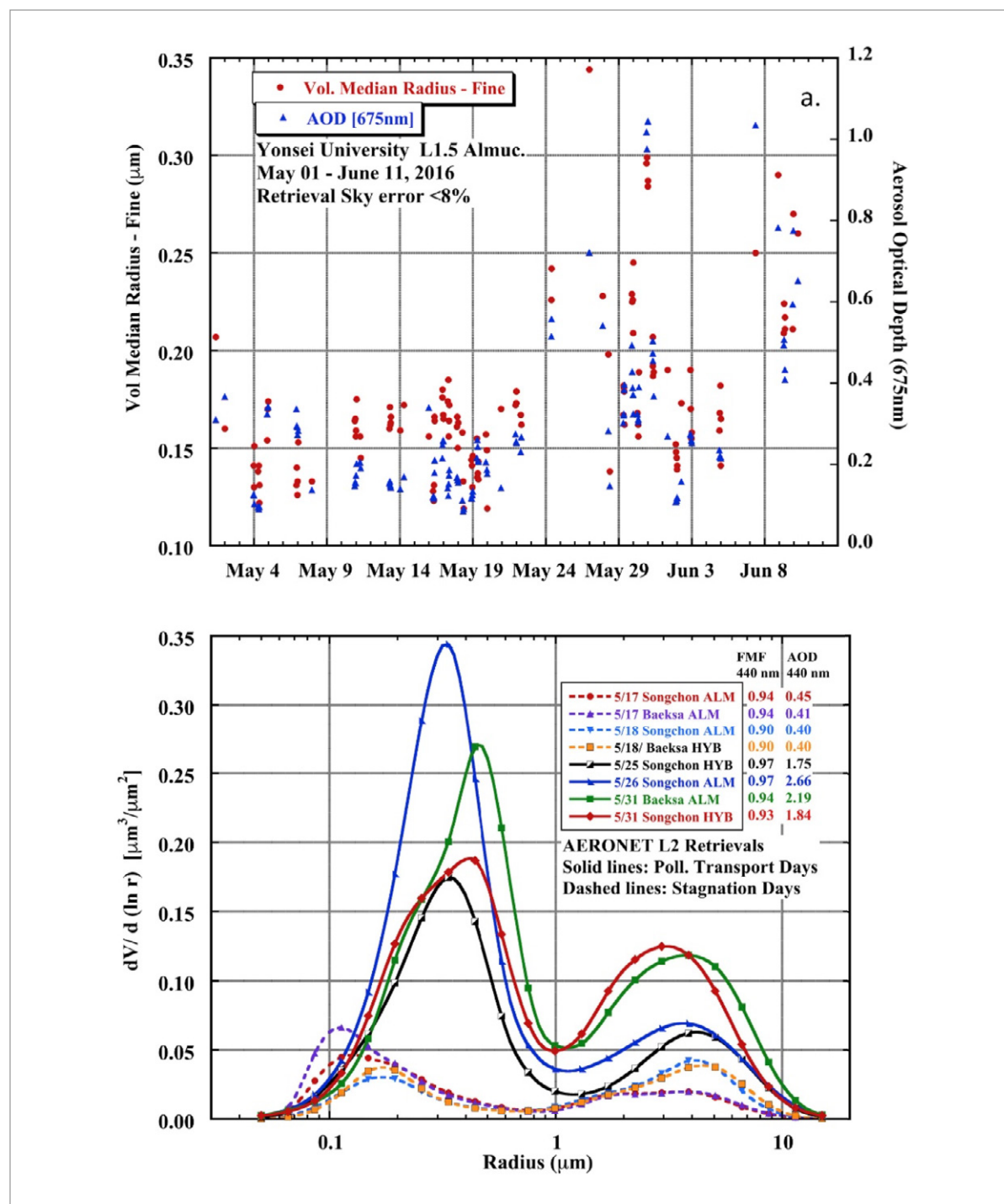


Figure 6-9. (a) Time series of the AERONET almucantar retrievals of volume median radius and measured AOD at 675 nm for the Yonsei University site in central Seoul from May 01 through June 10, 2016. (b) AERONET size distribution retrievals show an order of magnitude greater fine mode aerosol volume on

the days of pollution transport (May 25, 26, & 31) as compared to the stagnant days (May 17 & 18) with primarily local sources, low RH and no clouds. This is partly due to enhanced aerosol water on the high RH pollution transport days. (Figure taken from Eck et al., 2020).

Ultimately, satellite aerosol products are the only way to provide the spatial distribution of AODs over wider area around Korean Peninsula. Geostationary Earth Orbit (GEO) satellite products can further show the tracking of aerosol plumes in higher temporal resolution and the variation of plume movement patterns when combined with the wind fields. Connecting this valuable information to models will improve both forecasting and attribution of pollution sources affecting Korea.

6.5. Concluding remarks

Satellite remote sensing has evident advantages for measuring broad areas including regions which may not be accessible for making surface or airborne measurements. Low Earth orbit (LEO) satellites can provide daily information with global coverage. Geostationary Earth orbit (GEO) satellites provide additional value over a specific domain by enabling the investigation of diurnal variations of air pollutants due to photochemistry, meteorological variability, and emission changes.

Satellite remote sensing by GOCI and AHI provided a broad view of aerosol spatial distributions and their changes during the campaign. Satellite AODs coupled with back trajectories allowed the tracking of plume movement in high temporal resolution. GeoTASO successfully demonstrated the capability of GEMS to observe precursor gases in addition to aerosols. However, these remote sensing observations provide columnar information of aerosol extinction and gas concentrations, lacking critical surface concentration information. This limitation can be overcome with combined measurements of gas concentrations at the surface and mixing layer height information (e.g., by ceilometer), complemented by chemistry-transport models. Machine learning algorithms can be also used to develop methods for converting the columnar measurements to surface concentration (e.g., S. Park et al., 2020).

GEMS was launched from Kourou in French Guiana on February 19, 2020, onboard the GEOstationary KOREA Multi-Purpose SATellite-2B (GEO-KOMPSAT-2B). Column amounts of aerosol, ozone, and their precursors (NO_2 , SO_2 , HCHO , CHOCHO) are retrieved from GEMS spectra. GEMS starts a new era of GEO observation of atmospheric pollutants that will expand many areas of air quality management, including forecasting, top-down emission rate estimates, data assimilation, and public service.

Trace gas observations from satellites can be exploited for the assessment of existing emission inventories by a top-down approach. For example, NO_x emissions estimated from OMI NO_2 observations during KORUS-AQ suggest an underestimation in the current bottom-up NO_x emissions in Seoul (Goldberg et al., 2019). This top-down approach can also be applied to assess emissions of other gaseous species, such as SO_2 . When long-term satellite data sets are accumulated, they can even be used for exploring missing emission sources from bottom-up inventories. Eventually, the top-down assessment of emission inventories and the detection of missing sources using satellites will improve the performance of air quality models. Satellite trace gas observations can also contribute to the improvement of air quality modeling by data assimilation. Since these approaches have better performance with higher spatial and temporal resolution satellite data, GEMS is expected to contribute to air quality prediction significantly.

Satellite-based observation has provided spatio-temporal characteristics and information on long-range transport of aerosols and has also increased our understanding of air quality by reducing uncertainties in modeling for aerosols. Data assimilation and inverse modeling with satellite data have been applied to improve the accuracy of forecasting results (Saide et al., 2014, 2020; Pang et al., 2018). Since Korean geostationary satellite sensors for aerosol and trace gas observations were recently launched, their contributions to the air quality measurements and modeling over Korea and more broadly across Asia are expected through data fusion, top-down emission estimation and data assimilation (Figure 6-10).

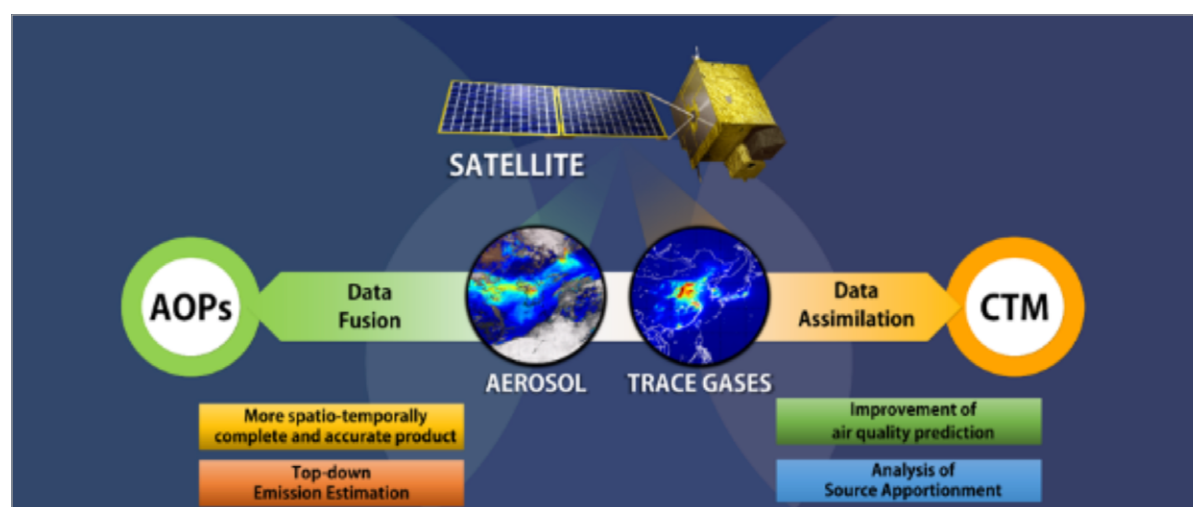


Figure 6-10. Framework for air quality application of satellite observations.

Chapter 7: Policy Recommendations

7.1. Air Quality Management Activities in Korea

7.1.1 Air quality and emission reduction targets in Korea

The Korean government has established national ambient air quality standards for eight air pollutants, CO, SO₂, NO₂, O₃, PM₁₀, PM_{2.5}, Pb, benzene, also known as criteria air pollutants. Considering the number of exceedances and human health impacts, PM_{2.5} and O₃ are regarded as the top two pollutants of concern.

The Korean national ambient PM_{2.5} and O₃ standards as of 2020 are as follows.

PM_{2.5}	15	µg/m ³	annual mean,	35	µg/m ³	24-hour mean
O₃	60	ppbv	8-hour mean,	100	ppbv	1-hour mean

As of 2016, no urban air monitoring station has attained any of the above mentioned national ambient PM_{2.5} and O₃ standards, and therefore these standards should be viewed as long-term objectives. The Korean Ministry of Environment declared the 9.26 comprehensive PM_{2.5} management plan (hereafter denoted as the 9.26 plan) in 2017 and set the following interim PM_{2.5} targets.

The annual mean concentration of Seoul: 18 µg/m³ (26 µg/m³ in 2016)

The number of days exceeding the 24-hr average of 50 µg/m³: 78 days, nationwide
(258 days in 2016)

The emission reduction target of the 9.26 plan is set to 30% by 2022. The targeted species for emission reduction not only includes PM_{2.5} but also NO₂, SO₂ and VOCs, which contributed to secondary PM_{2.5}. Comprehensive mitigation strategies included strengthening emission standards, fuel switching, institutionalizing economic incentives, and retrofitting air pollution control technologies.

The 9.26 plan focuses on four sectors of direct and indirect PM_{2.5} emissions, namely power generation, industry, transportation, and fugitive sources. The sectoral PM_{2.5} emission reduction targets are 25% for

power generation, 43% for industry, 32% for transportation, and 15% for fugitive sources. The industrial sector contributes 51% of the total emissions reduction and the transport sector to 28% of the total emissions reduction.

7.1.2 New Korean PM Regulation - Seasonal PM Management Strategies

Particulate matter pollution has long been recognized as the most serious air pollution problem in Korea. In 2003, the Korean Ministry of Environment promulgated a Special Act on the Improvement of the Air & Environment for Seoul Metropolitan Area, which greatly contributed to marked improvement of PM_{10} over the following decade.

As scientific evidence accumulated and public concern rose regarding the impact of $PM_{2.5}$ on human health, the $PM_{2.5}$ standard was promulgated in 2015. Upon enactment of the $PM_{2.5}$ standard, the Korean Ministry of Environment developed national reference and equivalent $PM_{2.5}$ monitoring methods and established the $PM_{2.5}$ monitoring network consisting of the $PM_{2.5}$ mass monitoring network, the $PM_{2.5}$ speciation monitoring network, and $PM_{2.5}$ super monitoring stations.

The 6.23 plan, announced in 2016, set a goal of 13% $PM_{2.5}$ emission reduction. This plan was superseded by the 9.26 comprehensive $PM_{2.5}$ management plan, setting a more ambitious goal of reducing $PM_{2.5}$ emission by 30%. Reflecting the ever escalating public concerns and anticipating the effects of $PM_{2.5}$ emission reduction, the 9.26 plan revised $PM_{2.5}$ standards by lowering the annual mean $PM_{2.5}$ standard to $15 \mu\text{g}/\text{m}^3$ from $25 \mu\text{g}/\text{m}^3$ and the 24-hour mean $PM_{2.5}$ standard to $35 \mu\text{g}/\text{m}^3$ from $50 \mu\text{g}/\text{m}^3$ in 2018.

As $PM_{2.5}$ policy development and implementation took form, the Seasonal PM Management Strategies (hereafter denoted as Seasonal Strategies) were crafted and implemented in 2019 to speed-up PM problem solving. From December to March, residential heating increases the emissions of $PM_{2.5}$ and its precursors in North-East Asia, and transport of $PM_{2.5}$ and its precursors from China occurs more frequently than in other seasons. Adding to these regional influences, radiation inversions form more frequently due to cold ground temperatures and suppress local wind circulation. During these months in 2018, the $PM_{2.5}$ concentration was 15~30 % higher than the annual average and 18 out of the 19 Seoul metropolitan $PM_{2.5}$ alerts for the year were issued.

The Seasonal Strategies implemented an additional 20% PM_{2.5} emission reduction by limiting coal power plant capacity utilization, shutting down old coal power plants, banning old diesel cars in downtown Seoul, voluntary emission reduction agreements with large point sources, three dimensional air emission surveillance system mobilizing drones, reducing port emission by enforcing the use of low sulfur oil, and regulating old construction equipment.

During the PM season in 2020, the first year of Seasonal Strategies, the nationally averaged PM_{2.5} concentration was improved by 27% and the number of days exceeding 50 µg/m³ was reduced to 2 from 18 days compared to the previous year. Modeling analysis attributed this improvement to not only implementation of the seasonal PM management Strategies but also meteorology dominated by easterly winds and emission activities reduced by COVID-19 in the upwind region.

All of these PM_{2.5} mitigation efforts were made after the KORUS-AQ campaign in 2016, thus, additional field studies are needed to assess these mitigation efforts and characterize the role of meteorological conditions in observed changes to PM pollution in Korea

7.2. Policy implications of KORUS-AQ findings

The following discussions summarize the policy implications of KORUS-AQ findings. More detail on these implications can be found in the chapters dedicated to each topic. It should be emphasized up front that these recommendations are focused on local actions that can be taken to improve PM_{2.5} and ozone pollution. This does not discount that there are substantial transboundary influences to consider and that regional cooperation is necessary to achieving sustainable improvements in air quality for Korea. Clear steps to reduce local emissions are good faith actions needed to support such regional cooperative efforts.

1) Improving both PM_{2.5} and ozone pollution relies on coordinated reductions in both NO_x and VOCs, specifically higher (C₇+) aromatic compounds.

Analysis of the KORUS-AQ observations revealed dominant roles for both NO_x and VOCs in the control of PM_{2.5} and ozone, but the impacts are manifested in different ways.

For $PM_{2.5}$, the observed composition changed from organic-dominated to inorganic-dominated conditions depending on meteorology. Organic aerosol was the dominant fraction of $PM_{2.5}$ during stagnant conditions when clearer skies and abundant sunlight were most favorable for photochemical processing of local VOC emissions. By contrast, inorganic aerosol dominated under transport/haze conditions with evidence that transboundary pollution influence was exacerbated by enhanced gas-to-particle conversion of local emissions under the humid conditions. The role of nitrate aerosol driven by local NO_x emissions enabled a positive feedback by enhancing aerosol liquid water content which facilitated additional particle formation.

For ozone, NO_x and VOC emissions work together in a complex fashion with VOC emissions having greater control of the rate of ozone formation and NO_x controlling the regional extent of ozone formation. Given the large abundance of NO_x , ozone formation in Seoul is limited by VOC availability such that if VOCs emissions alone are reduced, ozone formation rates in Seoul would decrease; however, NO_x reductions are necessary to reduce the regional extent of ozone formation affecting the greater Korean peninsula. Given that the NO_x abundance in Seoul is so great that it suppresses the catalytic chemical cycle of ozone formation, NO_x reductions could initially offset the impact of VOC reductions and lead to greater ozone in the short term for urban areas. To add to the complexity, the tendency toward faster chemical cycling as NO_x emissions are reduced would also shorten the lifetime of NO_x such that the atmospheric abundance should decrease faster than emissions.

Observation-constrained modeling revealed the importance of C_7+ aromatic compounds (e.g., toluene and xylenes), indicating that this single class of VOCs was responsible for a third of organic aerosol and ozone production.

While reductions in NO_x and VOCs will yield immediate benefits for $PM_{2.5}$, the rate of reduction between NO_x and VOCs is important for ozone. The more rapidly NO_x is reduced relative to VOCs raises the expectation of increases in ozone, especially in urban areas. In the face of such setbacks, it will be important to be patient and confident that continued reductions will lead to success in the long term.

2) Improved estimates place better bounds on current emissions, but specific sources for higher (C_7+) aromatic compounds need to be determined to enable effective control strategies to be developed.

Air quality control strategies can only be effective if emissions are well understood. An important outcome

of KORUS-AQ research was the improvement of emission inventories.

An underestimation in NO_x emissions was first diagnosed through top-down assessments using satellite observations and models. In response, the subsequent bottom-up assessment increased on-road mobile emissions based on better emission factors from Portable Emissions Measuring Systems (PEMS). This improves the understanding of what can be achieved with current NO_x control strategies.

For VOCs, emission speciation profiles were improved to allocate more mass to reactive VOCs, and model representation of aromatic compounds compared to observations improved as a result. The sources of these compounds, however, remain broadly distributed and are poorly understood in detail. An observation-based source apportionment analysis indicated that solvent use is primarily responsible for the large abundance of higher aromatic compounds in Seoul, with toluene being more associated with non-paint solvents and xylenes being more associated with paint solvents. These two categories, however, can be linked to a large number of potential products. Specific products to target for reduction are still needed.

3) Large underestimates of VOC emissions from industrial point sources warrant continued scrutiny and verification.

KORUS-AQ made several visits to sample emissions from point sources along the northwest coast of the Korean peninsula. The top-down assessments of NO_x and SO_2 emissions agreed well with CAPSS emissions given the supporting observations from the Continuous Emissions Monitoring System (CEMS). By contrast, multiple top-down assessments based on observations at the Daesan chemical facility showed VOC emissions to be underestimated by a factor of 2.5 to 4. Given the complex chemical mixtures containing multiple Hazardous Air Pollutants (HAPs) and their oxidation products, underestimation of these emissions carries additional risk to workers and local communities. VOC emissions are different than stack emissions of NO_x and SO_2 . They occur mainly as fugitive emissions that come from a multitude of facility components and activities such as: storage tanks, transport pipelines throughout the complex and to/from the nearby shipping port, petroleum production and handling, as well as combustion and flaring operations. Thus, they cannot be easily measured from a single point in the facility. The recent establishment of the Seosan supersite on the Taean peninsula is a positive step given its proximity to Daesan and other points sources along the northwest coast. However, the discrepancies at Daesan raise

questions about whether similar underestimates exist at other facilities, both large and small, across Korea. A top-down airborne survey of point sources may be the most efficient way to determine the extent of this underestimate.

4) Model simulations of air quality require a hierarchy of models to obtain the best representation and understanding of uncertainties to support decision making.

KORUS-AQ assembled a team of air quality modeling groups to support during the planning, execution, and research stages of the study. These groups employed a hierarchy of models covering regional-to-global domains with various resolutions and various complexity in their treatments of ozone and PM formation. Models play an important role in evaluating emissions estimates, providing the translation from emission inventories to ambient concentrations to be compared with observations. The average of several different models, with differing strengths and weaknesses, was generally better at matching observations than any individual model. This illustrates the value of having multiple models for determining the drivers of air quality, and placing uncertainty bounds on quantitative assessments. Ongoing model development, leading to more accurate simulations of ozone and secondary aerosol formation in individual models, is needed to guide policies on emissions controls and improve air quality forecasting.

7.3. A way forward

7.3.1 Monitoring

With the combination of the extensive AirKorea monitoring network and hourly monitoring from GEMS as well as GOCI-II, Korea will have unprecedented information to support continuous air quality monitoring of Korea and the larger regional impacts across Asia. This information will support improved forecasting, top-down emissions estimates, assessment of emission controls, and fundamental understanding of the factors driving air quality. Nevertheless, there are a few small additional investments that will benefit the interpretation of information coming from monitoring observations.

Given the ongoing need to understand local versus transboundary influences, high-quality measurements of CO and CO₂ would provide continuous information on the strength of transboundary influence based on the large difference in combustion efficiency in Korea as compared to China. Continuous research-grade

observations of aerosol composition would provide the details needed to better understand changes in the local rate of secondary aerosol production. Additional routine observations of humidified and dry aerosol scattering would allow for calculation of aerosol liquid water to better understand the coupled chemical and meteorological processes driving haze events. Finally, high-quality ammonia measurements would enable model assessments to be fully constrained in the evaluation of inorganic aerosol formation, aerosol acidity, and related aerosol reaction pathways. If these measurements were co-located at a single site in Seoul, the findings of KORUS-AQ and their relevance to understanding the drivers of $PM_{2.5}$ could be extended throughout the year. Finally, to provide increased attention on the role of mixed layer dynamics on $PM_{2.5}$ abundance, a real-time mixing height data product from the currently operating ceilometer network should be developed to provide continuous information on the diurnal cycle of mixing and ventilation of near-surface pollution.

7.3.2 Emission Inventories

Bottom-up emissions play an important role in setting up air quality management policies. Korea has made an effort in developing and refining bottom-up emissions for the last two decades. KORUS-AQ analysis provided a critical review of CAPSS, Korea bottom-up emissions, and Chinese emissions by comparing modeling results with field measurements and developing new sets of emission inventories (named as KORUS emissions) primarily for air quality modeling.

Because of differences in development and purposes, KORUS emissions may not be directly comparable to CAPSS. Discrepancies among multiple air quality modeling results also hamper full validation of KORUS-AQ emissions even for modeling purposes. However, the major assessments of CAPSS emissions which led to the development of KORUS emissions should be noted for future development of CAPSS. This refers specifically to the underestimations of mobile source NO_x and point source VOCs emissions deduced through top-down methods. With continuous GEMS observations and ongoing changes in emissions due to control policies, top-down assessments will continue to be critical to the scrutiny of bottom-up emissions.

7.3.3 Modeling

A number of state-of-the-science air quality models (WRF-Chem, CMAQ, CAMx, GEOS-Chem) are being used to study ozone and PM pollution in Korea and should continue to be supported for further

development and evaluation. Ongoing model improvements, based on improved scientific understanding of chemistry and the complex meteorology affecting Seoul and the Korean peninsula, are needed to improve air quality forecasts. The continued close collaboration begun during KORUS-AQ between the groups developing emissions inventories and models will lead to improved emissions and models. With greater confidence in air quality forecasts, real-time policy measures such as traffic restrictions based on air quality forecasts might be considered.

7.3.4 The next phase of US-KOREA cooperation

In December 2018, NIER and NASA signed a Memorandum of Understanding concerning “Cooperation in Pollution Studies, Calibration, and Validation”. Since that time, the GEMS satellite launched in February 2020 and the impending launch of TEMPO in 2022 will bring the Air Quality satellite constellation closer to fruition.

This agreement demonstrates the commitment to continued cooperation between the United States and Korea to the calibration and validation of GEMS and TEMPO observations and more importantly to the interpretation of the information from these satellites to inform air quality forecasts, improve understanding, and provide value to decision making.

The recent development of the Pandora Asia Network (PAN) has also been critical to expanding collaboration across Asia and globally through membership in the Pandora Global Network (PGN). This effort not only brings scientists together, but under the sponsorship of KOICA and the United Nations Economic and Social Commission for Asia and the Pacific (UNESCAP), brings decision makers into the discussion of local and shared impacts to air quality across Asia.

Continued field work will be necessary with current plans already underway for flights of the GCAS instrument for GEMS validation. Other projects in the near future include ACCLIP(Asian Summer Monsoon Chemical & CLimate Impact Project), GMAP(GEMS MAP of Air Pollution), SIJAQ(Satellite Integrated Joint Monitoring of Air Quality). Over the longer term, Korean and US scientists will continue to explore and discuss ideas for field study collaborations to evaluate the changing landscape of emissions and the resulting changes in air quality as we work to achieve our respective national goals.

References

- Bachmann, J. (2007). Will the circle be unbroken: a history of the U.S. National Ambient Air Quality Standards. *Journal of the Air & Waste Management Association*, 57(6), 652–697. <https://doi.org/10.3155/1047-3289.57.6.652>
- Beirle, S., Borger, C., Dörner, S., Li, A., Hu, Z., Liu, F., Wang, Y., & Wagner, T. (2019). Pinpointing nitrogen oxide emissions from space. *Science Advances*, 5(11), eaax9800. <https://doi.org/10.1126/sciadv.aax9800>
- Carter, W. P. L. (2000). Documentation of the SAPRC-99 chemical mechanism for VOC reactivity assessment. *Report to the California Air Resources Board*. <http://www.cert.ucr.edu/~carter/absts.htm#saprc99>
- Chang, C.-Y., Faust, E., Hou, X., Lee, P., Kim, H. C., Hedquist, B. C., & Liao, K.-J. (2016). Investigating ambient ozone formation regimes in neighboring cities of shale plays in the Northeast United States using photochemical modeling and satellite retrievals. *Atmospheric Environment*, 142, 152–170. <https://doi.org/10.1016/j.atmosenv.2016.06.058>
- Cho, C., S. Jeong, J. Liao, G.M. Wolfe, J.M. St. Clair, D. il Kang, J. Choi, M.-H. Shin, J. Park, T.F. Hanisco, and K.-E. Min. (2020). Volatile organic compounds (VOCs) emission rates estimation using airborne in-situ formaldehyde (HCHO) observation from a petrochemical complex in Korea, in preparation.
- Choi, Y., Kim, H., Tong, D., & Lee, P. (2012). Summertime weekly cycles of observed and modeled NO_x and O₃ concentrations as a function of satellite-derived ozone production sensitivity and land use types over the Continental United States. *Atmospheric Chemistry and Physics*, 12(14), 6291–6307. <https://doi.org/10.5194/acp-12-6291-2012>
- Choi, J., Park, R. J., Lee, H.-M., Lee, S., Jo, D. S., Jeong, J. I., Henze, D. K., Woo, J.-H., Ban, S.-J., Lee, M.-D., Lim, C.-S., Park, M.-K., Shin, H. J., Cho, S., Peterson, D., & Song, C.-K. (2019). Impacts of local vs. trans-boundary emissions from different sectors on PM_{2.5} exposure in South Korea during the KORUS-AQ campaign. *Atmospheric Environment*, 203, 196–205. <https://doi.org/10.1016/j.atmosenv.2019.02.008>

- Choi, M., Lim, H., Kim, J., Lee, S., Eck, T. F., Holben, B. N., Garay, M. J., Hyer, E. J., Saide, P. E., & Liu, H. (2019). Validation, comparison, and integration of GOCI, AHI, MODIS, MISR, and VIIRS aerosol optical depth over East Asia during the 2016 KORUS-AQ campaign. *Atmospheric Measurement Techniques*, 12(8), 4619–4641. <https://doi.org/10.5194/amt-12-4619-2019>
- Chong, H., Lee, S., Kim, J., Jeong, U., Li, C., Krotkov, N. A., Nowlan, C. R., Al-Saadi, J. A., Janz, S. J., Kowalewski, M. G., Ahn, M.-H., Kang, M., Joiner, J., Haffner, D. P., Hu, L., Castellanos, P., Huey, L. G., Choi, M., Song, C. H., ... Koo, J.-H. (2020). High-resolution mapping of SO₂ using airborne observations from the GeoTASO instrument during the KORUS-AQ field study: PCA-based vertical column retrievals. *Remote Sensing of Environment*, 241, 111725. <https://doi.org/10.1016/j.rse.2020.111725>
- Duncan, B. N., Yoshida, Y., Olson, J. R., Sillman, S., Martin, R. V., Lamsal, L., Hu, Y., Pickering, K. E., Retscher, C., Allen, D. J., & Crawford, J. H. (2010). Application of OMI observations to a space-based indicator of NO_x and VOC controls on surface ozone formation. *Atmospheric Environment*, 44(18), 2213–2223. <https://doi.org/10.1016/j.atmosenv.2010.03.010>
- Eck, T. F., Holben, B. N., Kim, J., Beyersdorf, A. J., Choi, M., Lee, S., Koo, J.-H., Giles, D. M., Schafer, J. S., Sinyuk, A., Peterson, D. A., Reid, J. S., Arola, A., Slutsker, I., Smirnov, A., Sorokin, M., Kraft, J., Crawford, J. H., Anderson, B. E., ... Park, S. (2020). Influence of cloud, fog, and high relative humidity during pollution transport events in South Korea: Aerosol properties and PM_{2.5} variability. *Atmospheric Environment*, 232, 117530. <https://doi.org/10.1016/j.atmosenv.2020.117530>
- Fried, A., et al. (2020). Airborne Formaldehyde and VOC Measurements over the Daesan Petrochemical Complex on Korea's Northwest Coast During the KORUS-AQ Study: Estimation of Emission Fluxes and Effects on Air Quality. *Elem. Sci. Anth.* 8(1), 121. <https://doi.org/10.1525/elementa.2020.121>
- Gaubert, B., Emmons, L. K., Raeder, K., Tilmes, S., Miyazaki, K., Arellano, A. F., Jr., Elguindi, N., Granier, C., Tang, W., Barré, J., Worden, H. M., Buchholz, R. R., Edwards, D. P., Franke, P., Anderson, J. L., Saunio, M., Schroeder, J., Woo, J.-H., Simpson, I. J., ... Ren, X. (2020). Correcting model biases of CO in East Asia: impact on oxidant distributions during KORUS-AQ. *Atmospheric Chemistry and Physics Discussions: ACPD*. <https://doi.org/10.5194/acp-2020-599>
- Gil, J., Kim, J., Lee, M., Lee, G., Lee, D., Jung, J., An, J., Hong, J., Cho, S., Lee, J., and Long, R. (2021).

The role of HONO in O₃ formation and insight into its formation mechanism during the KORUS-AQ Campaign. *Atmos. Env.* 247. <https://doi.org/10.1016/j.atmosenv.2020.118182>

Goldberg, D. L., Lu, Z., Streets, D. G., de Foy, B., Griffin, D., McLinden, C. A., Lamsal, L. N., Krotkov, N. A., & Eskes, H. (2019). Enhanced Capabilities of TROPOMI NO₂: Estimating NO_x from North American Cities and Power Plants. *Environmental Science & Technology*, 53(21), 12594–12601. <https://doi.org/10.1021/acs.est.9b04488>

Guo, H., Wang, T., Blake, D. R., Simpson, I. J., Kwok, Y. H., & Li, Y. S. (2006). Regional and local contributions to ambient non-methane volatile organic compounds at a polluted rural/coastal site in Pearl River Delta, China. *Atmospheric Environment*, 40(13), 2345–2359. <https://doi.org/10.1016/j.atmosenv.2005.12.011>

Gupta, P., Levy, R. C., Mattoo, S., Remer, L. A., Holz, R. E., & Heidinger, A. K. (2019). Applying the Dark Target aerosol algorithm with Advanced Himawari Imager observations during the KORUS-AQ field campaign. *Atmospheric Measurement Techniques*, 12(12), 6557–6577. <https://doi.org/10.5194/amt-12-6557-2019>

Halliday, H. S., DiGangi, J. P., Choi, Y., Diskin, G. S., Pusede, S. E., Rana, M., Nowak, J. B., Knute, C., Ren, X., He, H., Dickerson, R. R., & Li, Z. (2019). Using Short-Term CO/CO₂ Ratios to Assess Air Mass Differences Over the Korean Peninsula During KORUS-AQ. *Journal of Geophysical Research, D: Atmospheres*, 124(20), 10951–10972. <https://doi.org/10.1029/2018JD029697>

Jang, Y., Lee, Y., Kim, J., Kim, Y., & Woo, J.-H. (2019). Improvement China Point Source for Improving Bottom-Up Emission Inventory. *Asia-Pacific Journal of Atmospheric Sciences*, 56(1), 107–118. <https://doi.org/10.1007/s13143-019-00115-y>

Jin, X., & Holloway, T. (2015). Spatial and temporal variability of ozone sensitivity over China observed from the Ozone Monitoring Instrument. *Journal of Geophysical Research, D: Atmospheres*, 120(14), 7229–7246. <https://doi.org/10.1002/2015JD023250>

Jordan, C., Crawford, J. H., Beyersdorf, A. J., Eck, T. F., Halliday, H. S., Nault, B. A., Chang, L.-S., Park, J., Park, R., Lee, G., Kim, H., Ahn, J.-Y., Cho, S., Shin, H. J., Lee, J. H., Jung, J., Kim, D.-S., Lee, M., Lee, T., ... Schwarz, J. P. (2020). Investigation of factors controlling PM_{2.5} variability across the South Korean

Peninsula during KORUS-AQ. *Elem Sci Anth*, 8(1), 28. <https://doi.org/10.1525/elementa.424>

Judd, L., Al-Saadi, J., Valin, L., Pierce, R. B., Yang, K., Janz, S., Kowalewski, M., Szykman, J., Tiefengraber, M., & Mueller, M. (2018). The Dawn of Geostationary Air Quality Monitoring: Case Studies from Seoul and Los Angeles. *Frontiers of Environmental Science & Engineering in China*, 6. <https://doi.org/10.3389/fenvs.2018.00085>

Kim, H., Choi, W.-C., Rhee, H.-J., Suh, I., Lee, M., Blake, D. R., Kim, S., Jung, J., Lee, G., Kim, D.-S., Park, S.-M., Ahn, J., & Lee, S. D. (2018). Meteorological and Chemical Factors Controlling Ozone Formation in Seoul during MAPS-Seoul 2015. *Aerosol and Air Quality Research*, 18(9), 2274–2286. <https://doi.org/10.4209/aaqr.2017.11.0445>

Kim, H., Zhang, Q., & Heo, J. (2018). Influence of intense secondary aerosol formation and long-range transport on aerosol chemistry and properties in the Seoul Metropolitan Area during spring time: results from KORUS-AQ. *Atmospheric Chemistry and Physics*, 18(10), 7149–7168. <https://doi.org/10.5194/acp-18-7149-2018>

Kim, H., Gil, J., Lee, M., Jung, J., Whitehill, A., Szykman, J., Lee, G., Kim, D.-S., Cho, S., Ahn, J.-Y., Hong, J., & Park, M.-S. (2020). Factors controlling surface ozone in the Seoul Metropolitan Area during the KORUS-AQ campaign. *Elem Sci Anth*, 8(1), 46. <https://doi.org/10.1525/elementa.444>

Kim, J., Jeong, U., Ahn, M.-H., Kim, J. H., Park, R. J., Lee, H., Song, C. H., Choi, Y.-S., Lee, K.-H., Yoo, J.-M., Jeong, M.-J., Park, S. K., Lee, K.-M., Song, C.-K., Kim, S.-W., Kim, Y. J., Kim, S.-W., Kim, M., Go, S., ... Choi, Y. (2020). New Era of Air Quality Monitoring from Space: Geostationary Environment Monitoring Spectrometer (GEMS). *Bulletin of the American Meteorological Society*, 101(1), E1–E22. <https://doi.org/10.1175/BAMS-D-18-0013.1>

Kim, S., Jeong, D., Sanchez, D., Wang, M., Seco, R., Blake, D., Meinardi, S., Barletta, B., Hughes, S., Jung, J., Kim, D., Lee, G., Lee, M., Ahn, J., Lee, S.-D., Cho, G., Sung, M.-Y., Lee, Y.-H., & Park, R. (2018). The Controlling Factors of Photochemical Ozone Production in Seoul, South Korea. *Aerosol and Air Quality Research*, 18(9), 2253–2261. <https://doi.org/10.4209/aaqr.2017.11.0452>

Kim, Y. P., & Lee, G. (2018). Trend of Air Quality in Seoul: Policy and Science. *Aerosol and Air Quality Research*, 18(9), 2141–2156. <https://doi.org/10.4209/aaqr.2018.03.0081>

Kim, J., Al-Saadi, J., et al. Remote Sensing of air quality around Korea during the KORUS-AQ, in preparation.

Koo et al., Comparison of HCHO/NO₂ from the multiple observations during the KORUS-AQ, in preparation.

Kwon, H.-A., R.J. Park, Y. Oak, C.R. Nowlan, S.J. Janz, M.G. Kowalewski, A. Fried, J. Walega, K. Bates, J. Choi, D.R. Blake, and A. Wisthaler. (2021). Top-down estimates of anthropogenic emissions in South Korea using formaldehyde vertical column densities from aircraft platforms during the KORUS-AQ campaign. *Elem. Sci. Anth.* 9(1), 00109. <https://doi.org/10.1525/elementa.2021.00109>

Lamb, K. D., Perring, A. E., Samset, B., Peterson, D., Davis, S., Anderson, B. E., Beyersdorf, A., Blake, D. R., Campuzano-Jost, P., Corr, C. A., Diskin, G. S., Kondo, Y., Moteki, N., Nault, B. A., Oh, J., Park, M., Pusede, S. E., Simpson, I. J., Thornhill, K. L., ... Schwarz, J. P. (2018). Estimating Source Region Influences on Black Carbon Abundance, Microphysics, and Radiative Effect Observed Over South Korea. *Journal of Geophysical Research, D: Atmospheres*, 123(23), 295. <https://doi.org/10.1029/2018JD029257>

Lee, S., Kim, J., Choi, M., Hong, J., Lim, H., Eck, T. F., Holben, B. N., Ahn, J.-Y., Kim, J., & Koo, J.-H. (2019). Analysis of long-range transboundary transport (LRTT) effect on Korean aerosol pollution during the KORUS-AQ campaign. *Atmospheric Environment*, 204, 53–67. <https://doi.org/10.1016/j.atmosenv.2019.02.020>

Lennartson, E. M., Wang, J., Gu, J., Castro Garcia, L., Ge, C., Gao, M., Choi, M., Saide, P. E., Carmichael, G. R., Kim, J., & Janz, S. J. (2018). Diurnal variation of aerosol optical depth and PM_{2.5} in South Korea: a synthesis from AERONET, satellite (GOCI), KORUS-AQ observation, and the WRF-Chem model. *Atmospheric Chemistry and Physics*, 18(20), 15125–15144. <https://doi.org/10.5194/acp-18-15125-2018>

Lim, H., Choi, M., Kim, J., Kasai, Y., & Chan, P. W. (2018). AHI/Himawari-8 Yonsei Aerosol Retrieval (YAER): Algorithm, Validation and Merged Products. *Remote Sensing*, 10(5), 699. <https://doi.org/10.3390/rs10050699>

Lim, H., Go, S., Kim, J., Choi, M., Lee, S., Song, C.-K., & Kasai, Y. (2020). Integration of GOCI and AHI Yonsei Aerosol Optical Depth Products During the 2016 KORUS-AQ and 2018 EMeRGe Campaigns. *Atmospheric Measurement Techniques Discussions*, 1–32. <https://doi.org/10.5194/amt-2020-336>

- Lyu, X. P., Zeng, L. W., Guo, H., Simpson, I. J., Ling, Z. H., Wang, Y., Murray, F., Louie, P. K. K., Saunders, S. M., Lam, S. H. M., & Blake, D. R. (2017). Evaluation of the effectiveness of air pollution control measures in Hong Kong. *Environmental Pollution*, 220(Pt A), 87–94. <https://doi.org/10.1016/j.envpol.2016.09.025>
- Martin, R. V., Fiore, A. M., & Van Donkelaar, A. (2004). Space-based diagnosis of surface ozone sensitivity to anthropogenic emissions. *Geophysical Research Letters*, 31(6). <https://doi.org/10.1029/2004GL019416>
- Miyazaki, K., Sekiya, T., Fu, D., Bowman, K. W., Kulawik, S. S., Sudo, K., Walker, T., Kanaya, Y., Takigawa, M., Ogochi, K., Eskes, H., Boersma, K. F., Thompson, A. M., Gaubert, B., Barre, J., & Emmons, L. K. (2019). Balance of Emission and Dynamical Controls on Ozone During the Korea-United States Air Quality Campaign From Multiconstituent Satellite Data Assimilation. *Journal of Geophysical Research, D: Atmospheres*, 124(1), 387–413. <https://doi.org/10.1029/2018JD028912>
- Nault, B. A., Campuzano-Jost, P., Day, D. A., Schroder, J. C., Anderson, B., Beyersdorf, A. J., Blake, D. R., Brune, W. H., Choi, Y., Corr, C. A., de Gouw, J. A., Dibb, J., DiGangi, J. P., Diskin, G. S., Fried, A., Huey, L. G., Kim, M. J., Knote, C. J., Lamb, K. D., ... Jimenez, J. L. (2018). Secondary organic aerosol production from local emissions dominates the organic aerosol budget over Seoul, South Korea, during KORUS-AQ. *Atmospheric Chemistry and Physics*, 18(24), 17769–17800. <https://doi.org/10.5194/acp-18-17769-2018>
- NIER & NASA. (2017). *KORUS-AQ Rapid Science Synthesis Report*. <https://espo.nasa.gov/sites/default/files/documents/KORUS-AQ-ENG.pdf> <https://espo.nasa.gov/sites/default/files/documents/KORUS-AQ-RSSR.pdf>
- Oak, Y. J., Park, R. J., Schroeder, J. R., Crawford, J. H., Blake, D. R., Weinheimer, A. J., Woo, J.-H., Kim, S.-W., Yeo, H., Fried, A., Wisthaler, A., & Brune, W. H. (2019). Evaluation of simulated O₃ production efficiency during the KORUS-AQ campaign: Implications for anthropogenic NO_x emissions in Korea. *Elementa Science of the Anthropocene*, 7(1), 56. <https://doi.org/10.1525/elementa.394>
- Pang, J., Liu, Z., Wang, X., Bresch, J., Ban, J., Chen, D., & Kim, J. (2018). Assimilating AOD retrievals from GOCI and VIIRS to forecast surface PM_{2.5} episodes over Eastern China. *Atmospheric Environment*, 179, 288–304. <https://doi.org/10.1016/j.atmosenv.2018.02.011>

Park M., Y. Kim, A. Fried, I. J. Simpson, H. Jin, A. Weinheimer, G. Huey, J. Crawford, H. Hu, and J. -H. Woo. (2020). Evaluating South Korean large point source emissions using a NASA KORUS-AQ aircraft field campaign. *Elementa*, submitted.

Park, R.J., Oak, Y.J., Emmons, L.K., Kim, C.-H., Pfister, G.G., Carmichael, G.R., Saide, P.E., Cho, S.-Y., Kim, S., Woo, J.-H., Crawford, J.H., Gaubert, B., Lee, H.-J., Park, S.-Y., Jo, Y.-J., Gao, M., Tang, B., Stanier, C.O., Shin, S.S., Park, H.Y., Bae, C., Kim, E. (2021). Multi-model inter-comparisons of air quality simulations for the KORUS-AQ campaign. *Elem. Sci. Anth.* 9(1), 00139. <https://doi.org/10.1525/elementa.2021.00139>

Park, S., Lee, J., Im, J., Song, C.-K., Choi, M., Kim, J., Lee, S., Park, R., Kim, S.-M., Yoon, J., Lee, D.-W., & Quackenbush, L. J. (2020). Estimation of spatially continuous daytime particulate matter concentrations under all sky conditions through the synergistic use of satellite-based AOD and numerical models. *The Science of the Total Environment*, 713, 136516. <https://doi.org/10.1016/j.scitotenv.2020.136516>

Park, Taehyun, Jihee Ban, Gyutae Park, Seokwon Kang, Kyunghoon Kim, Beom-Keun Seo, Jongho Kim, Soobog Park, Taehyoung Lee. (2020). The physico-chemical evolution of atmospheric aerosols and the gas-particle partitioning of inorganic aerosol during KORUS-AQ. *Atmospheric Environment*, in preparation.

Peterson, D. A., Hyer, E. J., Han, S.-O., Crawford, J. H., Park, R. J., Holz, R., Kuehn, R. E., Eloranta, E., Knote, C., Jordan, C. E., & Lefer, B. L. (2019). Meteorology influencing springtime air quality, pollution transport, and visibility in Korea. *Elementa Sci Anth*, 7(1), 57. <https://doi.org/10.1525/elementa.395>

Saide, P. E., Kim, J., Song, C. H., Choi, M., Cheng, Y., & Carmichael, G. R. (2014). Assimilation of next generation geostationary aerosol optical depth retrievals to improve air quality simulations: Geostationary AOD improves simulations. *Geophysical Research Letters*, 41(24), 9188–9196. <https://doi.org/10.1002/2014GL062089>

Saide, P. E., Gao, M., Lu, Z., Goldberg, D. L., Streets, D. G., Woo, J.-H., Beyersdorf, A., Corr, C. A., Thornhill, K. L., Anderson, B., Hair, J. W., Nehrir, A. R., Diskin, G. S., Jimenez, J. L., Nault, B. A., Campuzano-Jost, P., Dibb, J., Heim, E., Lamb, K. D., ... Crawford, J. H. (2020). Understanding and improving model representation of aerosol optical properties for a Chinese haze event measured during KORUS-AQ. *Atmospheric Chemistry and Physics*, 20(11), 6455–6478. <https://doi.org/10.5194/acp-20-6455-2020>

Schroeder, J. R., Crawford, J. H., Fried, A., Walega, J., Weinheimer, A., Wisthaler, A., Müller, M., Mikoviny, T., Chen, G., Shook, M., Blake, D. R., & Tonnesen, G. S. (2017). New insights into the column $\text{CH}_2\text{O}/\text{NO}_2$ ratio as an indicator of near-surface ozone sensitivity. *Journal of Geophysical Research, D: Atmospheres*, 122(16), 8885–8907. <https://doi.org/10.1002/2017JD026781>

Schroeder, J. R., Crawford, J. H., Ahn, J.-Y., Chang, L., Fried, A., Walega, J., Weinheimer, A., Montzka, D. D., Hall, S. R., Ullmann, K., Wisthaler, A., Mikoviny, T., Chen, G., Blake, D. R., Blake, N. J., Hughes, S. C., Meinardi, S., Diskin, G., Digangi, J. P., ... Wennberg, P. (2020). Observation-based modeling of ozone chemistry in the Seoul metropolitan area during the Korea-United States Air Quality Study (KORUS-AQ). *Elementa Science of the Anthropocene*, 8(1), 3. <https://doi.org/10.1525/elementa.400>

Simpson, I. J., Blake, D. R., Blake, N. J., Meinardi, S., Barletta, B., Hughes, S. C., Fleming, L. T., Crawford, J. H., Diskin, G. S., Emmons, L. K., Fried, A., Guo, H., Peterson, D. A., Wisthaler, A., Woo, J.-H., Barré, J., Gaubert, B., Kim, J., Kim, M. J., ... Zeng, L. (2020). Characterization, sources and reactivity of volatile organic compounds (VOCs) in Seoul and surrounding regions during KORUS-AQ. *Elem Sci Anth*, 8(1), 37. <https://doi.org/10.1525/elementa.434>

Spinei, E., Whitehill, A., Fried, A., Tiefengraber, M., Knepp, T. N., Herndon, S., Herman, J. R., Müller, M., Abuhassan, N., Cede, A., Richter, D., Walega, J., Crawford, J., Szykman, J., Valin, L., Williams, D. J., Long, R., Swap, R. J., Lee, Y., ... Poche, B. (2018). The first evaluation of formaldehyde column observations by improved Pandora spectrometers during the KORUS-AQ field study. *Atmospheric Measurement Techniques*, 11(9), 4943–4961. <https://doi.org/10.5194/amt-11-4943-2018>

Spinei, E., Tiefengraber, M., Müller, M., Gebetsberger, M., Cede, A., Valin, L., Szykman, J., Whitehill, A., Kotsakis, A., Santos, F., Abuhassan, N., Zhao, X., Fioletov, V., Lee, S. C., & Swap, R. (2020). Effect of Polyoxymethylene (POM-H Delrin) offgassing within Pandora head sensor on direct sun and multi-axis formaldehyde column measurements in 2016–2019. *Atmospheric Measurement Techniques Discussions*, 1–24. <https://doi.org/10.5194/amt-2020-158>

Streets, D. G., Bond, T. C., Carmichael, G. R., Fernandes, S. D., Fu, Q., He, D., Klimont, Z., Nelson, S. M., Tsai, N. Y., Wang, M. Q., Woo, J.-H., & Yarber, K. F. (2003). An inventory of gaseous and primary aerosol emissions in Asia in the year 2000. *Journal of Geophysical Research*, 108(D21), 213. <https://doi.org/10.1029/2002JD003093>

Tang, W., Emmons, L. K., Arellano, A. F., Jr, Gaubert, B., Knote, C., Tilmes, S., Buchholz, R. R., Pfister, G. G., Diskin, G. S., Blake, D. R., Blake, N. J., Meinardi, S., DiGangi, J. P., Choi, Y., Woo, J., He, C., Schroeder, J. R., Suh, I., Lee, H., ... Kim, D. (2019). Source Contributions to Carbon Monoxide Concentrations During KORUS-AQ Based on CAM-chem Model Applications. *Journal of Geophysical Research, D: Atmospheres*, 124(5), 2796–2822. <https://doi.org/10.1029/2018JD029151>

Tonnesen, G. S., & Dennis, R. L. (2000). Analysis of radical propagation efficiency to assess ozone sensitivity to hydrocarbons and NO_x: 1. Local indicators of instantaneous odd oxygen production sensitivity. *Journal of Geophysical Research*, 105(D7), 9213–9225. <https://doi.org/10.1029/1999JD900371>

Wang, F., Li, Z., Ren, X., Jiang, Q., He, H., Dickerson, R. R., Dong, X., and Lv, F. (2018). Vertical distributions of aerosol optical properties during the spring 2016 ARIAs airborne campaign in the North China Plain, *Atmos. Chem. Phys.*, 18, 8995–9010, <https://doi.org/10.5194/acp-18-8995-2018>

Woo, J.-H., Choi, K.-C., Kim, H. K., Baek, B. H., Jang, M., Eum, J.-H., Song, C. H., Ma, Y.-I., Sunwoo, Y., Chang, L.-S., & Yoo, S. H. (2012). Development of an anthropogenic emissions processing system for Asia using SMOKE. *Atmospheric Environment*, 58, 5–13. <https://doi.org/10.1016/j.atmosenv.2011.10.042>

Woo, J.-H., Kim, Y., Kim, H.-K., Choi, K.-C., Lee, J.-B., Lim, J.-H., Kim, J., & Seong, M. (2020a). Development of the CREATE inventory in support of integrated climate and air quality modeling for Asia. *Sustainability*, *in press*.

Woo, J.-H, Y. Kim, Jinseok Kim, M. Park, Y. Jang, Jinsu Kim, C. Bu, Y. Lee, R. Park, Y. Oak, A. Fried, I. Simpson, L. Emmons, and J. Crawford. (2020b). KORUS Emissions: A Comprehensive Asian Emissions Information in Support of the NASA/NIER KORUS-AQ Mission. *Elementa*, *to be submitted*.

World Health Organization. (1987). Air quality guidelines for Europe. Copenhagen: WHO Regional Office for Europe. *Copenhagen: WHO Regional Office for Europe*. <https://apps.who.int/iris/handle/10665/107364>

World Health Organization Working Group on Volatile Organic Compounds. (1995). Updating and revision of the air quality guidelines for Europe: report on a WHO Working Group on Volatile Organic Compounds. *Copenhagen: World Health Organization Regional Office for Europe*. <https://apps.who.int/iris/handle/10665/107551>

World Health Organization. (2000). Air quality guidelines for Europe. *Copenhagen: WHO Regional Office for Europe*. <https://apps.who.int/iris/handle/10665/107335>

World Health Organization. (2006). Air quality guidelines global update 2005: particulate matter, ozone, nitrogen dioxide and sulfur dioxide. *Copenhagen: WHO Regional Office for Europe*. <https://apps.who.int/iris/handle/10665/107823>

Appendix

This appendix contains a series of tables to provide details on the investigators, institutions, and observations conducted during the study as well as modeling teams supporting the campaign. Tables are presented in the following order:

Table 1. Instrumentation at the Olympic Park Supersite

Table 2. Instrumentation at the Taehwa Research Forest Supersite

Table 3. Other Ground and Ship-Based Measurements

Table 4. Locations of AERONET Sunphotometers and Pandora Spectrometers

Table 5. Airborne Instrumentation onboard the NASA DC-8, NASA King Air, and Hanseo University King Air Research Aircraft

Table 6. Air Quality Modeling and Forecasting Groups

Table 1. Instrumentation at the Olympic Park Supersite (Lat/Lon: 37.5216 °N/127.1242 °E)

Investigator, Institution	Instrument Name/Technique	Species/Parameters Measured
Trace Gas Measurements		
Seogu Cho, Seoul Institute of Health and Environment	Ecotech gas sensors, AeroLaser 4021, Varian GC450, Met One weather sensors	O ₃ , NO, NO ₂ , NO _x , CO, SO ₂ , CH ₂ O, VOCs, Meteorology: T, RH, WD, WS, Solar and UV radiation
Jinsang Jung, Korea Research Institute of Standards and Science (KRISS)	KENTEK gas analyzers	O ₃ , NO _x , CO, SO ₂
Deug-Soo Kim, Kunsan National University	Teledyne T200U, Thermo Scientific 42i	NO, NO ₂ , NO _x , NO _y
Russell Long, US EPA	2B Tech 211, Teledyne T200U, Teledyne T500U CAPS, Aerodyne QCL	O ₃ , NO, NO ₂ , NO _x , CH ₂ O
Meehye Lee, Korea University	Fluorescence High Performance LC, Ion Chromatography	H ₂ O ₂ , CH ₃ OOH, HONO
Gangwoong Lee, Hankuk Institute of Foreign Studies	QCTILDAS	H ₂ O ₂ , HONO
Jae Hong Lee, Harim Engineering, Inc.	Teledyne T400, T265, and 430	O ₃
Saewung Kim, University of California, Irvine	CIMS (Chemical Ionization Mass Spectrometer)	PAN, ClNO ₂ , Cl ₂
Seogheon Kim, Yonsei University	TD-GC/MS	VOCs
Dongsoo Lee, Yonsei University	Ion Chromatography	Acidic Gases: HCl, HONO, HNO ₃ , H ₂ SO ₄
Jinseok Han, Anyang University	Ion Chromatography	Base Gases: NH ₃ , DMA, TMA
Aerosol Measurements		
Minsuk Bae, Mokpo National University	PILS-TOC	WSOC
Seogu Cho, Seoul Institute of Health and Environment	Sunset OCEC, Thermo FH62C14, XRF625, MARGA	OCEC, PM ₁₀ , PM _{2.5} , PM ₁ , Trace metals, water soluble ions
Kitai Kang, ART PLUS Co., Ltd.	SMPS	Particle size distribution
Sungroul Kim, Soonchunhyang University	Aethalometer AE-33, AE-51	Black Carbon
Jae Hong Lee, Harim Engineering, Inc.	Met One BC1050, Teledyne T640	EC, OC, PM ₁₀ , PM _{2.5}
Jeonghoon Lee, Korea Univ. of Technology and Education	Thermo MAAP 5012, Brechtel TAP 2901, PTI	Black Carbon; absorption at 467, 528, and 652 nm; UV absorption
Chul-Un Ro, Inha University	SEM/EDX	Particle imaging
Hye Jung Shin, NIER	HR-ToF-AMS	PM ₁ ionic composition
Seong Soo Yum, Yonsei University	HTDMA, TSI CPC3776, TSI CPC3010, DMT CCNC	dry diameter, kappa, condensation nuclei (3 nm and 10 nm cutoff), CCN
Remote Sensing Measurements and Soundings		
James Szykman, US EPA	Vaisala CL51	Mixed layer height
Russell Long, US EPA	iMet-1-RSB Radiosondes, DMT/EN-SCI ECC	O ₃ , T, P, RH, WS, WD soundings

**Table 2. Instrumentation at the Taehwa Research Forest Supersite****(Lat/Lon: 37.3123 °N/127.3105 °E)**

Investigator, Institution	Instrument Name/Technique	Species/Parameters Measured
Trace Gas Measurements		
Scott Herndon, Aerodyne	Aerodyne TILDAS mini spectrometer	CH ₂ O
Russell Long, US EPA	2B Tech 211, Aeroqual 500, Teledyne T500U CAPS	O ₃ , NO, NO ₂ , NO _x
Saewung Kim, University of California, Irvine	Thermo 42i, LGR CRDS, CIMS, PTR-ToF-MS, CRM-CIMS	NO, NO ₂ , ClNO ₂ , Cl ₂ , VOCs, OH reactivity
		VOCs
Meehye Lee, Korea University	Luminol-GC, GC-FID	PAN, VOCs
Youngjae Lee, NIER		O ₃ , CO, SO ₂ , NO _x , CO ₂ , H ₂ O, Meteorology: T, WS, WD
Thomas McGee, NASA GSFC	Thermo 42i, Lufft WS501	O ₃ , Meteorology: T, P, RH, WS, WD, Solar radiation
Aerosol Measurements		
Kitai Kang, ART PLUS Co., Ltd.	SMPS	Particle size distribution
Youngjae Lee, NIER		OC, EC
Remote Sensing Measurements and Soundings		
James Szykman, US EPA	Vaisala CL51	Mixed layer height
Thomas McGee, NASA GSFC	GSFC TROPOZ DIAL	Lidar ozone profile
Anne Thompson, NASA GSFC	iMet-1 -RSB Radiosondes, DMT/EN-SCI ECC	O ₃ , T, P, RH, WS, WD soundings

Table 3. Other Ground and Ship-Based Measurements

Investigator, Institution	Instrument Name/Technique	Species/Parameters Measured
Bulkwang Supersite (Lat/Lon: 37.6098 °N/126.9348 °E)		
Hye-Jung Shin	SMPS, APS, nephelometer, BAM 1020, XRF, AIM, Sunset SOCEC, Aethalometer	Particle size distribution, scattering, PM _{2.5} , PM ₁₀ , trace metals, soluble ions, OC, EC, BC
Bangnyung Supersite (Lat/Lon: 37.963 °N/124.644 °E)		
Jinseok Han, Anyang University	HEDS-IC	TMA, NH ₃
Meehye Lee, Korea University	Luminol-GC	PAN
Mindo Lee, NIER	Teledyne Gas Analyzers, Varian NL/450GC SMPS, APS, nephelometer, BAM 1020, XRF, AIM, Sunset SOCEC, Aethalometer	O ₃ , CO, NO _x , SO ₂ , VOCs Particle size distribution, scattering, PM _{2.5} , PM ₁₀ , trace metals, soluble ions, OC, EC, BC
Kitai Kang, ART PLUS Co., Ltd.	SMPS	Particle size distribution
Daejeon Supersite (Lat/Lon: 36.35 °N/127.38 °E)		
Jeong Ah Yu, NIER	Nephelometer, BAM 1020, XRF, AIM, Sunset SOCEC, Aethalometer	Scattering, PM _{2.5} , PM ₁₀ , trace metals, soluble ions, OC, EC, BC
Gwangju Supersite (Lat/Lon: 35.2278 °N/126.8428 °E)		
Cheol-Soo Lim, NIER	Nephelometer, BAM 1020, XRF, AIM, Sunset SOCEC, Aethalometer	Scattering, PM _{2.5} , PM ₁₀ , trace metals, soluble ions, OC, EC, BC
Kihong Park, Gwangju Institute of Science and Technology (GIST)	SMPS, OPC, QAMS	Particle size distribution, submicron chemical composition
Ulsan Supersite (Lat/Lon: 35.53 °N/129.31 °E)		
Mikyung Park, NIER	Teledyne gas analyzers, nephelometer, BAM 1020, XRF, AIM, Sunset SOCEC, Aethalometer	NO _y , NH ₃ , Scattering, PM _{2.5} , PM ₁₀ , trace metals, soluble ions, OC, EC, absorption
Jeju Supersite (Lat/Lon: 33.32 °N/126.40 °E)		
Soojin Ban, NIER	SMPS, APS, nephelometer, BAM 1020, XRF, AIM, Sunset SOCEC, Aethalometer	Particle size distribution, scattering, PM _{2.5} , PM ₁₀ , trace metals, soluble ions, OC, EC, absorption
Seoul National University (SNU) (Lat/Lon: 37.458 °N/126.951 °E)		
Sang-Woo Kim, SNU Robert Holz, U. Wisconsin	Mie Scattering Lidar High Spectral Resolution Lidar	Aerosol backscatter and depolarization
Korea Institute of Science and Technology (KIST) (Lat/Lon: 37.6015 °N/127.0452 °E)		
Hwajin Kim, KIST	HR-ToF-AMS (High Resolution Time-of-Flight Aerosol Mass Spectrometer)	Chemically-speciated submicron non-refractory particulate mass and size distribution
Hankuk University of Foreign Studies (HUFS) (Lat/Lon: 37.339 °N/127.266 °E)		
Young Sung Ghim, HUFS	SMPS, OPC, MAAP	Particle size distribution, PM ₁₀ , PM _{2.5} , PM ₁ , BC
Yonsei University (Lat/Lon: 37.564 °N/126.935 °E)		
Jinkyu Hong, Yonsei U.	Picarro CRDS, CL-31	CO ₂ , CH ₄ , BL height



Investigator, Institution	Instrument Name/Technique	Species/Parameters Measured
Jungnang (Lat/Lon: 37.5906 °N/127.0794 °E)		
Moon-Soo Park, HUFS	CL51, Automatic Weather Station	Aerosol backscatter, BL height, Met: T, P, RH, precip, WS, WD, radiation
Gosan (Lat/Lon: 33.292 °N/126.162 °E)		
Sang-Woo Kim, SNU	SMPS, nephelometer, aethalometer, Mie scattering lidar	Particle size distribution, scattering, BC, backscatter and depolarization
Pyeongtaek power plant (Lat/Lon: 36.865 °N/126.215 °E)		
Young J Kim, GIST	Mini MAX-DOAS	SO ₂
Fukue Island (Lat/Lon: 32.75 °N/126.68 °E)		
Yugo Kanaya, JAMSTEC	Thermo analyzers (49C, 48C, MAAP 5012, and SHARP 5030) COSMOS, Metcon spectroradiometer	O ₃ , CO, Black carbon, j(NO ₂), j(O ¹ D)
RV Onnuri		
Carolyn Jordan, National Institute of Aerospace	Brechtel TAP, Airphoton IN101 nephelometer, SpEx, filter sampling, MicroTOPS II	In situ aerosol absorption and scattering, spectral aerosol extinction (300-700 nm), aerosol composition and spectral optical properties, total-column multi-wavelength AOD
Anne Thompson, NASA GSFC	Thermo 49C, 48C, and 42C-Y; Aerodyne CAPS	O ₃ , CO, NO, NOy, NO ₂
Wonkook Kim, KIOST	RV Onnuri onboard AWS	Meteorology: T, P, RH, WS, WD, Solar radiation, precipitation
RV Jang Mok		
James Flynn, University of Houston	Thermo 49i, 42i-TL, 48i-TLE, and 43i-TL	O ₃ , NO, NO ₂ , CO, SO ₂
Young-Je Park, KIOST	RV Jang Mok onboard AWS	Meteorology: T, P, RH, WD, WS
RV Kisang		
Meehye Lee, Korea University	Thermo gas analyzers, KENTEK Mezus-110, Luminol-GC, nephelometer, aethalometer	O ₃ , CO, SO ₂ , NO ₂ , PAN, aerosol scattering, Black carbon

Table 4. Locations of AERONET Sunphotometers and Pandora Spectrometers

Site Name	Latitude(°N)	Longitude (°E)	AERONET	Pandora
Anmyeon	36.53889	126.33	L	K
Baengnyeong	37.963	124.644	L	
Busan	35.235	129.083	L	K
Daegwallyeong	37.687	128.759	K	
Gangneung	37.771	128.867	L	
Gosan	33.292	126.162	L	
Gwangju	35.22778	126.84278	L	K
Hankuk	37.339	127.266	L	
Iksan	35.962	127.005	K	
Kyungpook	35.89	128.606	K	
Mokpo	34.913	126.437	K	
NIER	37.569	126.64	K	
Olympic Park	37.5216	127.1243	K	K
Seoul	37.458	126.951	L	
Songchon (Baeksa)	37.412	127.569	K	K
Taehwa	37.3123	127.3105	K	K
UNIST	35.582	129.19	K	
Yeoju	37.338	127.489	K	K
Yonsei	37.564	126.935	L	K

K = KORUS-AQ site; L = Long-term site

Table 5. Airborne Instrumentation onboard the NASA DC-8, NASA King Air, and Hanseo University King Air Research Aircraft

Investigator, Institution	Instrument Name/Technique	Species/Parameters Measured
NASA DC-8 Trace Gas Measurements		
Andrew Weinheimer, NCAR	NCAR 4-Channel Chemiluminescence Instrument	O ₃ , NO, NO ₂ , NO _y
Glenn Diskin, NASA Langley	DACOM (Diode Laser Spectrometer)	CO, CH ₄ , N ₂ O
Glenn Diskin, NASA Langley	DLH (Diode Laser Hygrometer)	H ₂ O(v)
Joshua DiGangi, NASA Langley	Non-dispersive IR Spectrometer	CO ₂
Donald Blake, University of California, Irvine	WAS (Whole Air Sampler)	C ₂ -C ₁₀ alkanes, C ₂ -C ₄ alkenes, C ₆ -C ₉ aromatics, C ₅ -C ₆ cycloalkanes, C ₁ -C ₅ alkyl nitrates, C ₁ -C ₂ halocarbons (CFCs, HCFCs, HFCs, halons, methyl halides, etc.), isoprene, monoterpenes, ethyne, COS, DMS
Alan Fried, University of Colorado, Boulder	CAMS (Compact Atmospheric Multi-Species Spectrometer)	CH ₂ O, C ₂ H ₆
L. Gregory Huey, Georgia Institute of Technology	GT-CIMS (Georgia Tech - Chemical Ionization Mass Spectrometer)	PAN, PPN, APAN, PBZN, SO ₂ , HCl
William Brune, Penn State	ATHOS (Airborne Tropospheric Hydrogen Oxides Sensor)	OH, HO ₂ , OH reactivity
Ronald Cohen, University of California, Berkeley	TD-LIF (Thermal Dissociation-Laser Induced Fluorescence)	NO ₂ , sum of peroxy nitrates, sum of alkyl nitrates, aerosol-phase organic nitrates
Saewung Kim, University of California, Irvine	CIMS (Chemical Ionization Mass Spectrometer)	ClNO ₂ , Cl ₂
Kyung-Eun Min, Gwangju Institute of Science and Technology	CEASAR (Cavity Enhanced Absorption Spectroscopy for Atmospheric Research)	NO ₂ , CHOCHO
Jeong-Hoo Park, National Institute of Environmental Research	PTR-HR-ToF-MS (Proton Transfer, High-Resolution, Time-of-Flight, Mass Spectrometer)	Toluene
Paul Wennberg, California Institute of Technology	CIT-CIMS (Caltech Chemical Ionization Mass Spectrometer)	HNO ₃ , HCN, H ₂ O ₂ , organic peroxides, organic nitrates, organic hydroxynitrates, peroxyacetic acid, cresol, glycoaldehyde
Armin Wisthaler, University of Oslo	PTR-ToF-MS (Proton Transfer Time-of-Flight Mass Spectrometer)	methanol, acetonitrile, acetone, methyl ethyl ketone, acetaldehyde, benzene, toluene, C8-alkylbenzenes, isoprene, isoprene oxidation products, monoterpenes
NASA DC-8 Aerosol Measurements		
Bruce Anderson, NASA Langley	LARGE (Langley Aerosol Research Group Experiment)	Aerosol number, size distribution, optical and microphysical properties
Jack Dibb, University of New Hampshire	SAGA (Soluble Acidic Gases and Aerosol)	Bulk aerosol ionic composition, fine aerosol sulfate, HNO ₃ (and submicron NO ₃ aerosol)

Investigator, Institution	Instrument Name/Technique	Species/Parameters Measured
Jose Jimenez, University of Colorado-Boulder	HR-ToF-AMS (High Resolution Time-of-Flight Aerosol Mass Spectrometer)	Chemically-speciated submicron non-refractory particulate mass and size distribution
Taehyoung Lee, Hankuk University of Foreign Studies	AMS (Aerosol Mass Spectrometer)	Chemically speciated submicron non-refractory particulate mass
Joshua Schwarz, NOAA	HS-SP2 (Humidified Dual Single Particle Soot Photometer)	Black carbon (BC) concentration, size distribution, mixing state, and hygroscopicity of BC containing particles
Seong Soo Yum, Yonsei University	Condensation Nuclei Counter	
NASA DC-8 Remote Sensing Measurements		
Samuel Hall, NCAR	CAFS (CCD Actinic Flux Spectrometers)	4- π sr actinic flux and derived photolysis frequencies
John Hair, NASA Langley	DIAL-HSRL (Differential Absorption Lidar and High Spectral Resolution Lidar)	Zenith and Nadir O ₃ ; aerosol backscatter, depolarization, extinction, and other retrieved aerosol parameters
Jens Redemann, NASA Ames	4STAR (Spectrometers for Sky-Scanning, Sun-Tracking Atmospheric Research)	Zenith measurements of AOD; column water vapor, O ₃ , and NO ₂
NASA King Air Remote Sensing Measurements		
Scott Janz, NASA Goddard	Geo-TASO (Geostationary Trace gas and Aerosol Sensor Optimization)	Nadir column densities of NO ₂ and CH ₂ O
Hanseo University King Air Trace Gas Measurements		
Jinsoo Park, National Institute of Environmental Research	Teledyne API T400 AeroLaser AL5002 LGR GGS 24 EP Thermo TEI 43i	O ₃ CO CH ₄ , CO ₂ , H ₂ O SO ₂
Tom Hanisco, NASA Goddard	CAFÉ (Compact Airborne Formaldehyde Experiment)	CH ₂ O

**Table 6. Air Quality Modeling and Forecasting Groups**

Investigator, Institution	Model Name/Role	Domain/Resolution
Rokjin Park, Seoul National University	GRIMs-Chem	70-150°E, 15-55°N / 0.25° x 0.3125° (~27 km over Korea)
Louisa Emmons, NCAR	CAM-Chem WRF-Tracer	Global / 0.9° x 1.25° East Asia / 15 km, Korea / 3 km
Chul Han Song, GIST	WRF-CMAQ	100-145°E, 20-45°N / 15 km
Arlindo DaSilva, NASA GSFC	GEOS-5	Global / 12.5 km
Gregory Carmichael, University of Iowa	WRF-Chem	East Asia / 20 km, Korea / 4 km
Cheol-Hee Kim, Pusan National University	WRF-Chem	East Asia / 27 km
Soontae Kim, Ajou University	WRF-CAMx	Flexi-nesting 27 km / 9 km / 3 km
Jung-Hun Woo, Konkuk University	KU-CREATE emissions database	
David Peterson, Naval Research Laboratory (NRL) and Sang-Ok Han, National Institute of Meteorological Sciences (NIMS)	Regional Weather Forecasting	

Glossary of Terms and Acronyms

AERONET - Aerosol Robotic Network

AHI - Advanced Himawari Imager (satellite instrument operated by Japan)

ALW - Aerosol Liquid Water

AMS - Aerosol Mass Spectrometer

BC - Black Carbon

BL - Boundary Layer (bottom layer of the troposphere that is in contact with the Earth's surface)

Bottom-Up Emissions - An estimate of emissions based on activity data from representative samples

CAMx - Comprehensive Air Quality Model with Extensions

CAPSS - Clean Air Policy Support System

CEMS - Continuous Emissions Monitoring System

CleanSYS - A smokestack telemonitoring system

CMAQ - Community Multiscale Air Quality model

CO - Carbon Monoxide

CO₂ - Carbon Dioxide

COS - Carbonyl sulfide

CREATE - Comprehensive Regional Emissions inventory for Atmospheric Transport Experiment

CTM - Chemical Transport Model

DMA – Dimethylamine

E-AIM - Extended Aerosol Inorganic Model

EC - Elemental Carbon

FSSR - Final Science Synthesis Report



GEMS - Geostationary Environment Monitoring Spectrometer

GEO - Geostationary (satellite)

GEOS-Chem - Goddard Earth Observing System – Chemistry model

GeoTASO - Geostationary Trace gas and Aerosol Sensor Optimization (airborne instrument)

GOCI - Geostationary Ocean Color Imager (satellite instrument operated by Korea)

HCHO - Formaldehyde

HOA - Hydrocarbon-like Organic Aerosol

HONO - Nitrous Acid

H₂O₂ - Hydrogen Peroxide

Kappa - parameter for aerosol hygroscopicity

KIST - Korea Institute of Science and Technology

KMOE - Korean Ministry of Environment

KORUS-AQ - Korea-United States Air Quality Study

KORUS-OC - Korea-United States Ocean Color Study

LEO - Low Earth Orbit (satellite)

LFT - Lower Free Troposphere (the layer of the atmosphere above the boundary layer)

LPG - Liquefied Petroleum Gas

MAPS-Seoul - Megacity Air Pollution Study - Seoul

MEIC - Multi-resolution Emission Inventory for China

Mixed Layer - A type of atmospheric boundary layer characterized by turbulence and mixing

MLH - Mixed Layer Height

NASA - National Aeronautics and Space Administration

NH_3 - Ammonia

NIER - National Institute of Environmental Research

NMB - Normalized Mean Bias

NO - Nitric Oxide

NO_2 - Nitrogen Dioxide

NO_x - Nitrogen Oxides ($\text{NO} + \text{NO}_2$)

OA - Organic Aerosol

OC - Organic Carbon

OH - Hydroxyl radical (a molecule)

OFR - Oxidation Flow Reactor

OMI - Ozone Monitoring Instrument (satellite instrument operated by USA/Netherlands/Finland)

OPE - Ozone Production Efficiency

O_3 - Ozone

P - Pressure

PBL - Planetary Boundary Layer

PM_{10} - Particulate Matter (diameter $< 10 \mu\text{m}$)

$\text{PM}_{2.5}$ - Particulate Matter (diameter $< 2.5 \mu\text{m}$)

POA - Primary Organic Aerosol

$\text{P}(\text{O}_3)$ - Net Ozone Production

RH - Relative Humidity

RMSE - Root Mean Square Error

RSSR - Rapid Science Synthesis Report



SIA - Secondary Inorganic Aerosol

S/IVOC - Semi-volatile and Intermediate-volatility Volatile Organic Compounds

SMA - Seoul Metropolitan Area

SMOKE-Asia - Sparse Matrix Operator Kernel Emissions-Asia

SOA - Secondary Organic Aerosol

SO₂ - Sulfur Dioxide

T - Temperature

T/B - Toluene/Benzene

TMA – Trimethylamine

Top-Down Emissions - An estimate of emissions based on observations at a regional scale

UV - Ultraviolet

VOC - Volatile Organic Compound

WAS - Whole Air Sampling

WD - Wind direction

WS - Wind speed

WRF-Chem - Weather Research and Forecasting - Chemistry model

0-D - Zero-dimensional

3-D - Three-dimensional

KORUS-AQ Final Science Synthesis Report
한-미 협력 국내 대기질 공동조사
KORUS-AQ 최종 종합보고서

